ROBUSTNESS AND POWER DISSIPATION IN QUANTUM-DOT CELLULAR AUTOMATA

A Dissertation

Submitted to the Graduate School
of the University of Notre Dame
in Partial Fulfillment of the Requirements
for the Degree of

Doctor of Philosophy

by

Mo Liu, B.S.E.E., M.S.

Craig S. Lent, Director

Graduate Program in Electrical Engineering
Notre Dame, Indiana
March 2006

ROBUSTNESS AND POWER DISSIPATION IN QUANTUM-DOT CELLULAR AUTOMATA

Abstract

by

Mo Liu

Quantum-dot cellular automata (QCA) is a new computation paradigm which encodes binary information by charge configuration within a cell instead of the conventional current switches. No current flows within the cells. The columbic interaction is sufficient for computation. This revolutionary paradigm provides a possible solution for transistor-less computation at the nanoscale. QCA logic devices such as binary wires, majority gates, shift registers and fan-outs made of metal islands and small capacitors have been successfully fabricated. Experimental and theoretical research on the switching of molecular QCA cells has been underway. This thesis will focus on robustness and power dissipation in QCA circuits. The robustness of both metallic and molecular QCA circuits are studied. The power dissipation and power flow in clocked molecular QCA circuits are explored. Our results show that QCA approach is inherently robust and ultra low power dissipation is possible in QCA.

To my parents and sister

with

Love and Gratitude

CONTENTS

FIGURES

ACKNOWLEDGMENTS

To begin with, I want to acknowledge my profound debt of gratitude to Professor Craig S. Lent. I could not have asked for a more supporting and caring advisor. It was an exceptionally exciting and rewarding experience working for and with Prof. Lent. I am lucky to have associated with such a mentor.

I am very grateful to Prof. Merz, Prof. Snider and Prof. Bernstein for being on my advisory committee and reviewing my dissertation. I would like to express my gratitude to Prof. Orlov for his generous help in both research level and personal level.

Also let me mention my appreciation for our research group members: John Timler, Beth Robinson, Enrique Blair and Yuhui Lu with whom I share the research interests and friendship. Same thanks to Department Assistant Susan Willams and Pat Base, for their kind assistance.

This career goal of mine would have never materialized had it not been for the sacrifices and support of my family. Words cannot adequately acknowledge their undying support. Finally, special thanks to Qi Gong, my fiancee, for his unfailingly support and stood behind me in all my endeavors.

CHAPTER 1

QCA INTRODUCTION

1.1 Introduction of QCA

In today's computers, binary information is encoded using current switches. The on and off states of current switches represent bit "1" and "0" respectively. In a transistor, when the gate voltage is less than the threshold voltage, there is no current flow; the transistor is off. Only when the gate voltage is greater than the threshold voltage is there current flow.

The conventional transistor-based CMOS technology has followed Moore's Law, doubling transistors every 18 months. Shrinking transistors has been the major trend to achieve circuits with fast speed, high densities and low power dissipation. However, when scaling comes down to submicron level, many problems occur. Physical limits such as quantum effects and non-deterministic behavior of small currents and technological limits like power dissipation and design complexity may hinder the further progress of microelectronics using conventional circuit scaling. A new paradigm, beyond current switches to encode binary information, may be needed.

Quantum-dot cellular automata (QCA) emerges as such a paradigm. It was proposed by Lent et al. in 1993 [1]. Since then, a significant amount of research has been done in QCA both theoretically and experimentally [2-58]. It has become one of the promising candidates for nano-computing. QCA encodes binary information in the charge configuration within a cell. Coulomb interaction between cells is suffi-

cient to accomplish the computation in QCA arrays—thus no interconnect wires are needed between cells. No current flows out of the cell so that low power dissipation is possible.

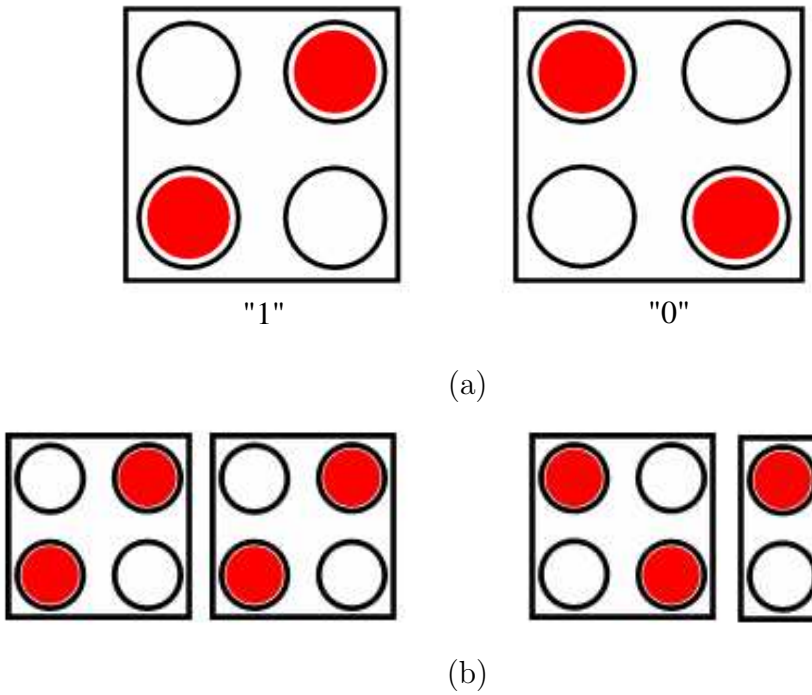

Figure 1.1. Schematic of a QCA cell. (a) Two states "1" and "0" in a single cell; (b) Coulomb interactions couple the states of neighboring cells.

A simple QCA cell consists of four quantum dots arranged in a square, shown in Figure 1.1. Dots are simply places where a charge can be localized. There are two extra electrons in the cell that are free to move between the four dots. Tunneling in or out of a cell is suppressed. The numbering of the dots in the cell goes clockwise starting from the dot on the top right. A polarization P in a cell, which measures the extent to which the electronic charge is distributed among the four dots, is therefore defined as

$$P = \frac{(\rho_1 + \rho_3) - (\rho_2 + \rho_4)}{\rho_1 + \rho_2 + \rho_3 + \rho_4}$$

where ρ_i denotes the electronic charge at dot i. Because of Coulomb repulsion, the electrons will occupy antipodal sites. The two polarized charge configurations $P = -1$ and $P = 1$ correspond bit value of 0 and 1 respectively. These two states are used to encode the binary information. When a polarized cell is placed close to another cell in line, the Coulomb interaction between them will force the second cell switch into the same state as the first cell, minimizing the electrostatic energy in the charge configuration of the cells. Based on the Coulomb interaction between cells, fundamental QCA devices can be built.

Figure 1.2 shows the layout of some basic QCA devices. A binary wire can be realized with a line of cells to transmit information from one cell to another. Two diagonally aligned cells will have the opposite polarization. Inverters can therefore be implemented with lines of diagonally aligned cells. A majority gate can be built with five cells. The top, left and bottom cells are inputs. The device cell in the center interacts with the three inputs and its result (the majority of the input bits) will be propagated to the cell on the right. A majority gate is the basic logic gate in QCA, as it can function as an "OR" gate with one of the inputs fixed to "1" and function as an "AND" gate with one of the inputs fixed to "0". More complex circuits like full adders and memories can be constructed hierarchically in QCA with appropriate layout [5, 9].

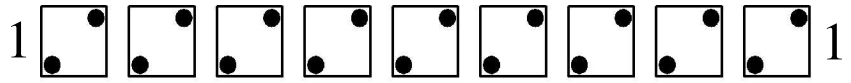

(a)

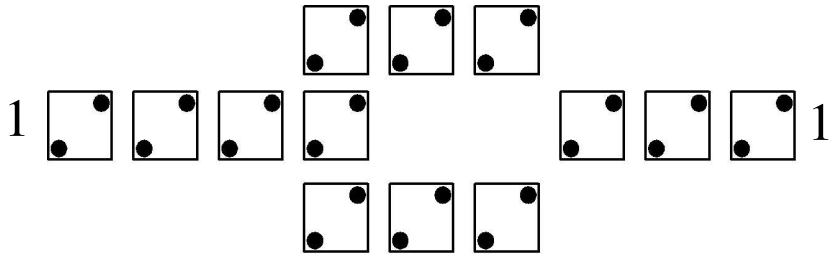

(b)

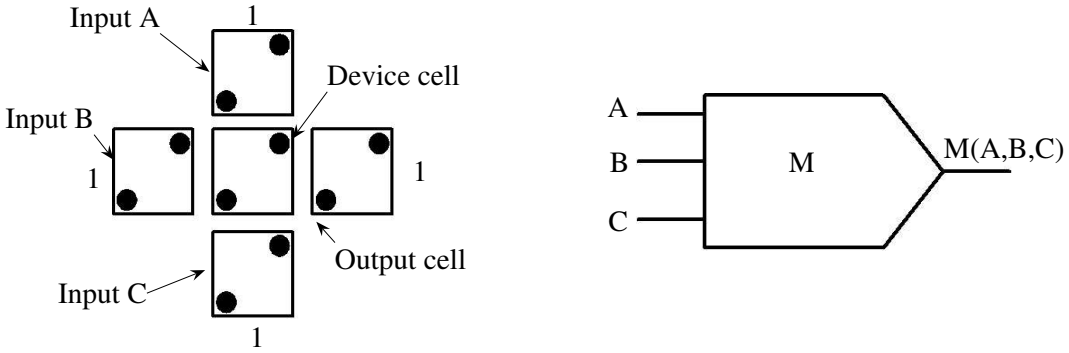

(c)

Figure 1.2. Basic QCA devices. (a) A binary wire which propagates information through the line; (b) An inverter which uses the interaction of diagonally aligned cells to invert bits; (c) A three input majority gate. The output is the majority vote of the three inputs.

1.2 Implementations of QCA cell

QCA cells can be realized with semiconductor, metal, magnets and molecules. Semiconductor material is used to form the dots which are capacitively coupled in semiconductor QCA. In [15], charge detection scheme is realized for AlGaAs/GaAs QCA cell and Coulomb coupling between quantum dots is observed. In [16, 17], a four dot silicon based QCA cell constructed with two adjacent double dots is fabricated and measured at 4.2 K. In magnetic QCA, the logic states are signaled by the magnetization direction of the single domain magnetic dots which couple to the neighbors through magnetic interactions. Room temperature magnetic QCA has been demonstrated in [18]. Other theoretical and experimental research on magnetic QCA devices has been studied in [19, 20]. A three input majority gate in magnetic QCA has been fabricated [21]. Those work provide useful demonstrations of QCA cell implementations. In this research, we focus on metallic QCA cell and molecular QCA cell.

1.2.1 Metallic QCA cells

QCA devices exist. Metal dot QCA cells are built with metallic tunnel junctions and very small capacitors. Aluminum islands form the dots and aluminum oxide tunnel junctions serve as the tunneling paths between dots. Figure 1.3 illustrates the implementation of a four-dot QCA cell [22]. Electrons can tunnel between dot 1 and dot 2 and between dot 3 and dot 4 through tunnel junctions. Figure 1.4 is a scanning electron micrograph of the four-dot cell. The four red dots indicate the positions of the four metal islands. The two magenta dots represent single electron transistor electrometers that are used to measure the output. The fabrication technique uses a combination of electron beam lithography and dual-angle evaporation to deposit thin lines of aluminum that form overlaps with a small area. The lines of aluminum

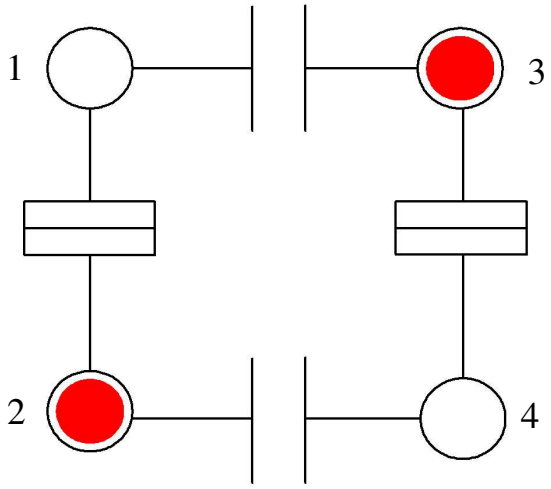

Figure 1.3. The implementation of a metal dot QCA cell, built with tunnel junctions and small capacitors. Dot 1, 2, 3, 4 are four quantum dots formed by aluminum islands.

thus form dots and the thin layer of aluminum oxide within the overlaps form the tunnel junction. The area of the tunnel junction is about 50nm $\times$ 50nm and the thickness of the aluminum oxide is about 2nm. The experiment is performed in a dilution refrigerator at a magnetic field of 1 Tesla to suppress the superconducting effect in aluminum. Figure 1.5 shows the measured characteristics of a four-dot cell [27]. The differential input $(V_1 - V_2)$ is applied between dot 1 and 2 with coupling capacitors. Φ_{D1}, Φ_{D2}, Φ_{D3}, Φ_{D4} are the measured dot potentials. When a positive input is applied, an electron tunnels from dot 2 to dot 1, which in turn will switch an electron from dot 3 to dot 4 due to the capacitively coupling between dot 1 and dot 3 and between dot 2 and dot 4.

Metal dot QCA devices have been successfully demonstrated at low temperatures. Majority logic gates, binary wires, memories, and clocked multi-stage shift registers have all been fabricated [25, 26, 27, 28]. Figure 1.6 shows the schematic

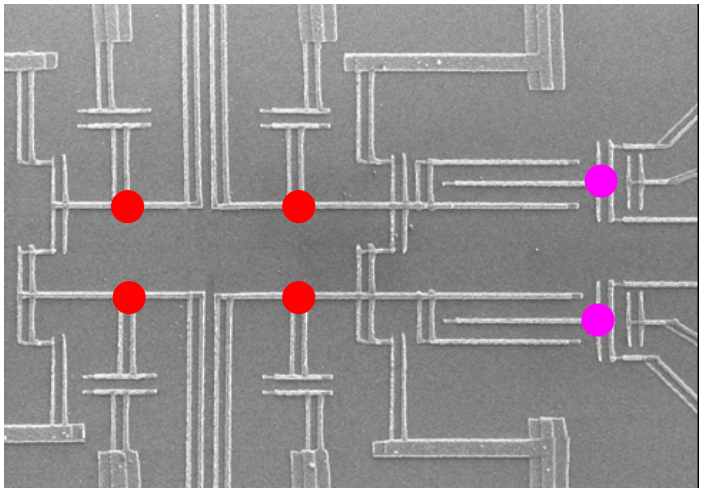

Figure 1.4. Scanning electron micrograph of a four-dot cell.

of the majority gate experiment which corresponds to Figure 1.2(c) [25]. Four aluminum dots are connected in a ring by tunnel junctions. Each dot is coupled to a metal gate through a gate capacitor. The differential signal A(between gate 1 and 3), B (between gate 1 and 2) and C (between gate 2 and 4) constitute the three inputs. The output is the differential potential between dot 3 and dot 4. Electrometers are used to measure the potential in dot 3 and dot 4. Figure 1.7 demonstrates the operation of the majority gate. The experiment result and theory matches very well. The data confirms the majority gate operation in QCA. These metal-dot QCA devices, though limited by the fabrication method to low temperature operation, provide valuable demonstrations of QCA circuits. They serve as prototypes for molecular systems that will function at room temperature.

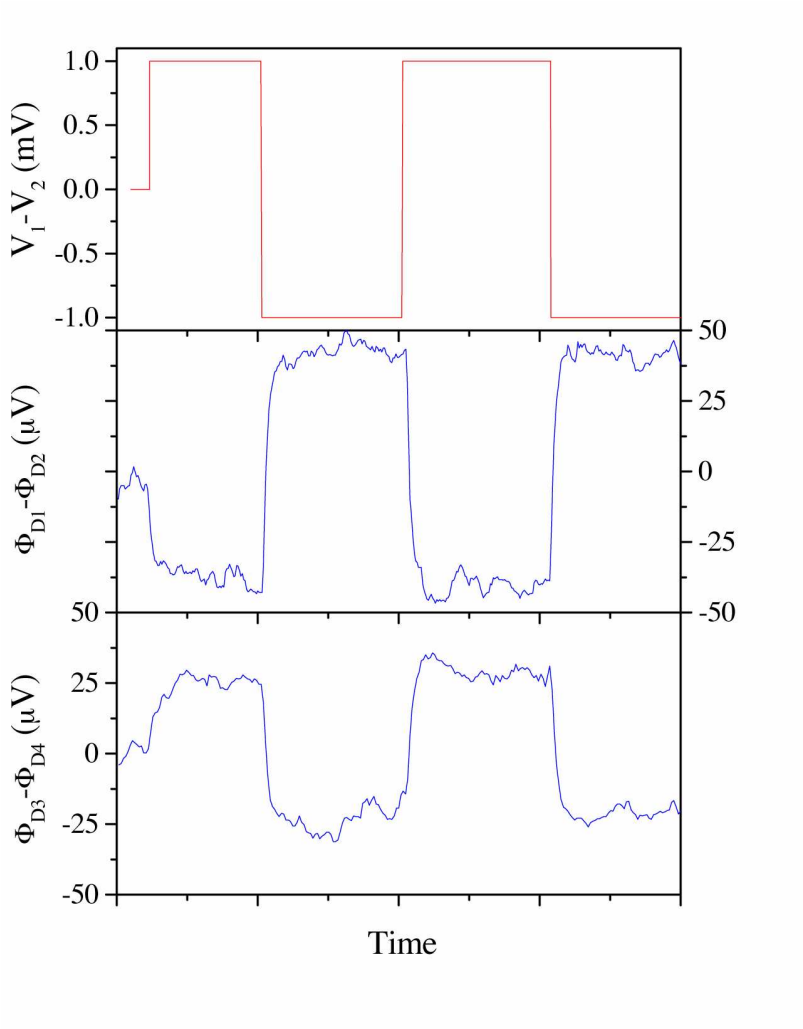

Figure 1.5. The experiment measurement of a demonstrated four-dot cell. It plots differential potential between dot 1 and dot 2, dot 3 and dot 4.

1.2.2 Molecular QCA cell

Molecular QCA cell holds a more promising future with room temperature operation. Compared to metal dot QCA, molecular QCA cell offers additional benefits other than small size and high densities. Molecules are very good charge containers. Also the molecular self-assembly creates identical devices so that the fabrication cost might be lowered. Of course many problems remain to be solved in synthesis

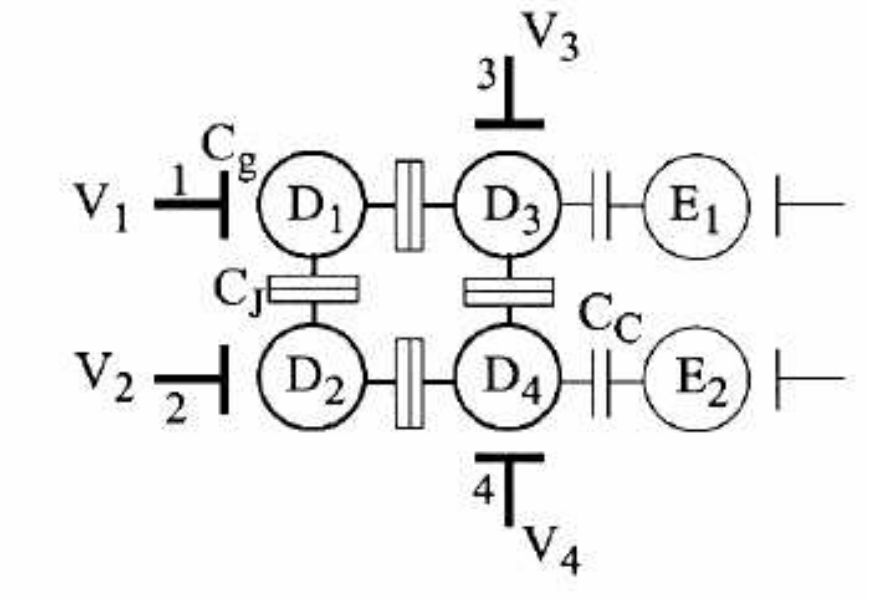

Figure 1.6. Schematic of the QCA majority gate experiment. Four dots are connected in a ring by tunnel junctions. Each dot is coupled to a metal gate through a gate capacitor. E1 and E2 are the electrometers.

and positioning of molecular devices, and there are few specific candidates for the QCA devices. In molecular QCA, each cell is a single molecule. Non-bonding π or d orbital serves as dots, so that electron transfer from dot to dot has minimal effect on the overall molecular structure [34-41]. Two-dot half-cells [38, 39, 40] and four-dot cells [41] have been recently synthesized. The two-dot cells are functionalized for attachment to a silicon substrate by covalent bonding. Supporting groups act as "struts" which hold the molecule perpendicular to the surface. Direct measurements of the bistable switching required for QCA operation have been reported in [40]. Charge tunneling from one dot to another can be sensed by capacitance measurements. Figure 1.8 shows the highest occupied molecular orbital (HOMO) of two stable states in a four-dot molecular QCA cell synthesized by Fehlner's group

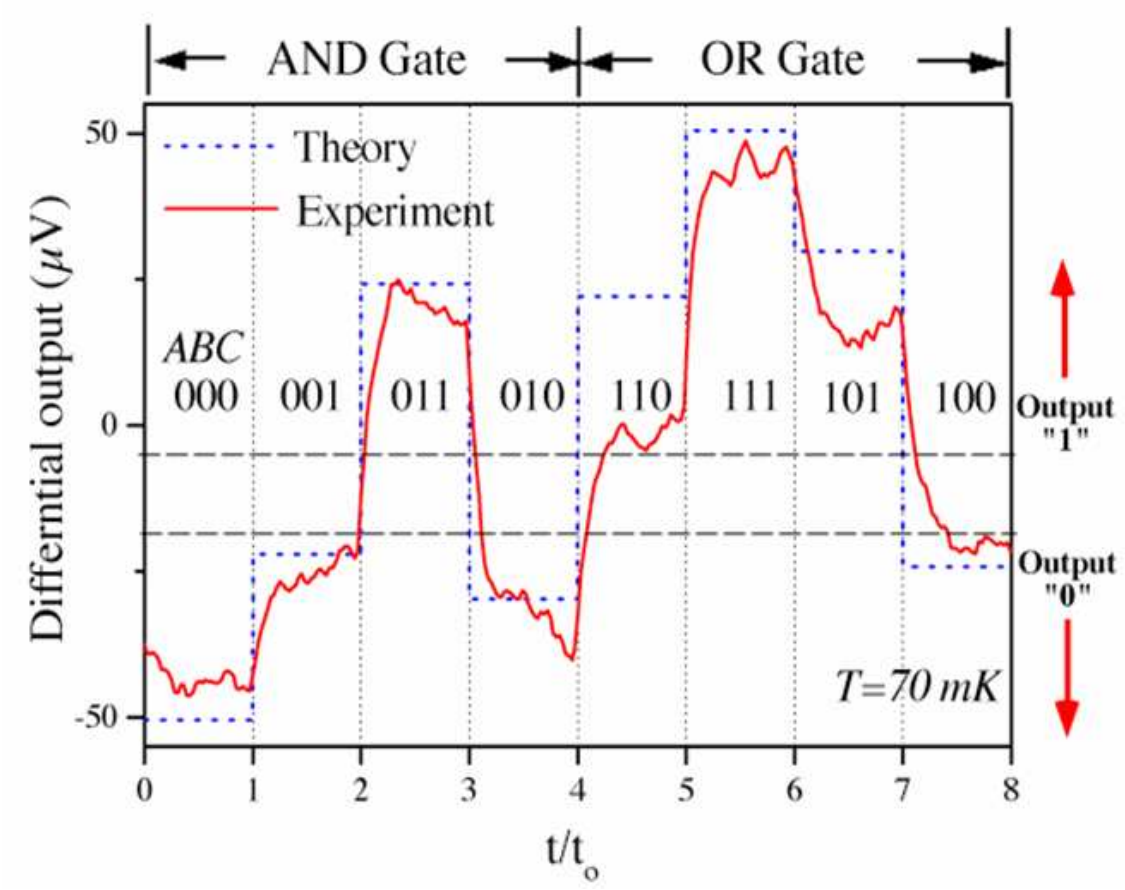

Figure 1.7. Demonstration of majority gate operation. Solid line represents the experimental result. Dashes line is the theoretical result.

[41]. Four ferrocene groups occupy four corner dots and each group acts as a quantum dot. The Co group in the center of the square provides a bridging ligand, which serves as the tunnelling path between four dots. The investigation of other molecular QCA candidates are under way.

1.3 Clocking in QCA

Clocking is a key architectural feature in QCA. It not only controls the information flow in the circuit, but also provides power gain and reduces power dissipation.

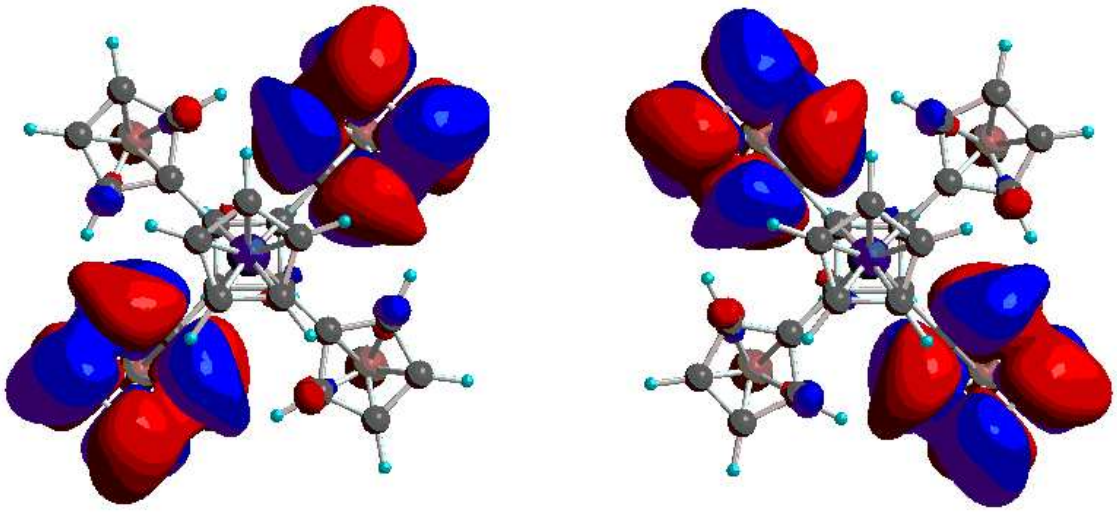

Figure 1.8. The HOMOs two stable states of a four-dot molecular QCA cell model.

A robust circuit should be able to restore signal at each transport stage so that information will not be lost due to unavoidable dissipative process. Therefore the circuit must have power gain at each stage, augmenting a weak input signal to restore logical levels. In conventional CMOS circuit, the power gain is provided by the power supply. In clocked QCA, the energy from the clock provides the energy needed to restore the signal.

The adiabatic clocking in QCA cells is based on the idea from Keys and Landauer [66]. Suppose a system is placed in a potential well that can be externally controlled to change between monostable and bistable state continuously. The system in one of the potential wells encodes bit "1" or "0", shown in Figure 1.9 (b), (c). At the initial state as in Figure 1.9 (a), the system is in a monostable state. Then a small input is applied as is shown in Figure 1.9 (d). The blue dashed curve represents the state before any change is made. If the input is held and a clock is applied

to slowly change the system from monostable to bistable state shown in Figure 1.9 (e), the system will be in one of the potential wells that is more energetically favorable, indicated by the input. In the end, the system remains in the potential well even when the input is removed as is shown in Figure 1.9 (f). The signal is thus amplified in the last stage. The cyclic modulation of the potential well is made slowly and gradually to ensure the system always operated under ground state so that the energy dissipation to the environment is reduced to minimal.

Two additional dots are added in the middle of the simplest QCA cell to form a clocked QCA cell. The four dots in the corner of the square function as active dots and the middle dots function as null dots. The clock is applied to change the potential energy of the middle dots. The clock can lower the potential energy in the middle dots, pull electrons to middle dots, which is a monostable state corresponding to Figure 1.9 (a). The cell is in a null state and holds no information. The clock can also raise the potential energy in the middle dots and push electrons to active dots, corresponding to Figure 1.9 (b) and Figure 1.9 (c). The cell is in an active state, holding a bit "0" or "1", decided by the input. Figure 1.10 shows the schematic of three states in a clocked six-dot QCA cell. In metal dot QCA cell, the clock is applied directly to the middle dots through a capacitive coupling to adjust the energy barrier.

Figure 1.11 (a) shows a simple three-dot clocked half-cell composed of only carbon and hydrogen [83]. The molecule lacks any functionalization for attachment and orientation, but is useful as a model system and is made computationally tractable by its simplicity. Ethylene groups form the dots in this structure. The molecular cation has a mobile hole which can occupy one of the three dots. Isopotential surfaces plotted in Figure 1.11 (b) show the molecular cation in the three states corresponding to "0", "1", and null. An electric field in the z-direction acts as a

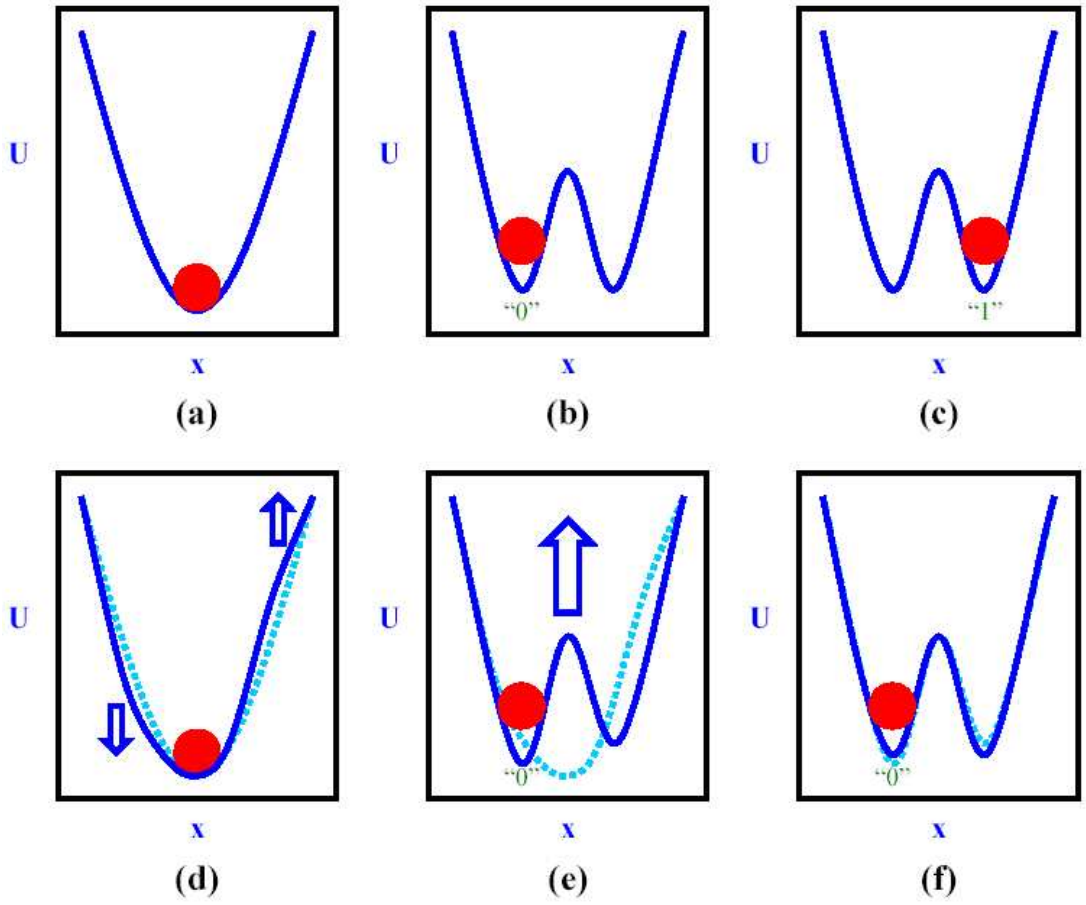

Figure 1.9. A system in a potential well varied between monostable state and bistable state continuously and adiabatically. The dashed curve represents the state before any change is made. (a) Monostable state (b) bistable state with bit "0" (c) bistable state with bit "1". (d) A small input is applied in the system. (e) A clock is applied to change the system from monostable state to bistable state. (f) The system remained in the well when the input is removed.

clocking field which moves the cell between one of the active states and null state and the field in the y-direction, presumably due to neighboring molecules, is the input signal. Quantum chemistry calculations of simple molecules with QCA properties can be useful in understanding molecular QCA switching behavior. The information content of the molecule is represented by the y-component of the dipole moment.

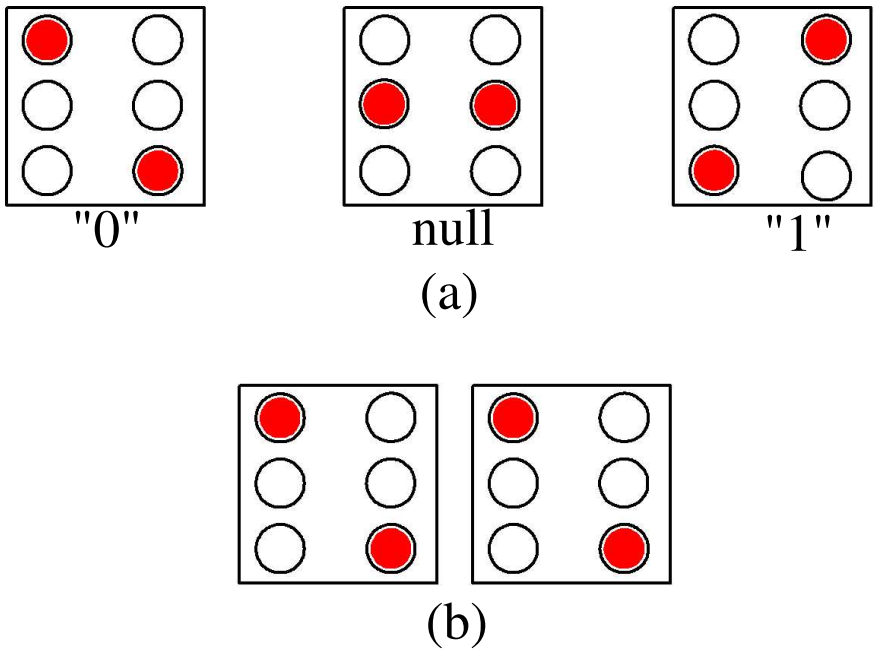

Figure 1.10. The schematic of three states in a clocked six-dot QCA cell.

We define the polarization to be the normalized dipole moment

$$P = \frac{\mu_y}{|\mu_y(max)|}$$

Figure 1.12 shows the calculated polarization as a function of the clocking field in the presence of a signal (driver) field of either sign [83]. The clocking field activates the cell, pushing it into the appropriate state depending on the sign of the driver field.

In molecular QCA cell, the clock is distributed over a large scale rather than an individual cell as it is impractical to make contact to individual cells due to the small size of the molecules [32, 33, 36]. Figure 1.13 shows a model of a six-dot molecular QCA cell [33]. The white molecule represents the input. Four active dots

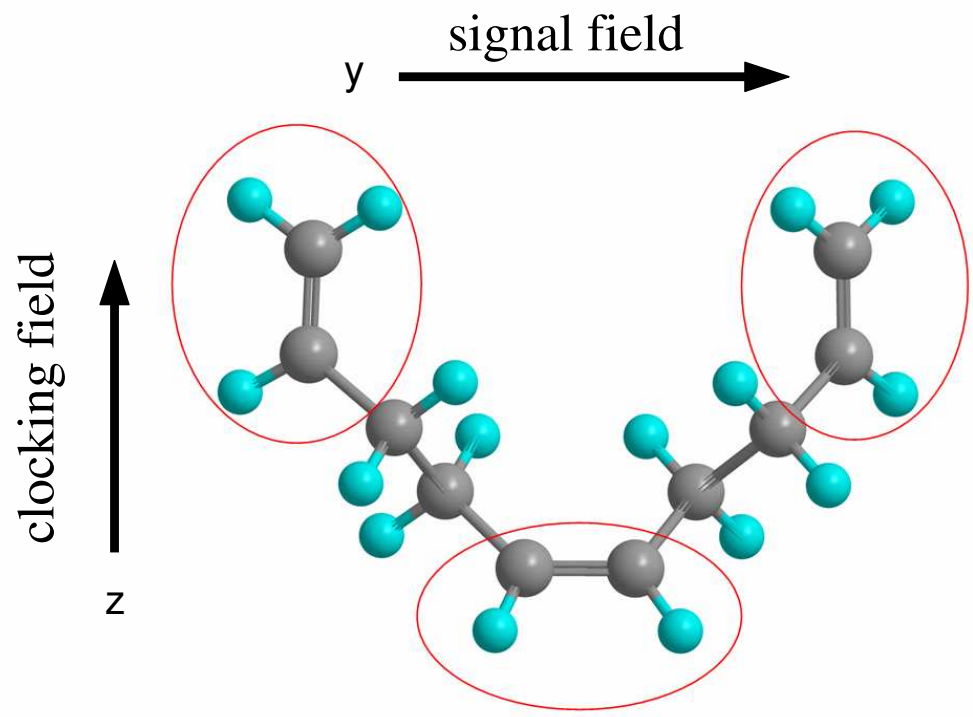

(a)

(b)

Figure 1.11. (a) A three-dot clocked half-cell composed of only carbon and hydrogen. Ethelyne groups form the dots in this structure. The molecular cation has a mobile hole which can occupy one of the three dots. (b) Isopotential surfaces in three states “0”, “1”, and null.

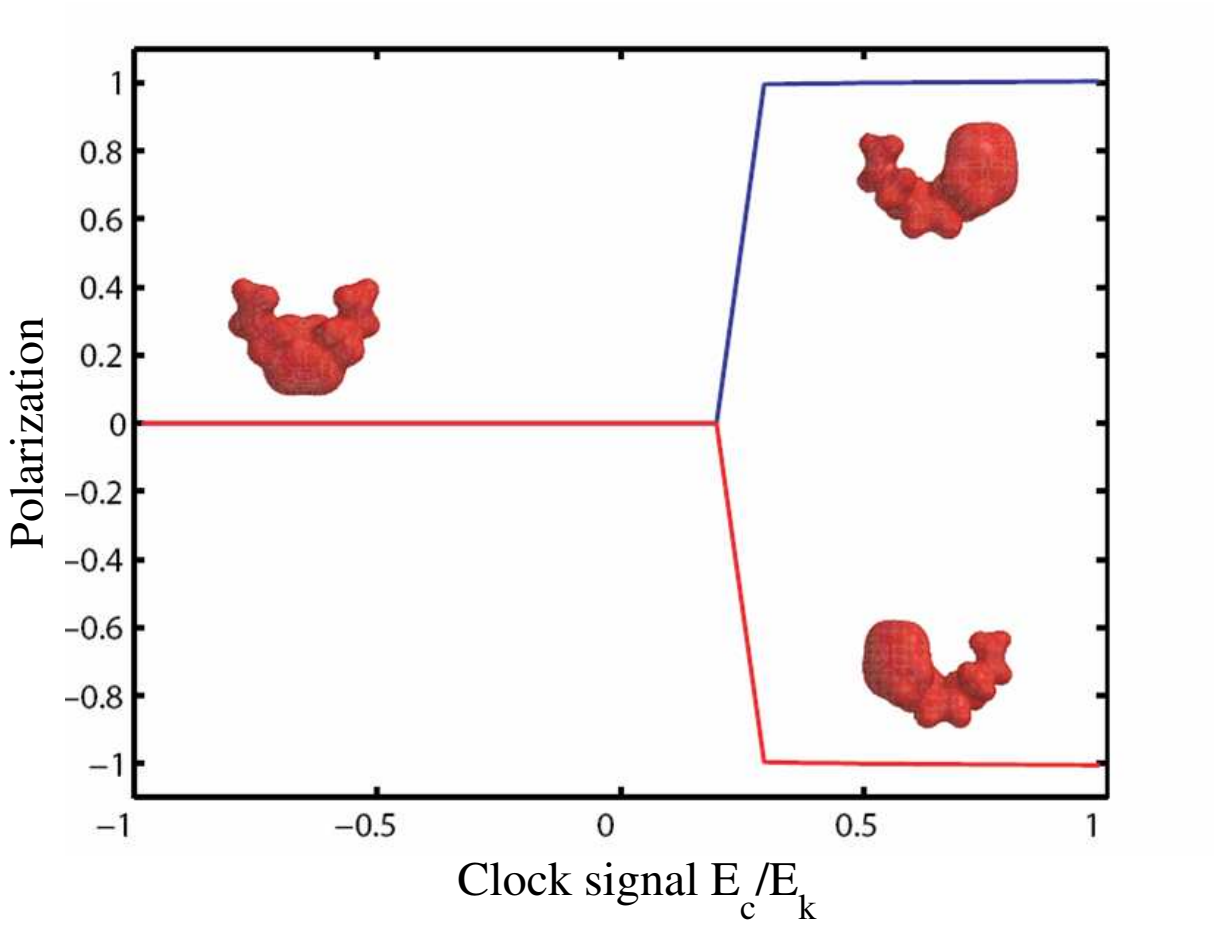

Figure 1.12. Calculated response for molecular QCA. The response of the molecule shown in Figure 1.11 to a clock signal in the presence of a signal field. The clocking field shifts the relative potential energies of the upper dots and the lower dots by an amount E_c. The horizontal axis is the ratio of this energy shift to the kink energy E_k which represents the interaction between two molecules. The cell polarization is the normalized molecular dipole moment. The two curves are for signal fields of opposite signs. The clock causes the molecule to move from the null state to the appropriate polarized cell.

are located above the two null dots in the middle. Buried underneath the surface is a conductor, which can create an electric field perpendicular to QCA plane when charged with signals. A positively charged conductor will attract electrons, pulling them to null dots. A negatively charged conductor will repel electrons, pushing

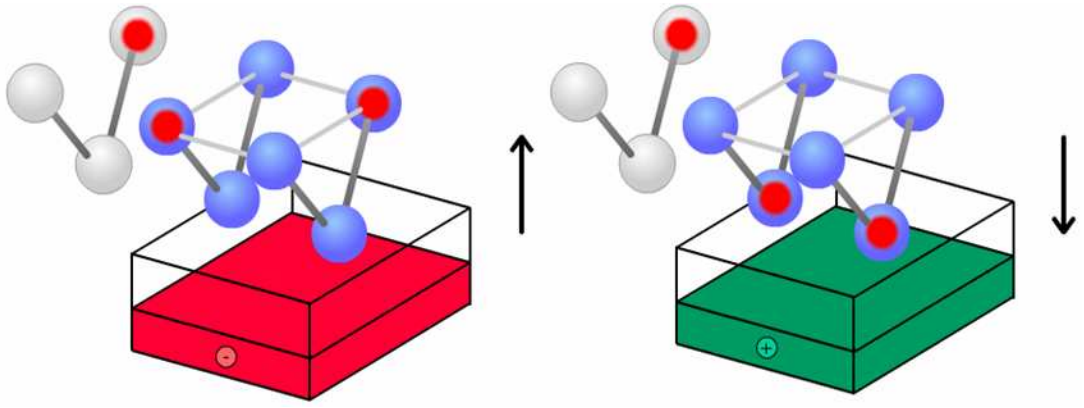

Figure 1.13. The implementation of a six dot molecular cell. A conductor is buried underneath the QCA surface, which can create an electric field perpendicular to QCA plane when charged with signals. The positively charged conductor generates an electric filed pointing downwards, pulling electrons to null dots. The negatively charged conductor creates an electric field pointing upwards, pushing electrons to active dots.

In an array of molecular QCA cells shown in Figure 1.14, each clocking wire is charged with a time-dependent multi-phase clock signal. The clocking wires form a patterned time-varying inhomogeneous electric field across the QCA plane. Shifted sinusoidal clocking phases applied to successive wires results in a continuously varying distributed clock signal that smoothly sweeps information along the QCA array. The upward pointing electric field across the QCA plane activate cells and downward pointing electric field deactivate cells. The transition region between them is the switching domain, where the computation is actually done. Adjacent molecules see clocking signals that are only fractionally out-of-phase with one another. This makes the adiabatic transition smoother, but still directs the propagation down the circuit toward the output. The clocking wires can be 10 to 100 times larger than

molecular QCA cells and can be fabricated with electron beam lithography. The fabrication of multi-phased clocking circuitry is under investigation in Bernstein's group. Notice that there is no need to contact individual molecules, which avoids the interconnect problems in conventional CMOS technology.

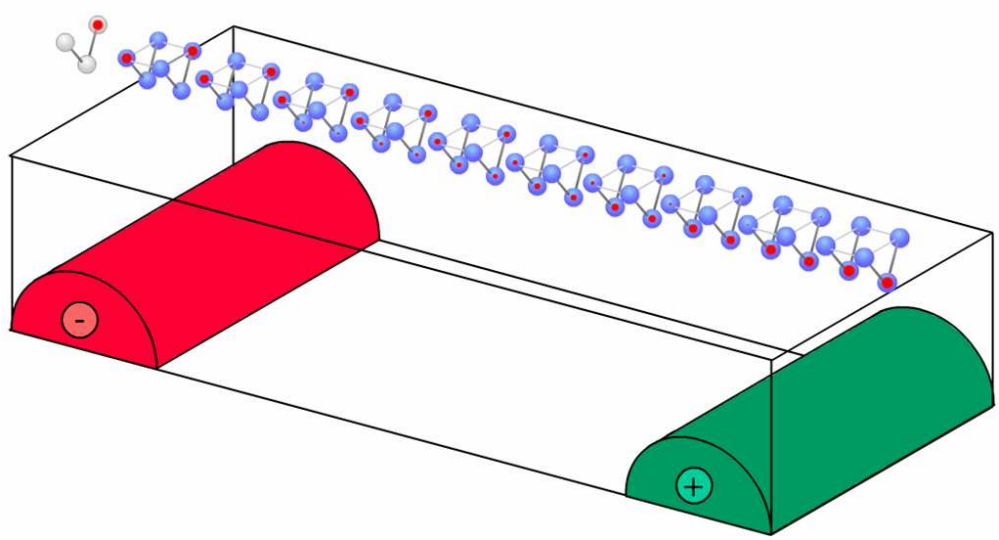

Figure 1.14. Clocking in a molecular QCA array. By driving adjacent wires with phase-shifted sinusoidal voltages, the active regions in the molecular layer shift smoothly across the surface.

1.4 Research overview

The computation paradigm known as QCA may provide transistor-less computation at the nanoscale. This revolutionary approach requires rethinking circuits and

architectures. Significant research in QCA has been done. Metal dot QCA devices operating at low temperatures have been successfully fabricated and the fabrication of molecular QCA devices are under way. Preliminary work on power gain and power dissipation in QCA shift registers has been conducted. Research on creating new architectures to match new computational paradigm has been done in [47-60]. This thesis will focus on the robustness and power dissipation in QCA system.

System robustness is critical because it ensures the reliability of a system in presence of defects and disorders which are unavoidable in a system especially in circuits at the molecular scale. A well functioned circuit should tolerate enough variations in the circuit parameters. For QCA circuits, a study of the robustness is essential for both theoretical and practical purposes. In this research, we provide a theoretical study on the robustness in both metallic QCA and molecular QCA implementations. Power dissipation is important because a high density chip will melt before it can function unless each device generates a very small amount of heat. In QCA system, clocking is employed to achieve adiabatic switching to reduce the power dissipation. Detailed research on this topic provides not only better understanding of the power dissipation in QCA circuits, but also suggests that there is no fundamental lower limit on the energy dissipation cost of information transportation. The power flow and dissipation in clocked molecular QCA circuits is examined in the thesis.

The thesis is organized as follows: Chapter 2 provides overview of the performance in metal-dot QCA circuits. Robustness in a semi-infinite metal-dot QCA shift register in terms of thermal effects, switching speed and capacitance variations is detailed. Chapter 3 elaborates the power dissipation in Landauer clocking and Bennett clocking for molecular QCA circuits. A coherence vector formalism with dissipation included is adopted to study thermodynamics in QCA systems.

The results of the two different clocking schemes are compared. The power flow in molecular QCA circuits in presence of information flow is studied in Chapter 4. The power flow in QCA fan-ins, fan-outs and majority gates is demonstrated. Chapter 5 concentrates on the robustness in molecular QCA circuits. The robustness in a semi-infinite single cell and three-cell wide shift register in view of manufacturing defects, displacement disorders and rotational disorders, is investigated. Concluding remarks are listed in Chapter 6.

CHAPTER 2

METAL DOT QCA CELL

2.1 Introduction

Functioning metal-dot QCA circuits working at low temperatures serve as prototypes for QCA. In this chapter, we explore a theoretical study of the robustness in metal-dot QCA circuits. In particular, we elaborate on the effect of speed, temperature and capacitance defects on the performance of a semi-infinite QCA shift register. A complete phase diagram of working parameter space as a function of temperature and speed, with defects included, shows that QCA is a robust system. The results of two simulation approaches—master equation and Monte-Carlo method are presented.

The chapter is organized as the following. In Section 2.2, the theory of single electron systems is reviewed. Section 2.3 describes the master equation and Monte-Carlo methods. Section 2.4 introduces power gain in QCA circuits. Section 2.5 displays the operation of a semi-infinite QCA shift register. The robustness in the semi-infinite QCA shift register is elaborated in Section 2.6.

2.2 Single electron system theory

Metal-dot QCA can be understood within the so-called "orthodox theory" of Coulomb blockade [78]. The circuit is described by charge configuration states, which are determined by the number of electrons on each of the metal islands.

Islands are metal grains surrounded by thin layers of insulators where electrons can be localized. Metal *islands* are coupled to the environment through tunnel junctions and capacitors. *Leads* are metal electrodes whose voltages are fixed by external sources. The schematic of islands and leads is shown in Figure 2.1. We define dot charges as the charge on the islands and lead charges as the charge on the electrodes. The free energy of charge configuration is the electrostatic energy of the capacitors and junctions minus the work done by the leads [75]:

$$F = \frac{1}{2}\begin{pmatrix} q \\ q' \end{pmatrix}^T C^{-1} \begin{pmatrix} q \\ q' \end{pmatrix} - v^T q' \tag{2.1}$$

where C is the capacitor matrix including all the junctions and capacitors, v is the column vector of lead voltages, and q and q' are the column vectors of dot charges and lead charges.

At zero temperature, the number of electrons on each island is an integer. The equilibrium charge configuration is the one that has the minimum free energy. A tunneling event happens only when the free energy decreases. At finite temperatures, the number of charges is no longer an integer but rather a thermal average of the charges over all possible configurations. Even if the free energy increases, there is still a certain probability that a tunneling event might happen. The transition rate of tunneling between two charge configuration states derived from first order perturbation theory is given by [75]

$$\Gamma_{ij} = \frac{1}{e^2 R_T} \frac{\Delta F_{ij}}{1 - e^{-\Delta F_{ij}/(k_B T)}} \tag{2.2}$$

where R_T is the tunneling resistance, ΔF_{ij} is the energy difference between the initial state i and final state j, k_B is Boltzmann constant and T is the temperature. The second order cotunneling is neglected as cotunneling can be suppressed in QCA system.

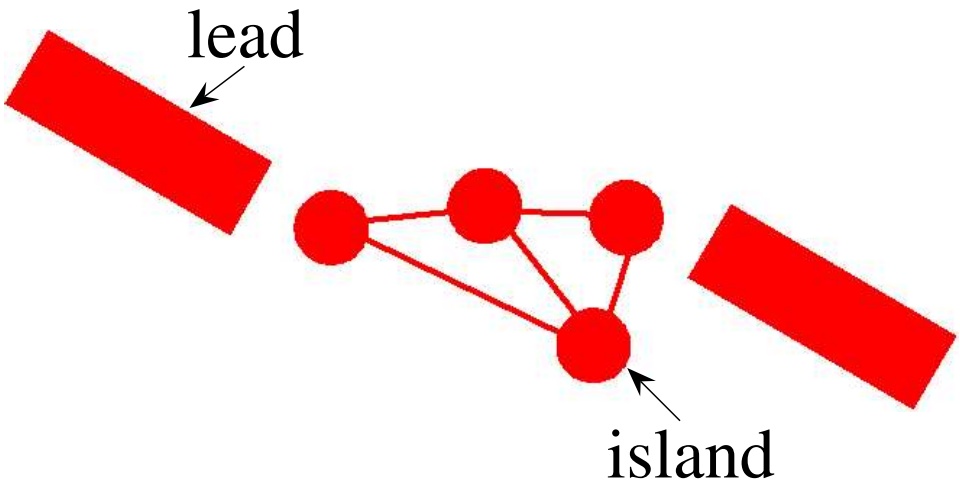

Figure 2.1. The schematic of a model with islands and leads. The four red dots are islands which are coupled to the environment through tunnel junctions and capacitors. The red line between the four dots can be tunnel junctions or capacitors. The two red square represent leads which are metal electrodes whose voltage are fixed by external sources. Leads are coupled to islands through capacitors.

For this single electron-tunneling phenomenon to occur, two prerequisites need to be satisfied. Firstly, the system must have metallic islands that are connected to other metallic regions through tunnel barriers with a tunnelling resistance R_T much greater than the resistance quantum $h/e^2 \simeq 26k\Omega$ to ensure that the electrons are localized on islands. Secondly, the charging energy $(e^2/2C)$ of the tunnel junction must be much greater than the thermal energy k_BT so that thermal fluctuation can be suppressed. Those two conditions ensure that the transport of charge from island to island is dominated by Coulomb charging energy.

2.3 Simulation methods

A tunneling event is an instantaneous and stochastic process; each successive tunneling event is uncorrelated and constitute a Poisson process. The tunneling events of many electrons can be described by a master equation, a conservation law for the temporal change of the probability distribution function of a physical quantity [75].

$$\frac{dP}{dt} = \Gamma P \tag{2.3}$$

P is the vector of state probabilities of charge configurations and is the ensemble average of the charge in the islands. Γ is a time dependent transition matrix, where the non-diagonal element is the transpose of $\Gamma_{i,j}$ and the diagonal element is $-\sum_{j \neq i} \Gamma_{i,j}$. In the master equation method, (2.3) is solved directly, which requires explicitly tracking all the possible states of the system. The drawback of this method is that it becomes impractical when the number of the states involved is too large. However because QCA operates so near the ground state, only a few states need to be considered, so a master equation approach is tractable.

The Monte-Carlo method, on the other hand, is based on a stochastic simulation of single electron tunneling events. The probability for a tunnel event out of state 0 happens at τ and not earlier in a Poisson distribution is given by

$$P_0(\tau) = e^{-\Gamma\tau} \tag{2.4}$$

where Γ is the tunnelling rate from (2.2).

To construct random numbers which are distributed in (2.4), one can take the inverse of (2.4)

$$\tau = -\frac{\ln(r)}{\Gamma} \tag{2.5}$$

where r is an evenly distributed random number in the interval $[0, 1]$. A good random number generator is needed in this method. One major disadvantage of this method is that it has problems with rare events, which results in very long simulation time. The application software SIMON [76] that uses Monte-Carlo method is widely used in single electron system simulations.

In this work, we focus on the master equation method. The results reported below are from master equation. Monte-Carlo simulation results, from the software package SIMON, are compared to master equation solutions.

2.4 Power gain in metal-dot QCA

A robust circuit has to be able to exhibit power gain in order to restore weakened signals due to unavoidable dissipative processes at each stage of information transportation. In conventional CMOS, the power supply provides the energy for signal and power gain. In QCA system, however, the energy needed for power gain is offered by the clock. A weak input is augmented to restore logic levels by the energy provided by the clock. Power gain has been studied theoretically in molecular QCA circuits [13] and measured experimentally in metal-dot QCA circuits [29]. Experimental results have shown a power gain greater than 3 in a metal-dot QCA shift register. In QCA circuits, power gain is defined by the ratio of the work done by the cell on its neighbor to the right (the output of the cell), to the work done on the cell by its neighbor to the left (the input to the cell). The work done on a cell by a voltage (V), applied through a capacitor (C) over a time interval $[0, T]$ is given by:

$$W = \int_0^T V(t) \frac{d}{dt} Q_c(t) dt \tag{2.6}$$

where $V(t)$ is the lead voltage, $Q_c(t)$ is the charge on the capacitor which couples the lead to the island and T is the clock period. In the time range of one clock

period, the cell goes back to its initial state which eliminates the possibility of the gain obtained by the energy temporarily stored in it. The power gain is thus the ratio of output to input signal power W_{out}/W_{in}.

2.5 Performance of QCA shift register

The schematic of a clocked half QCA cell is shown in Figure 2.2. The capacitances are taken to be $C_j = 1.6aF$, $C_g = 0.32aF$, $C_c = 0.8aF$, and the tunnelling resistance $R_T = 100k\Omega$. The circuit is charge neutral. Input is applied to the top and bottom dot through coupling capacitors. The clock is applied to the middle dot through a gate capacitor C_g. The differential potential between the top and bottom dot is the output V_{cell}.

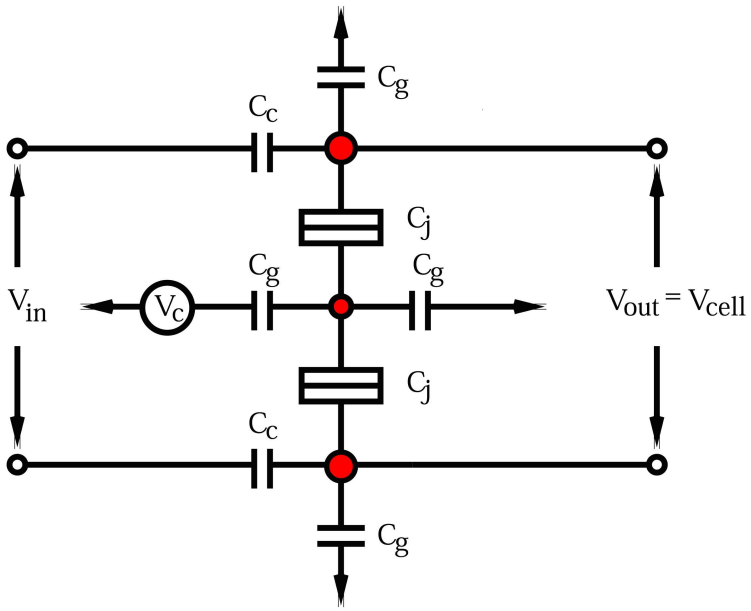

Figure 2.2. Schematic of a clocked triple dot. The input is applied to the top and bottom dot. The clock is set to the middle dot. The output defined as V_{cell} is the differential potential between the top and the bottom dot. $C_j = 1.6aF$, $C_g = 0.32aF$, $C_c = 0.8aF$. The capacitance to ground is 0.32 aF, and $R_T = 100k\Omega$.

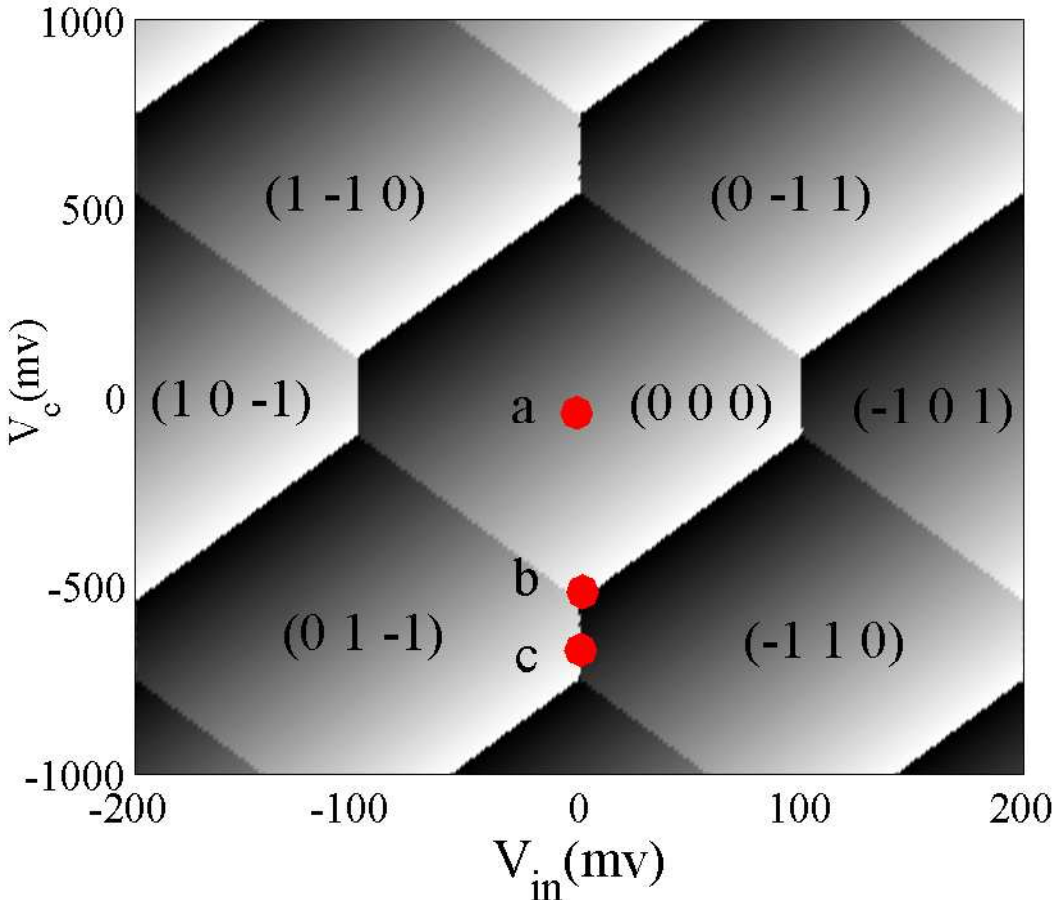

Figure 2.3. The equilibrium state configuration of a triple dot cell described in Fig.2.2. (n1, n2, n3) are the number of charges in the top, middle and bottom dot respectively. The cell is in the null state in point a. The cell is in the active state in point b. The cell is in locked state in point c.

A phase diagram of the equilibrium state configuration in Figure 2.2 is plotted in Figure 2.3 to illustrate the operating mode in clocked QCA system. The diagram is a gray scale map of the differential potential between top dot and bottom dot as a function of input and clock potential. (n1, n2, n3) is the number of charges in the top, middle and bottom dot respectively. A positive number indicates a

hole and negative number represents an electron. Each honeycomb cell represents a configuration state that has the lowest free energy. The brightest shade corresponds to the most positive value and darkest shade indicates the most negative value. The colors in between are intermediate values. A small input bias is applied, when the clock is high (less negative, correspond to point a), no electron switching event happens and the cell is in a null state, holding no information. When the clock is low (more negative, correspond to point b) an electron is switched to either top dot or bottom dot, determined by the input; the cell is then in the active state. If the clock is held very negative (point c), the electron is locked in the active state, since the energy barrier in the middle dot is too high to overcome. The locked cell is essentially a single bit memory; its present state depends on its state in the recent past, not on the state of neighbors. Varying the clock potential gradually between point a and c will switch the cell between null, active and locked state adiabatically. Notice that electrons can switch between the top and middle dot or the bottom and middle dot. Direct transition between top dot and bottom dot is suppressed.

A QCA shift register can be constructed with a line of capacitively coupled half QCA cells described in Figure 2.2, where the output in each cell acts as the input to its right neighbor. The schematic of the QCA shift register is shown in Figure 2.4. The transport of information from cell to cell is controlled by clock signals. Initially all of the cells are in the null state since the clocks are high even when input signal is applied. Then the clock for the first cell is lowered, the first cell switches to the opposite state of the input and holds that state even when input is removed. When the clock for the second cell is lowered, the second cell switches to the state opposite to the first cell and locks the bit. The information is thereby propagated along cell lines with clock signals. A cell always copies a bit from its left neighbor when the left neighbor is in the locked state and erases the bit when its right neighbor is in

the locked state. The copying of the bit can be accomplished gradually so that the right-most cell is always close to its instantaneously ground state and thus dissipates very small amount of energy.

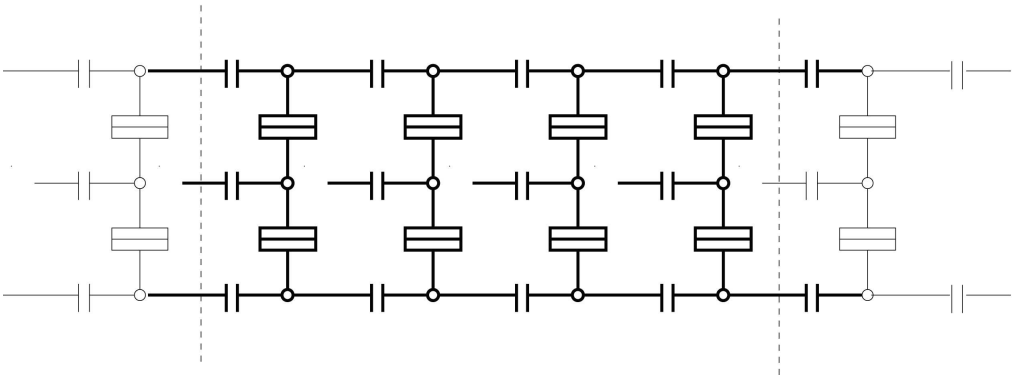

Figure 2.4. Schematic of a shift register composed of a line of identical triple dots in Fig. 2.2 The thick line described the actual four cells simulated.

It's instructive to build a semi-infinite shift register in order to study the robustness in the QCA circuit since each stage of the shift register can be replaced with more complex circuits. A semi-infinite shift register can be simulated with four half QCA cells. A four phase clocking scheme is adopted to achieve adiabatic switching, shown in Figure 2.5. Each clock signal is shifted a quarter period. At the end of the first clock period when the fourth cell switches to the locked state, the first cell is connected to the fourth cell so that the output of the fourth cell serves as the input of the first cell.

Figure 2.6 shows the calculated time evolution of the cell potential of the neighboring four cells in the shift register. The shaded area indicates the stream of stored bit information. Each cell has the opposite signal to the neighboring cells with one quarter period shifted; the information is inverted and shifted at each stage. The

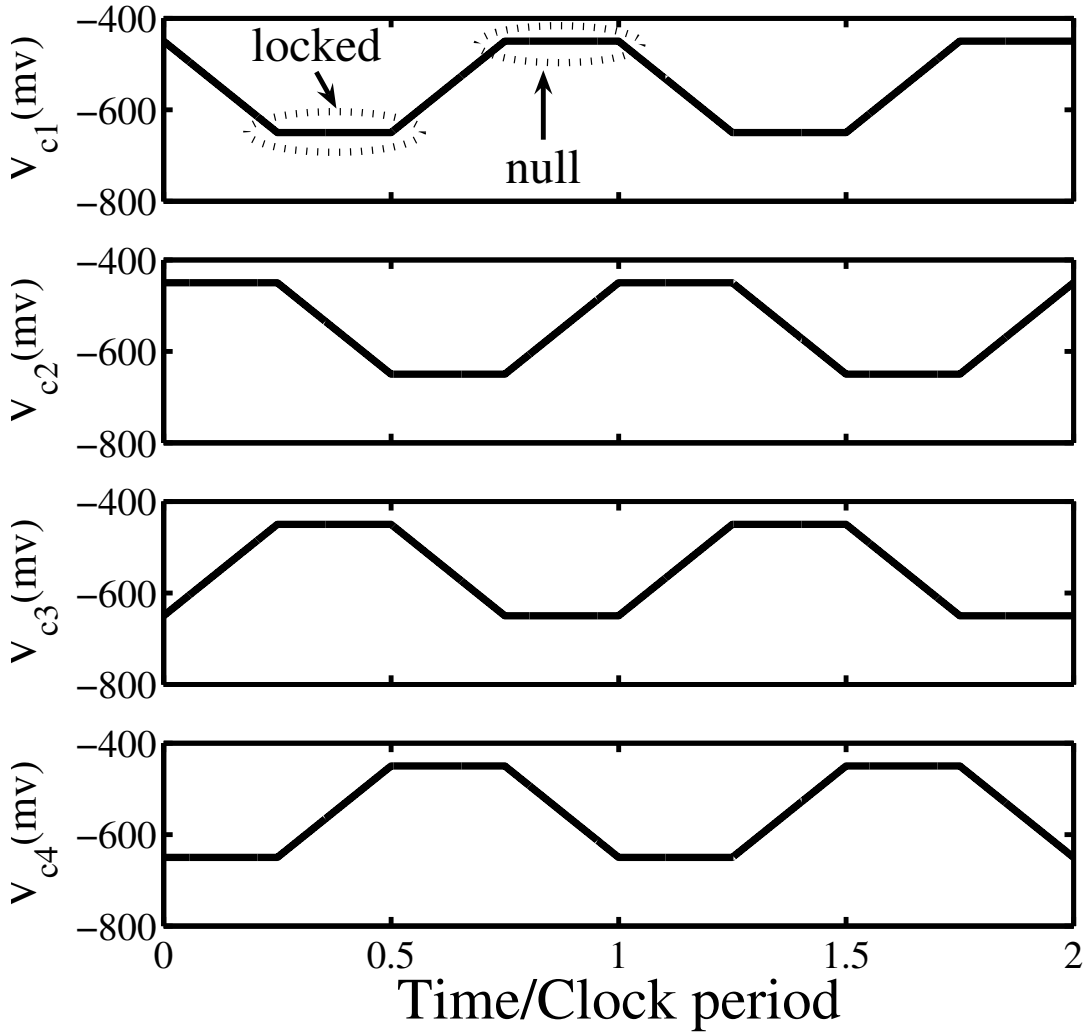

Figure 2.5. A four phase clocking scheme in metal-dot QCA.

arrow points to the direction of the information flow. At the end of the first quarter clock period, the first clock is set to low so that the first cell latches the input and locks it while the second cell is in the null state. By the time the second clock goes low, the first cell is still kept locked. The second cell thus copies the bit from the first cell. By the end of the third quarter period, the bit in the first cell is erased as its clock is set to high. The third cell copies the bit from the second cell and holds it.

The process goes on and the bit information is transported along the chain. Notice that there are always at least two copies of the bit at one time. When there are three copies of the bit, the cell potential (absolute value) in the middle cell decreases while cell potential in its left and right neighbor increase. This is because that the cell in the middle is coupled with both left and right neighbor, which will distribute its electrostatic dot potential to its neighboring cells. While there are two copies of the bit, the dot potential is distributed in only two cells.

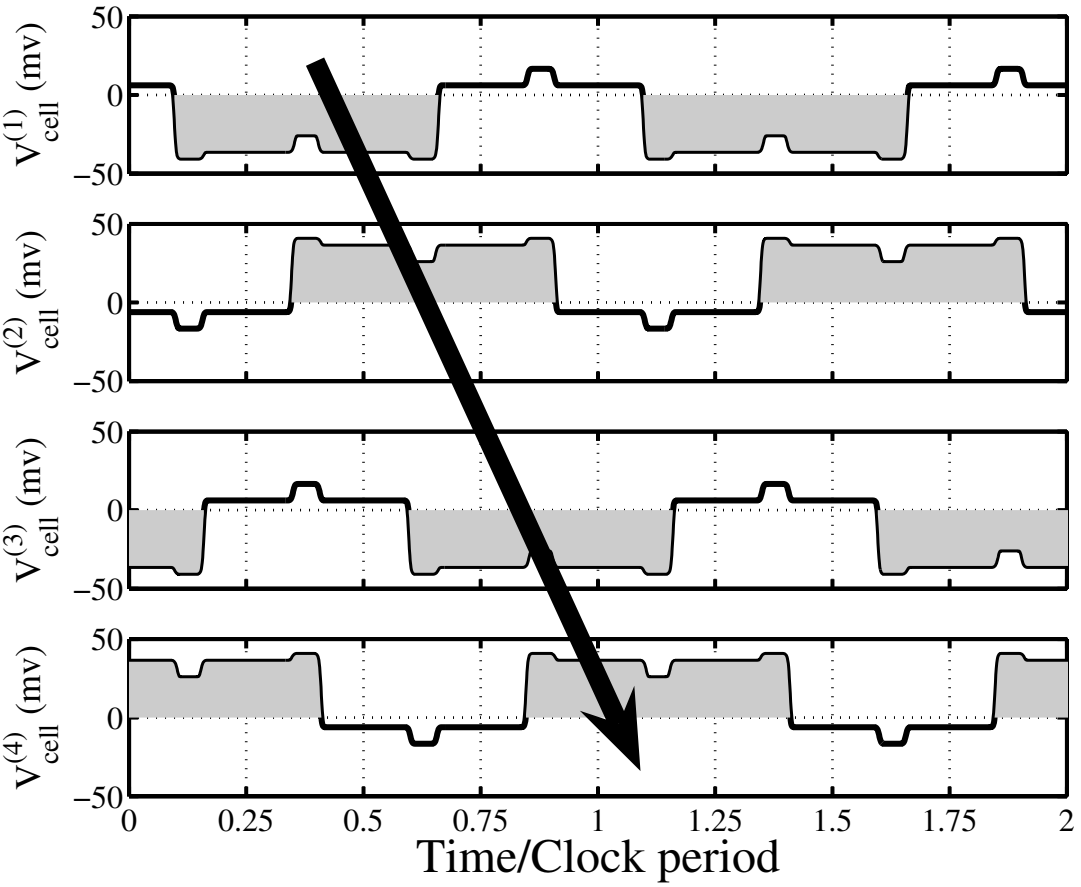

Figure 2.6. Time evolution of cell potential in the neighboring cells. $V^{(n)}_{cell}$ is the differential potential between the top and the bottom dot of the nth cell.

2.6 Robustness in metal-dot QCA shift register

The robustness in metal-dot QCA system is important because perturbations from the environment and manufacturing defects in devices are unavoidable. The performance of the metal-dot QCA circuit is subject to thermal fluctuation, random background charge fluctuation, non-adiabatic switching at high speeds and manufacturing defects in the circuits. Of course, the charging energy in the circuit must be much greater than the thermal energy for the circuit to be stable and reliable. Errors due to random background charges have been studied in [7]. A QCA binary wire is unaffected by stray charge at a distance greater than the cell-to-cell distance. The adiabatic switching of the QCA cells make sure the QCA circuit operate near ground state. The switching speed of the QCA circuit is limited by the electron tunneling rate across tunnel barriers. The capacitance variation due to fabrication imperfections is another factor which can cause errors in metal-dot QCA circuit. We focus here on the robustness of metal-dot QCA in view of the effect of temperature, clock speed, and capacitance variation.

2.6.1 Effect of clock speed and temperature

Because of the difficulty of fabricating very small capacitors, metal-dot QCA circuits can only operate at low temperatures. Thermal fluctuation is therefore a major source of causing errors in meta-dot QCA circuits. To understand the effect of temperature on performance of the semi-infinite shift register, we examine the cell potential as a function of cell number at different temperatures as shown in Figure 2.7. Below 5K, cell potential remains the same along the chain. The semi-infinite shift register is error-free since there is no degradation of information in a long range. Above 10 K, cell potential drops significantly along the chain. It will drop to zero with half of electrons in the right state and half in the wrong state at

the end of the chain. In this case, the circuit fails, as the information will be lost in a long run. It's noteworthy that at 8K, although the cell potential will drop to zero eventually in the chain, the circuit can still work up to the 90th cell.

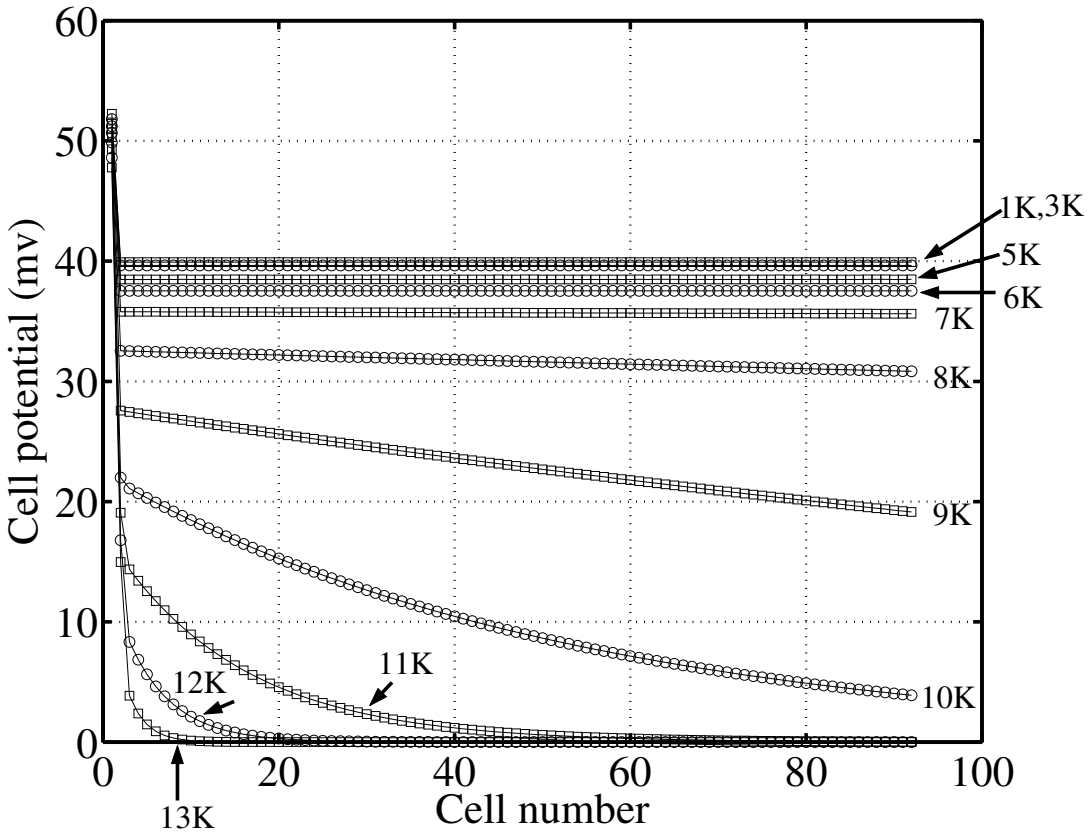

Figure 2.7. Cell potential as a function of cell number at different temperatures.

The degradation of performance with increasing temperature can be explained in terms of power gain. We calculate the power gain of each individual cell in the chain. Power gain remains the same along the chain, which implies that bit information decays at the same rate per propagation. Power gain is unity for each cell when the chain functions perfectly since all the cells are identical. Deviation from unity

power gain of an individual cell as a function of temperature is plotted in Figure 2.8. The power gain is unity for temperatures from 1 K to 5 K. The signal at each level is restored by the energy from the clock. When the temperature is above 5 K, power gain is less than unity. At this temperature, the flow of energy from the clock can no longer compensate for the energy loss to the thermal environment, with the result that the signal decays at each stage.

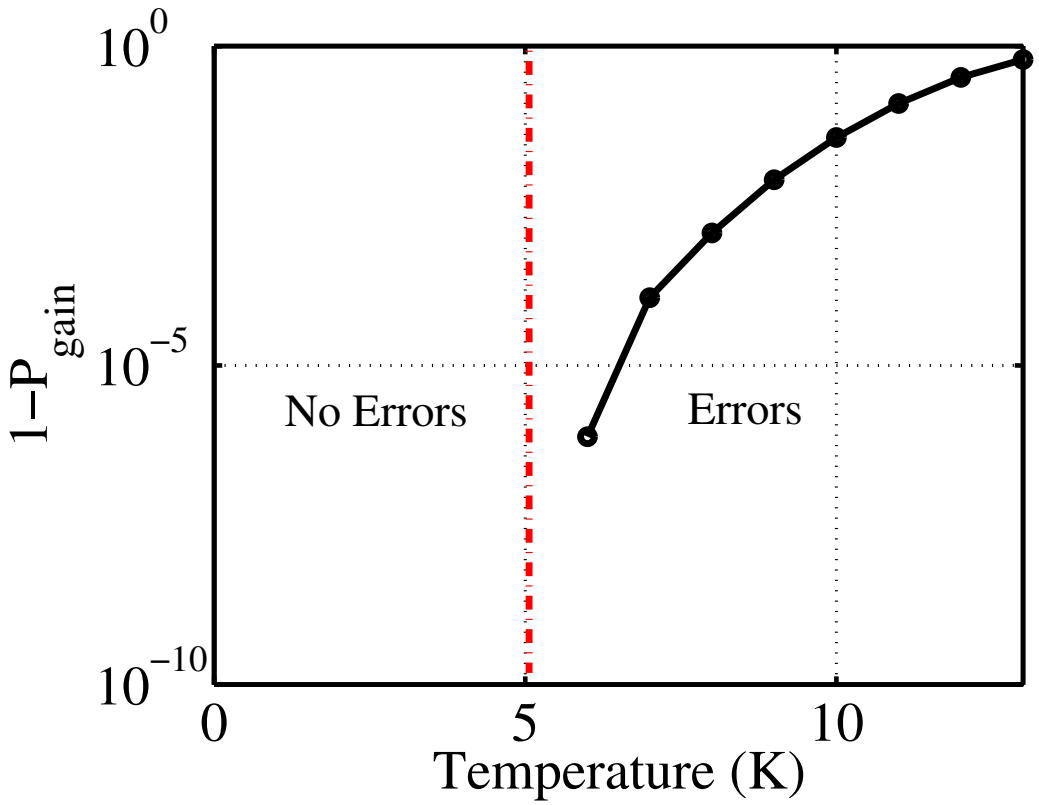

Figure 2.8. Deviation from unity power gain for an individual cell as a function of temperature.

A complete phase diagram of the operational space of the circuit as a function of clock speed and temperature with our standard parameters when C_j is 1.6 aF and with the scaled parameters when C_j is 0.16 aF is demonstrated in Figure 2.9 and Figure 2.10. All capacitances and voltages are scaled appropriately according

to C_j. The scaled parameter is provided to show the scalability of QCA circuits. The performance of the circuit increases greatly with scaling down capacitors with higher operating temperature and switching speed. The shaded area below the curve indicates speeds and temperatures for which the circuit is robust. The white area is where the bit information decays along the chain.

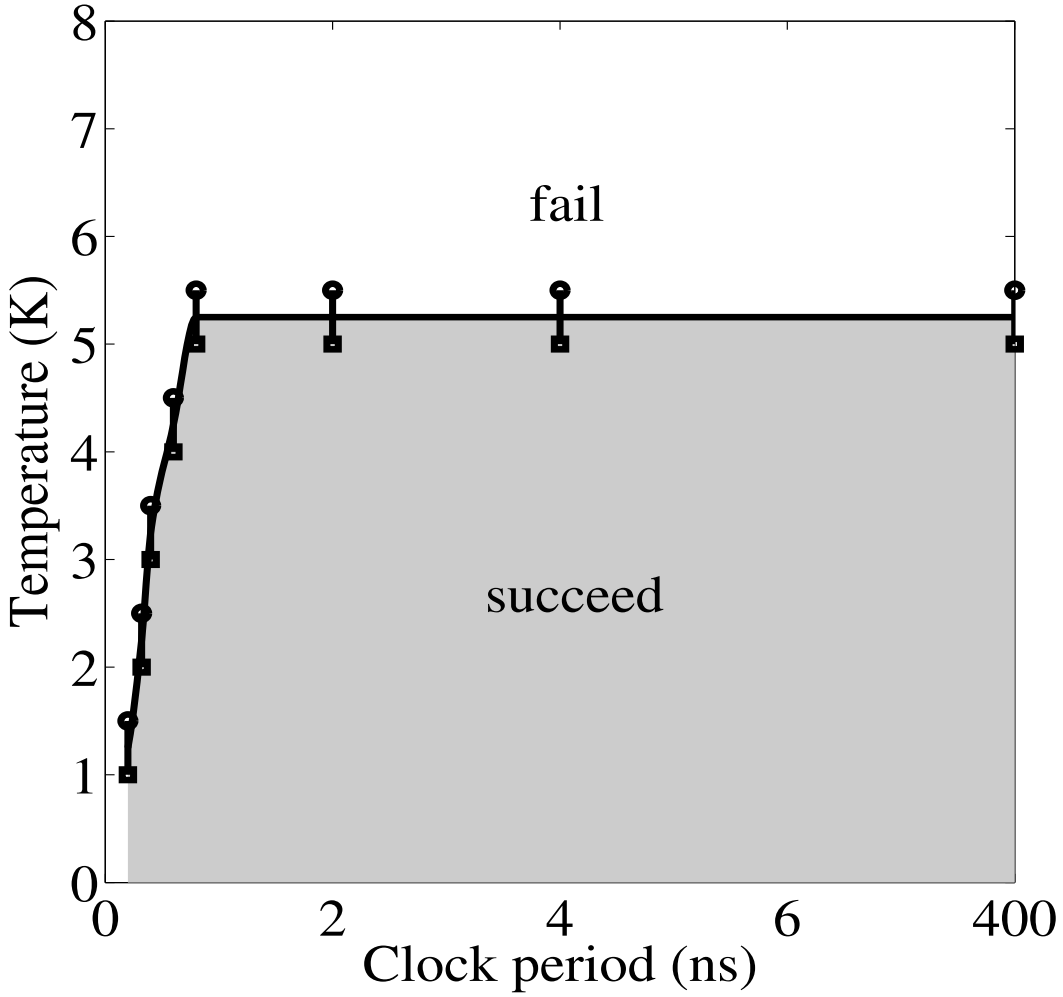

Figure 2.9. The phase diagram of the operation space as a function of temperature and clock period when $C_j = 1.6$ aF. The shaded area below the curve is where the circuit succeeds and the white area is where the circuit fails..

The two figures are identical, except that the clock speed in Figure 2.10 is 10

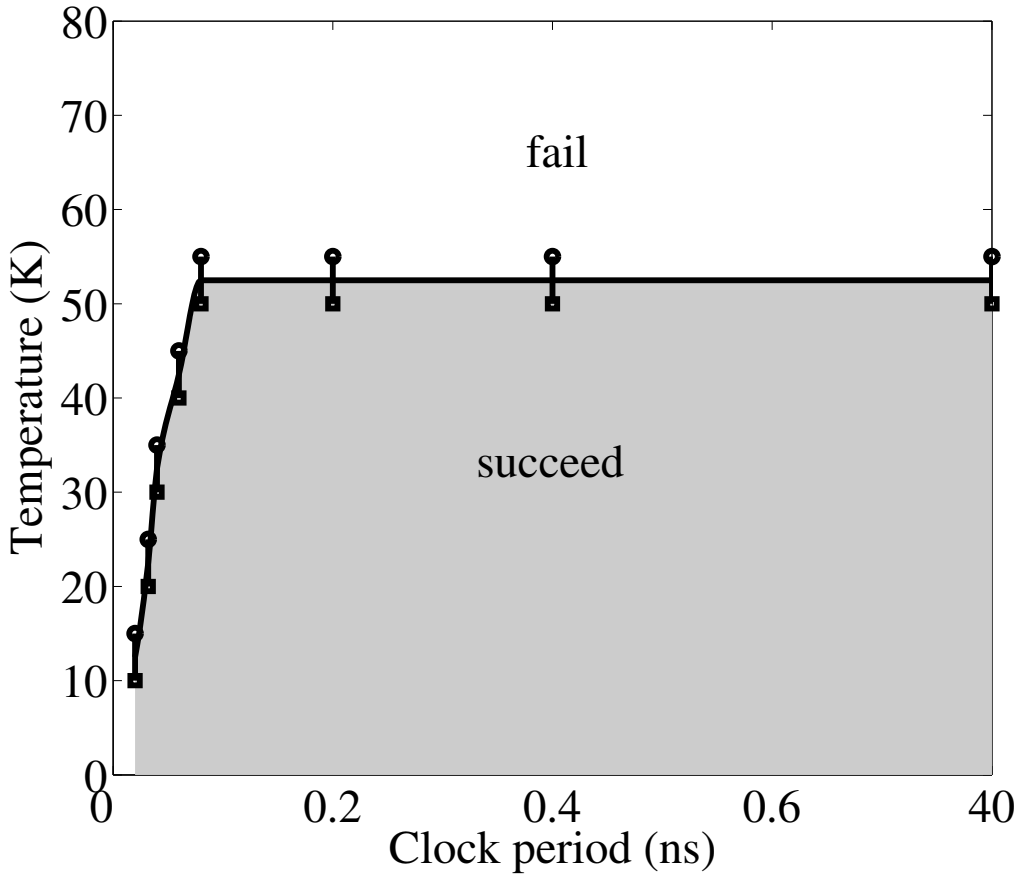

Figure 2.10. The phase diagram of the operation space as a function of temperature and clock period when $C_j = 0.16$ aF. The shaded area below the curve is where the circuit succeeds and the white area is where the circuit fails.

times of Figure 2.9 and the maximum operating temperature ten times higher in Figure 2.10. The maximum clock speed achieved in Figure 2.9 is 5 GHz. In Figure 2.9, when the clock period is less than the critical period of about 0.2 ns, the circuit fails even at zero temperature. This occurs when clock speed approaches the electron tunneling rate. When the clock speed is too fast, the electrons do not have enough time to tunnel reliably from one dot to another. There will be some electrons left in the wrong state. The error will accumulate as the information moves along the chain. Increasing the clock period will increase the probability of electrons being

in the right states, thus will increase the operating temperature. But the operating temperature remains the same when further increasing the clock period since the electrons have had enough time to be in the correct state.

The upper limit on operating temperature is limited by kink energy, the energy difference between the ground state and first excited state. The kink energy in our circuit is calculated as 65.8K. If we want the expectation value of electrons being in the wrong states (e^{-E_k/k_BT}) to be less than 10^{-6}, the kink energy should be about 13 times of k_BT, which gives us a maximum operating temperature of about 5K. The upper limit on operating speed is constrained to RC time constant. It is not exactly RC_j however, since the circuit effect and adiabatic switching have to be considered.

It's worthwhile to simulate the same circuit with Monte-Carlo method as a comparison. We construct the same circuit in SIMON, run the simulation over 200 times and measure how often it ends up in the wrong states. The error rate is defined as the percentage of the wrong states over many runs. Figure 2.11 shows the transient time evolution of top and bottom dot charge in the four neighboring cells at 8K when an error occurs. In the first clock period, the bit information is correctly carried on through the four neighboring cells. In the second clock period, the third cell copies the wrong bit from the second cell, which causes the second cell flips to the wrong state during holding stage when the bit of the first cell is erased.

The phase diagram of the operating space as a function of temperature and clock period when C_j is 1.6aF is displayed in Figure 2.12. A maximum operating speed of 2.5GHz and temperature of 7K is obtained, which is close to the master equation result.

We plot the error rate of Monte Carlo simulation and master equation as a function of temperature at the 50th cell in Figure 2.13. When the temperature is

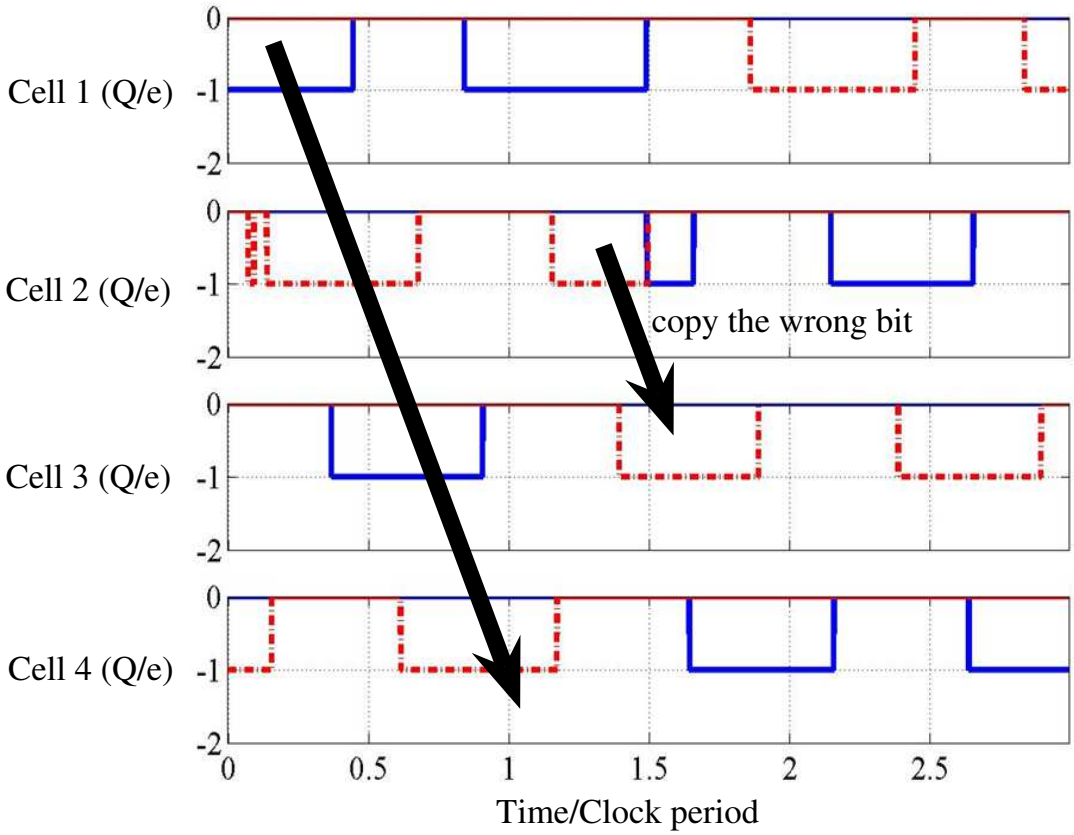

Figure 2.11. Time evolution of dot charge in the four neighboring cells of shift register at 8K when an error happens with Monte-Carlo simulation. The blue solid line represents the top dot and the red dashed line represents the bottom dot. In the first clock period, the bit information is correctly carried on through the four neighboring cells. In the second clock period, the third cell copies the wrong bit from the second cell, which causes the second cell flips to the wrong state during holding stage when the bit at the first cell is erased.

as high as 11K, the error rate in both methods is 50%, indicating that information is no longer distinguishable due to thermal fluctuations. It's noticeable that the Monte-Carlo method has trouble calculating the error rate less than 1% because of the inherent problem Monte-Carlo has dealing with rare events.

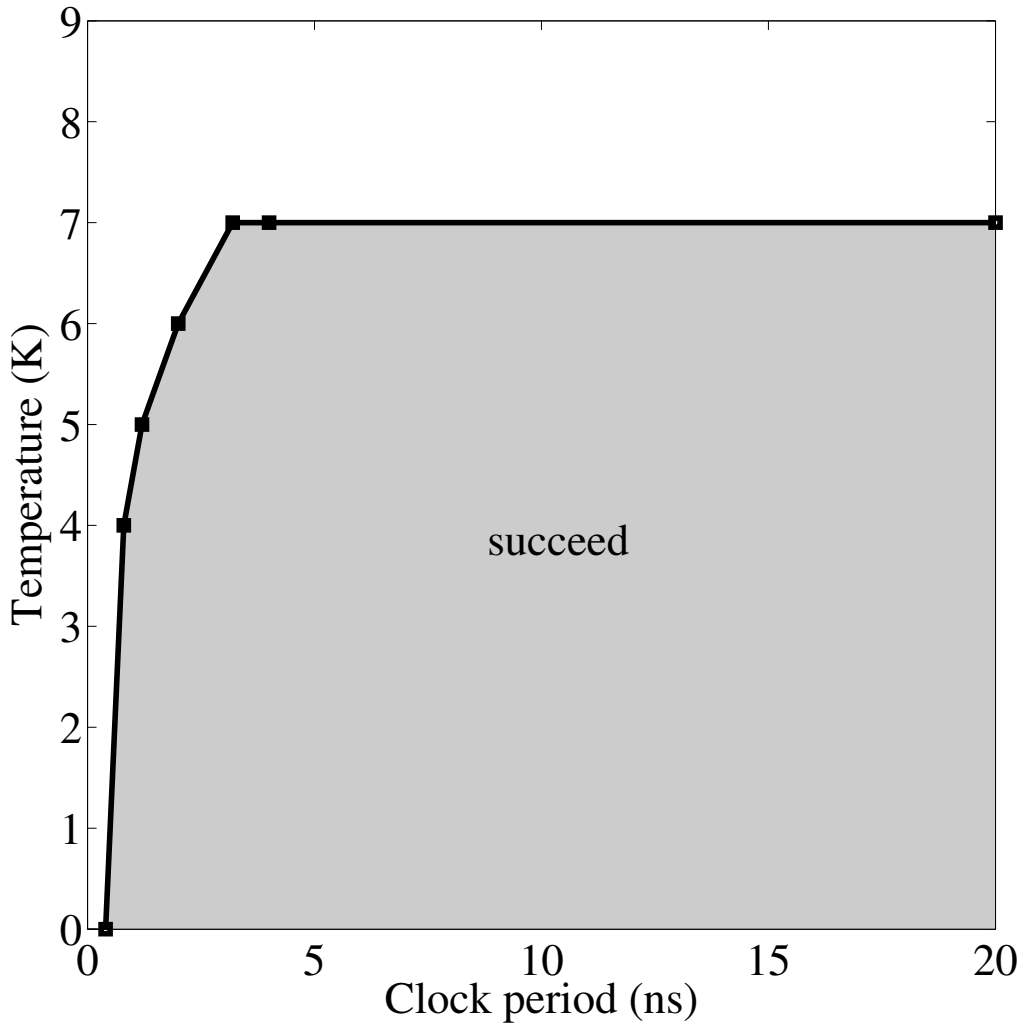

Figure 2.12. The phase diagram of the operation space as a function of temperature and clock period when C_j is 1.6aF with Monte-Carlo simulation.

2.6.2 Defect tolerance in semi-infinite QCA shift register

From the manufacturing point of view, a capacitor might deviate from its standard value because of variation in fabrication procedures. A robust circuit needs to display tolerance on manufacturing defects. Here we provide a theoretical study in the capacitor tolerance in the semi-infinite QCA shift register. Each capacitance is varied randomly within a certain percentage (both positive and negative) from

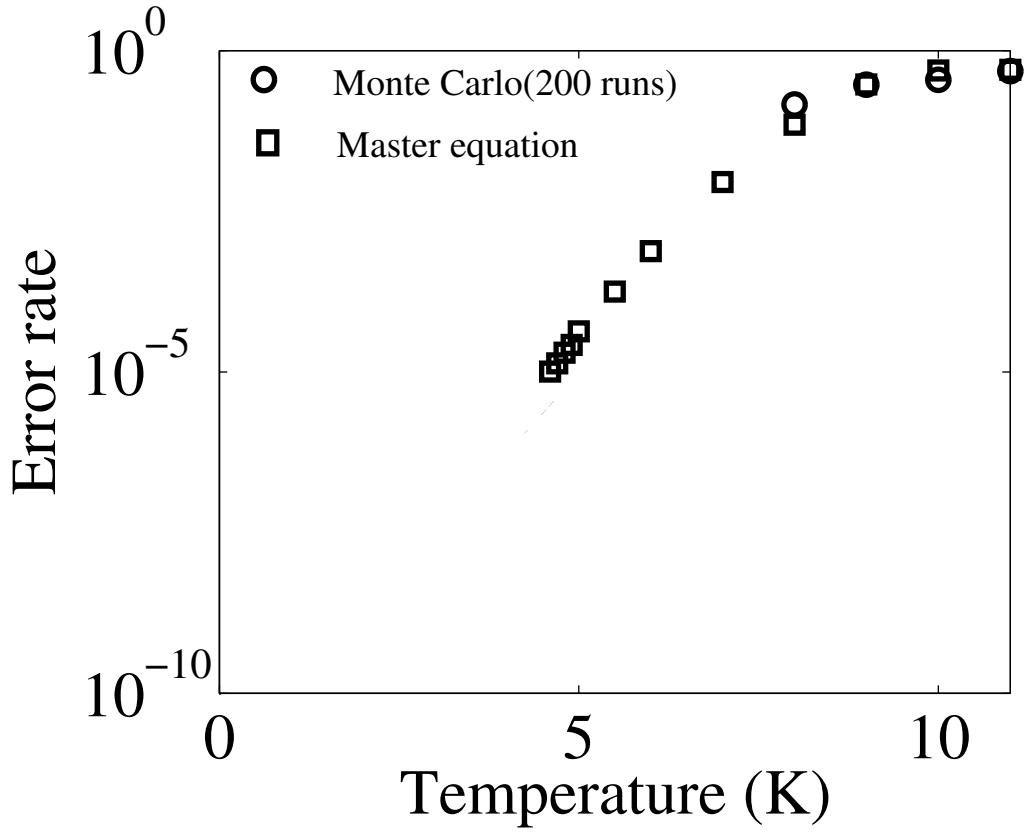

Figure 2.13. The comparison of error rate at 50th cell with master equation and Monte Carlo simulation in QCA shift register. The circle marker represents a Monte-Carlo simulation result and the square marker represents a master equation simulation.

its standard parameter. The circuit is reliable if the perturbation of the capacitances does not influence the performance of the circuit. We pick up a working point in Figure 2.9 where clock period is 5ns, temperature is 4K and vary all the capacitances randomly by $\pm 10\%$ and $\pm 15\%$ to their original values. Figure 2.14 and Figure 2.15 show the cell potential as a function of cell number with random capacitance variation. Each color represents a separate simulation result of random capacitance variation within the certain percentage range. When the variation is $\pm 10\%$ in Figure 2.14, despite of small deviations on the cell potential along the chain

of 2000 cells, it's remarkable that all the cells are in the "1" state (cell potential around $40mv$) and none of the cells flip to the wrong state. This result indicates that there is no degradation in the signal propagation in the shift register and the circuit is error-free. When the variation increases to ±15% in Figure 2.15, the deviations of the cell potential along the chain become large and many cells are flipped to the wrong bit "0" (cell potential negative value). The circuit is no longer reliable since errors occur during the information propagation. This calculation shows that metal-dot QCA circuit can successfully function without an error within ±10% of capacitance variation.

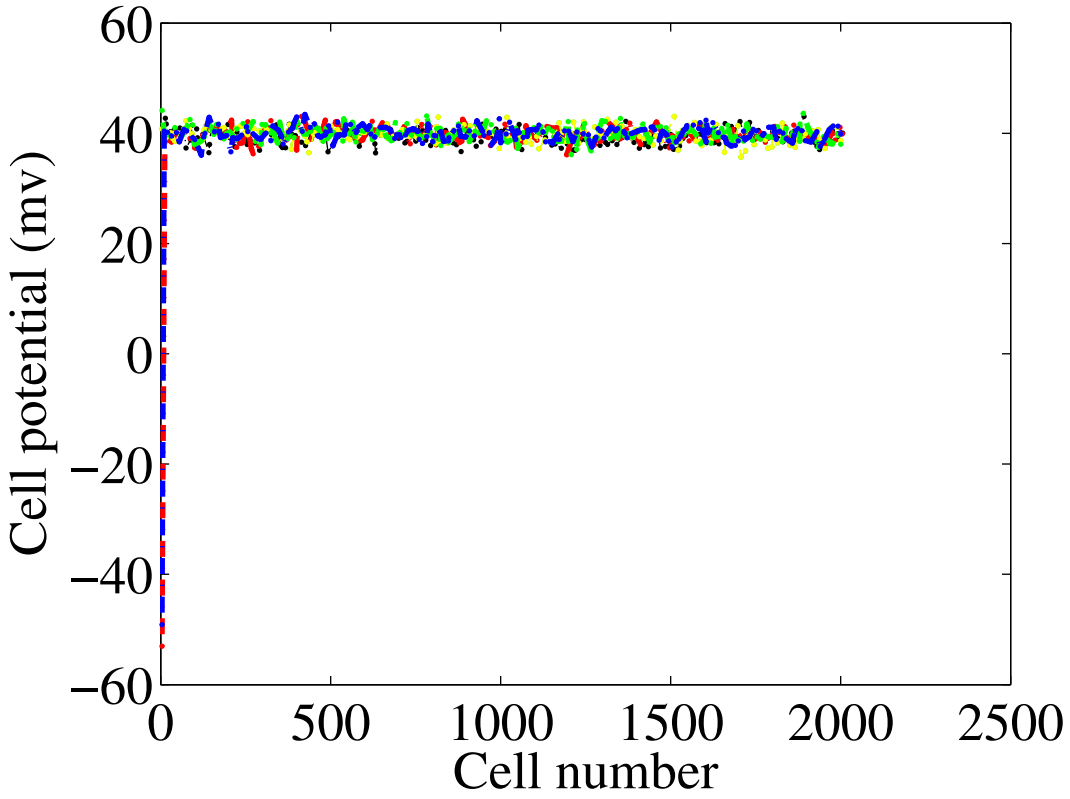

Figure 2.14. Cell potential as a function of cell number at 4K when capacitance variation is ±10%.

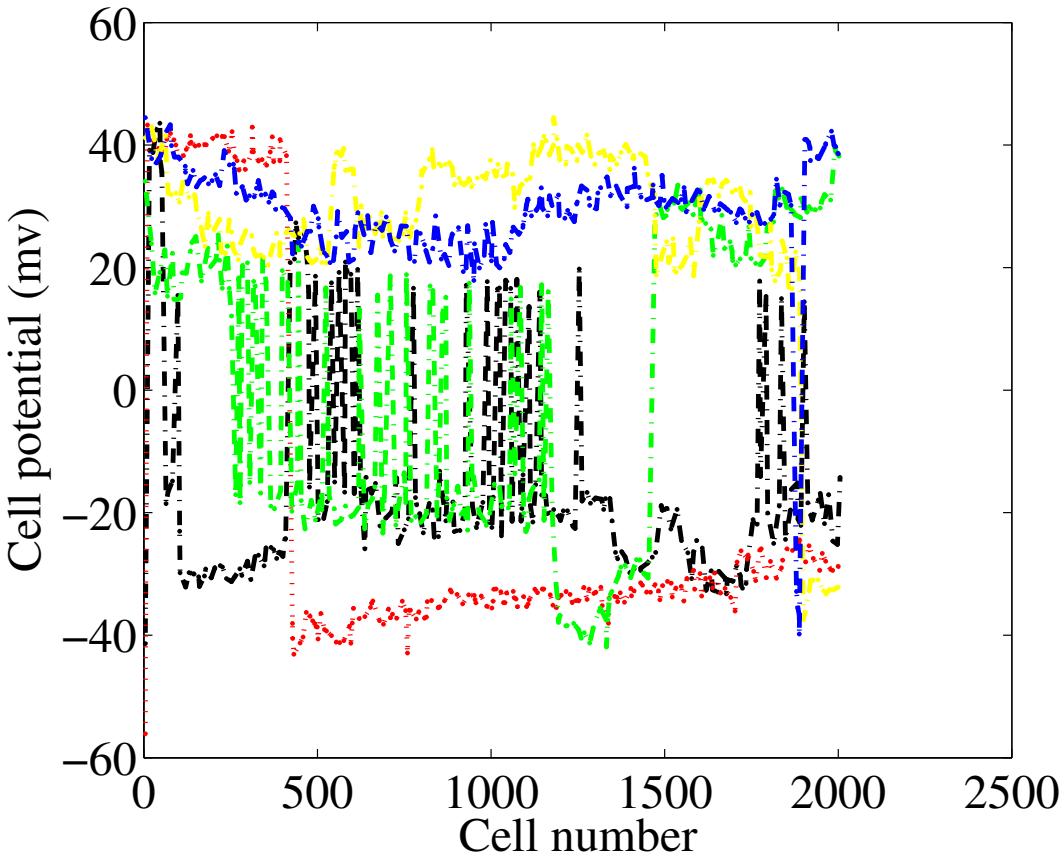

Figure 2.15. Cell potential as a function of cell number at 4K when capacitance variation is ±15%.

2.7 Conclusion

This chapter is focused on metal-dot QCA system. Although limited by low temperature operation, metal-dot QCA provides useful demonstrations of QCA circuits. We explore a theoretical study of the robustness in a semi-infinite metal-dot QCA shift register. A complete phase diagram of the operational region in the QCA shift register as a function of temperature and speed and the defect tolerance on the capacitance are obtained from master equation calculations. These results provide evidences of a robust metal-dot QCA system.

CHAPTER 3

LANDAUER CLOCKING AND BENNETT CLOCKING IN MOLECULAR QCA CIRCUITS

3.1 Introduction of energy dissipation for computation

As device feature sizes decrease steadily with the shrinking of semiconductor transistor technology, power dissipation has become clearly identified as a key limiter of continued CMOS scaling. Fundamental questions of heat dissipation and device operation rose naturally. Just how small can a computational device be? How much heat must it generate to compute a bit? The fundamental structural limit of scaling is single-molecule devices, since it appears impossible to structure matter at a smaller length scale. The connection, at first counter-intuitive, between information computation and heat has its roots in the very beginnings of statistical mechanics, discussions of Maxwell's demon, and the Second Law of Thermodynamics. The history of the question has been ably reviewed by others [60, 61, 62] and a brief summary will suffice here.

Szilard and Brillouin, argued that the measurement associated with the READ operation causes an energy dissipation of $k_B T ln(2)$ per bit [63, 64]. Landauer refuted this notion, showing that there is no necessary minimum energy dissipation associated with reading a bit, but rather with erasing information [65, 66]. He argued that logically reversible functions, in which no information is lost, could be performed with as little dissipation of heat as desired, though at the cost of speed.

The ERASE operation, or any logically irreversible function, by contrast, must dissipate at least $k_B T ln(2)$ per bit, independent of the operation speed. If a copy of the bit that is to be erased is kept, the operation can dissipate an arbitrary small amount of energy.

By "energy dissipation" we mean the transfer of energy from the system to the environment. This is irreversible because of the thermodynamically large number of degrees of freedom of the environment. Energy dissipation is not the same as energy transfer from one part of a circuit to another. Confusion often results from imprecise language, e.g. "the amount of energy it takes to compute a bit," which fails to distinguish device-to-device energy transfer from energy dissipation (the distinction is observed, for example in [67]).

Bennett extended the Landauer result by showing that in principle any computation could be embedded in a logically reversible operation [68]. The simplest version of this is simply to echo a copy of the inputs to the output. One can accumulate the intermediate results, information that would normally thrown away, and then erase these results by reversing the functions that created them. By using the inverse operations of the forward computation process, the system could be returned to its original state. Unless the original inputs to the calculation are stored, unavoidable dissipation occurs when they are erased. The minimum of $k_B T ln(2)$ can be understood from a simple statistical mechanical consideration. Let W be the number of physical configurations the system can be in. If initially the bit system can be in a 1 or 0 state, then $W = 2$. If the information is erased then for the final state $W = 1$. This 2-to-1 transition results in an entropy change for the system of

$$\Delta S \;=\; k_B \ln(1) - k_B \ln(2) \;=\; -k_B \ln(2).$$

Since the Second Law of Thermodynamics requires that the environment must increase in entropy by at least $k_B ln(2)$. This results in a free energy transfer to the

environment of $\Delta F = T\Delta S = k_B T \ln(2)$.

There remains a question of practicality. Is it a practical possibility to do computing in a reversible (or nearly reversible) way? Keyes, a coauthor with Landauer on some of the pioneering papers, assessed the situation in a 2001 article on the "Fundamental Limits of Silicon Technology [69]." The paper states that it seems likely that pressing transistors into service to implement reversible computing will prove finally not to be a practical approach because a costly layout is needed to keep all the intermediate results.

In contrast to transistors which function as current switches, QCA employs cells through which no current flows. Binary information is encoded in the charge configuration within a cell. A local electric field provides a clocking signal which controls the activity of the cell and can smoothly switch it from an information-bearing "active" state to a non-information-bearing "null" state. The QCA clocking scheme that has been developed relies on switching the cell to an active state adiabatically so that the cell is always operating very close to instantaneous ground state, applying the idea of Landauer [32, 36]. This approach reduces power dissipation, dissipating significant amounts only when information is erased [13, 14].

In this chapter, we study the energy dissipation in clocked molecular QCA circuits, especially in a QCA shift register where information is moved from cell to cell and a three input majority gate where information is processed. We explore the applications of the ideas of Bennett to switching QCA devices in the most power-efficient manner possible, keeping intermediate results in place so that power dissipation is reduced even further. The efficacy of Landauer-Bennett approach is made clear by directly solving the equations of motion for irreversible, reversible and Bennett-clocked gates. We show that QCA provides a natural implementation of Bennett switching which could offer both a practical realization of reversible

computing and one that could be scaled to the limit of single-molecule devices.

This chapter is organized as the following. In Section 3.2, the quantum theory of dissipative dynamics in a three state QCA system is presented. Landauer clocking and Bennett clocking in a QCA shift register and a three-input majority gate is studied in Section 3.3, and Section 3.4 shows the direct comparison for irreversible, reversible and Bennett clocked shift register and "OR" gate. Finally, we give the conclusion in Section 3.5.

3.2 Modeling QCA dynamics with dissipation

To examine the dissipation dynamics in QCA, the quantum system is coupled to the thermal bath. The quantum dynamics is modeled with coherence vector formalism where the dissipative coupling to the thermal bath is included through an energy relaxation time approximation [71]. The clocked QCA system can be simplified with a three-state approximation [79], where the three basic states are "0", "1" and null. The three basic vectors are $\varphi_- = |1\ 0\ 0\rangle$ which corresponds to "0"; $\varphi_+ = |0\ 1\ 0\rangle$ corresponding to "1" and $\varphi_0 = |0\ 0\ 1\rangle$ corresponding to "null". A Hamiltonian is constructed that includes the effect of the clocking field which shifts the energies of the active states relative to the null state, neighboring cell interaction which shifts the relative energies of the "0" and "1" states and the tunnelling between the states. The three-state Hamiltonian for the jth cell of a QCA array is given by

$$\hat{H}_j = \begin{bmatrix} -\frac{E_k}{2}\sum_{m\neq j} f_{j,m}P_m, & 0, & -\gamma \\ 0, & \frac{E_k}{2}\sum_{m\neq j} f_{j,m}P_m, & -\gamma \\ -\gamma, & -\gamma, & E_c \end{bmatrix} \tag{3.1}$$

where γ is tunneling energy between one of the two polarized states ($P = 1$, $P = -1$) and the null state ($P = 0$). This can be obtained for a particular

molecule from quantum-chemistry calculations. E_c is the potential energy of the null state which is altered by the clock. The zero of energy is here chosen to be that of an active isolated cell. E_k is the kink energy, which is the energy difference between two horizontally adjacent polarized cells having the same polarization or the opposite polarization. It can be calculated from simple electrostatics. P_m is the polarization of the mth cell. $f_{j,m}$ is a geometric factor depending on the distance and relative orientation between the jth cell and the mth cell. It is computed from electrostatics. For uniformly spaced and orientated cells, the geometric factor is simply one.

The coherence vector $\vec{\lambda}$ is developed by projecting the density matrix $\hat{\rho}$ onto the generators of $SU(3)$. The generators of the Lie group $SU(3)$ are

$$\hat{\lambda}_1 = \begin{pmatrix} 0 & 1 & 0 \\ 1 & 0 & 0 \\ 0 & 0 & 0 \end{pmatrix}, \qquad \hat{\lambda}_2 = \begin{pmatrix} 0 & 0 & 1 \\ 0 & 0 & 0 \\ 1 & 0 & 0 \end{pmatrix},$$

$$\hat{\lambda}_3 = \begin{pmatrix} 0 & 0 & 0 \\ 0 & 0 & 1 \\ 0 & 1 & 0 \end{pmatrix}, \qquad \hat{\lambda}_4 = \begin{pmatrix} 0 & i & 0 \\ -i & 0 & 0 \\ 0 & 0 & 0 \end{pmatrix},$$

$$\hat{\lambda}_5 = \begin{pmatrix} 0 & 0 & i \\ 0 & 0 & 0 \\ -i & 0 & 0 \end{pmatrix}, \qquad \hat{\lambda}_6 = \begin{pmatrix} 0 & 0 & 0 \\ 0 & 0 & i \\ 0 & -i & 0 \end{pmatrix},$$

$$\hat{\lambda}_7 = \begin{pmatrix} -1 & 0 & 0 \\ 0 & 1 & 0 \\ 0 & 0 & 0 \end{pmatrix}, \qquad \hat{\lambda}_8 = \frac{1}{\sqrt{3}} \begin{pmatrix} -1 & 0 & 0 \\ 0 & -1 & 0 \\ 0 & 0 & 2 \end{pmatrix}.$$

where the generators $\hat{\lambda}_7$ and $\hat{\lambda}_8$ correspond to the system's classical degrees of freedom.

The coherence vector for the jth cell is given by

$$\lambda_i^{(j)} \;=\; Tr\{\hat{\rho}_j \hat{\lambda}_i\} \tag{3.2}$$

where $\hat{\lambda}_i$ is one of the generators in $SU(3)$. These generators play the same role for $SU(3)$ that the Pauli spin matrices play for $SU(2)$. The state of each cell j is then described by the eight-dimensional vector, $\vec{\lambda}^{(j)}$. The cell polarization can be defined in terms of the expectation value of a particular generator.

$$P_j \;=\; -Tr(\hat{\rho}_j \hat{\lambda}_7) \;=\; -\lambda_7^{(j)}$$

Similarly, by projecting Hamiltonian onto the generators of $SU(3)$, we have an eight dimensional vector $\vec{\Gamma}$,

$$\Gamma_i^{(j)} \;=\; \frac{Tr\{\hat{H}^{(j)} \hat{\lambda}_i\}}{\hbar} \tag{3.3}$$

The 8×8 matrix

$$\Omega_{mn}^{(j)} \;=\; \sum_p \alpha_{mpn} \Gamma_p^{(j)}$$

where the structure constants α_{ijk} are determined by the commutator relation

$$4i\alpha_{mpn} \;=\; Tr\left\{ \left[\hat{\lambda}_m, \hat{\lambda}_p\right]_- \hat{\lambda}_n \right\}$$

In isolation from the environment, the unitary evolution of the density matrix can be expressed as the equation of motion for the coherence vector

$$\frac{d}{dt}\vec{\lambda}^{(j)} \;=\; \Omega^{(j)} \vec{\lambda}^{(j)} \tag{3.4}$$

Equation (3.4) represents the first order differential equations for the motion of coherence vector. If each cell is in a pure state, (3.4) will be equivalent to the

Schrdinger equation. For mixed states, (3.4) is equivalent to quantum Liouville equation. The Coulomb interaction between the cells is included in a mean-field Hartree approximation through (3.1).

With coupling to a heat bath, dissipation is introduced through an energy relaxation time approximation where the system relaxes to its instantaneous thermal equilibrium state. The steady state density matrix for a time dependent Hamiltonian is

$$\hat{\rho}_{ss}(t) = \frac{e^{-\frac{\hat{H}(t)}{k_B T}}}{Tr\{e^{-\frac{\hat{H}(t)}{k_B T}}\}} \tag{3.5}$$

The steady state coherence vector is given by

$$\lambda_{ss}^{(i)} = Tr\{\hat{\rho}_{ss}(t)\hat{\lambda}_i\} \tag{3.6}$$

The coherence vector is driven by the Hamiltonian forcing terms, and relaxes to the instantaneous thermal equilibrium value. The non-equilibrium dissipative motion equation now becomes

$$\frac{\partial}{\partial t}\vec{\lambda} = \Omega\vec{\lambda} - \frac{1}{\tau}\left[\vec{\lambda} - \vec{\lambda}_{ss}(t)\right] \tag{3.7}$$

where τ is the energy relaxation time representing the strength of the coupling between the system and the thermal bath. When τ is infinity, equation (3.7) becomes equation (3.4).

The equation of motion represents a set of coupled first order differential equations for the coherence vectors of QCA cells in contact with the thermal environment. As above, the cell-to-cell coupling is treated in a mean-filed approach. Coupling with the environment allows thermal fluctuations to excite the cells, and for cells to dissipate energy to the environment. This equation is essential in the study of thermodynamics of computation in an open system.

QCA cells exchange energy with neighboring cells, the clock and the thermal bath. The energy dissipated to the thermal bath can be derived from the instantaneous expectation value of the three-state Hamiltonian. The energy transferred to the bath over time interval Ts is given as

$$E_{diss} = \frac{\hbar}{2\tau}\int_{t}^{t+Ts}\vec{\Gamma}(t')[\vec{\lambda}_{ss}(t') - \vec{\lambda}(t')]dt'$$

The details of energy flow in QCA will be discussed in the next chapter.

3.3 Landauer clocking and Bennett clocking

The motion of the information across the QCA array is not ballistic, but controlled by the clocking signals. The clocking signals are controlled by a swept perpendicular electric field produced by local clocking wires as shown in Figure 1.14. The effect of the clocking field is to gradually drive cells in a particular region from null to active and back to null. Whether the active state is a 0 or 1 is determined by the state of the neighbors.

The perpendicular clocking electric field distributed along the horizontal direction of the QCA plane at different stages in one clock period in Landauer clocking is shown in Figure 3.1. The first plot is the sinusoidal clocking wave along the horizontal direction along the QCA array. To visualize, the shading of the clocking field is shown in the second plot. The blue area represents the null domain where the electric field is negative (pointing downward perpendicular to QCA plane) and the cells are in the null state. The white area indicates the active domain where the electric field is positive (pointing upward perpendicular to QCA plane) and the cells are in the active state. The color between them is the switching region where the transition between the null state and active state is made. In the beginning ($t = 0$) in Figure 3.1(a), all of the clocks are set to low. Then the clocks are slowly raised to high from left to right ($t = T_c/4$, $t = T_c/2$, T_c is one clock period) as is shown in

Figure 3.1 (b) (c) . Next, the clocks in the leftmost cells that were first switched on are turned off, while the clocks in the rightmost cells are still kept high ($t = 3Tc/4$). In the end, all of the clocks are set to low ($t = T_c$). The system goes back to the initial state.

Bennett style clocking is a new clocking scheme which aims to convert a logically irreversible circuit into a reversible form without changing circuit architecture by clocking in the information forward through the cell array and then backwards. The time evolution of Bennett clocking wave distributed along the QCA array is shown in Figure 3.2. The shading of the clocking field is plotted. All the clocks start as low. Then each clock in the cell array is slowly turned on along the array, until all of the clocks are high. Next, the clocks in the cell array are slowly turned off from right to left, until all of the clocks are returned back to low. Therefore, the white area in the figure sweeps forward the QCA array and then sweeps backward.

Figure 3.3 illustrates information flow in Landauer and Bennett clocking of QCA circuits. A QCA shift register is implemented by a single line of cells, which copies information from cell to cell. A three-input majority gate is formed when three QCA shift registers converge. The additive effect of the Coulomb interaction from the input cells determine which state the device cell (at the junction) will switch into when its clock is raised. The left column (L1-L5) represents snapshots of the circuit at different times as it is clocked using the Landauer clocking scheme and the right column (B1-B7) shows snapshots using the Bennett clocking scheme. It is assumed that the input signals come from other QCA circuitry to the left of the circuit shown and that the output signals are transported to the right to other QCA circuits.

In the initial state (L1), all the cells in the Landauer-clocked circuit are in the null state. As the clocking signal activates the left-most cells, they copy the incoming

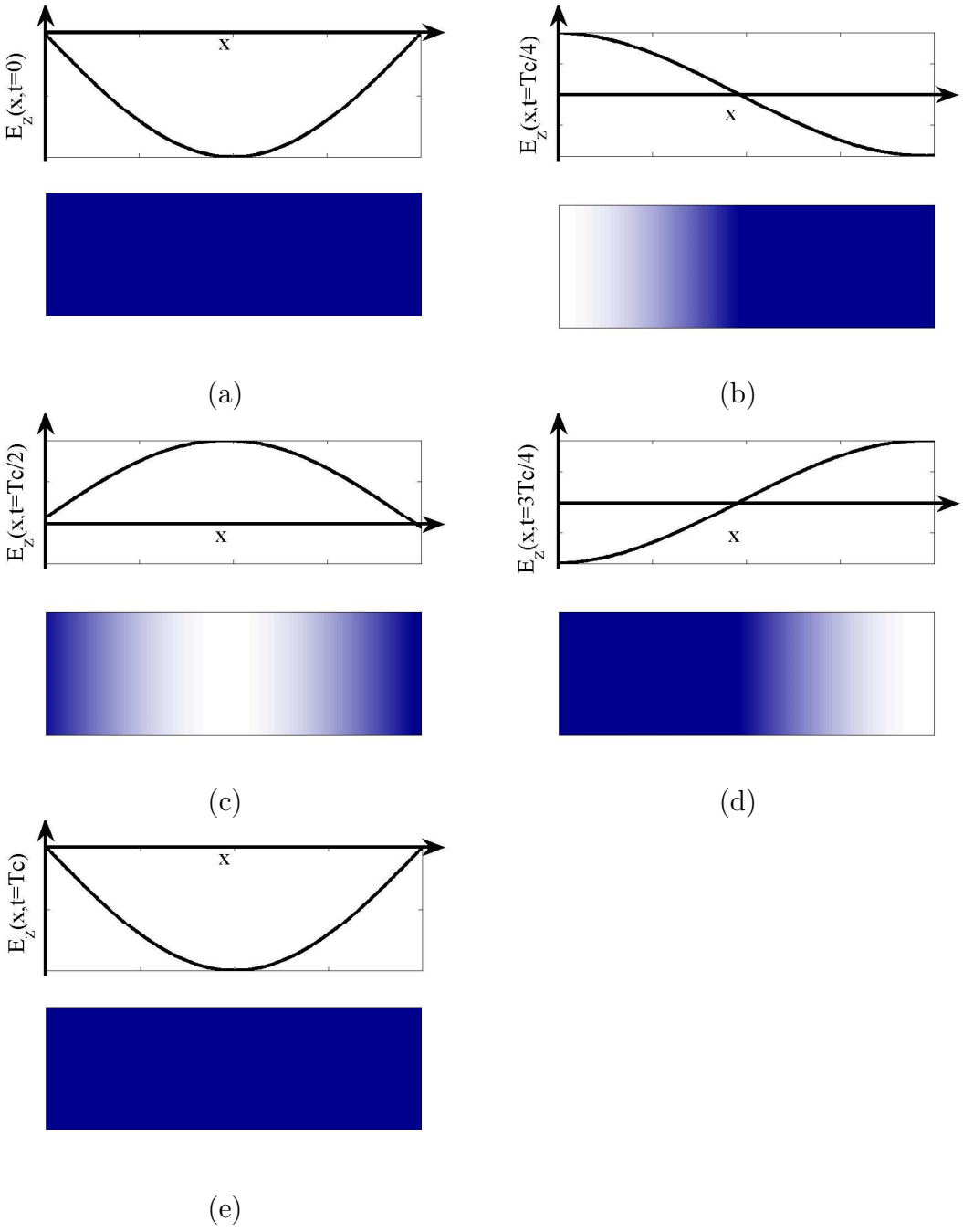

Figure 3.1. Landauer clocking field distributed along the QCA plane at different stages of one clock period T_c. (a)$t = 0$ (b) $t = T_c/4$ (c)$t = T_c/2$ (d) $t = 3T_c/4$ (e) $t = T_c$.

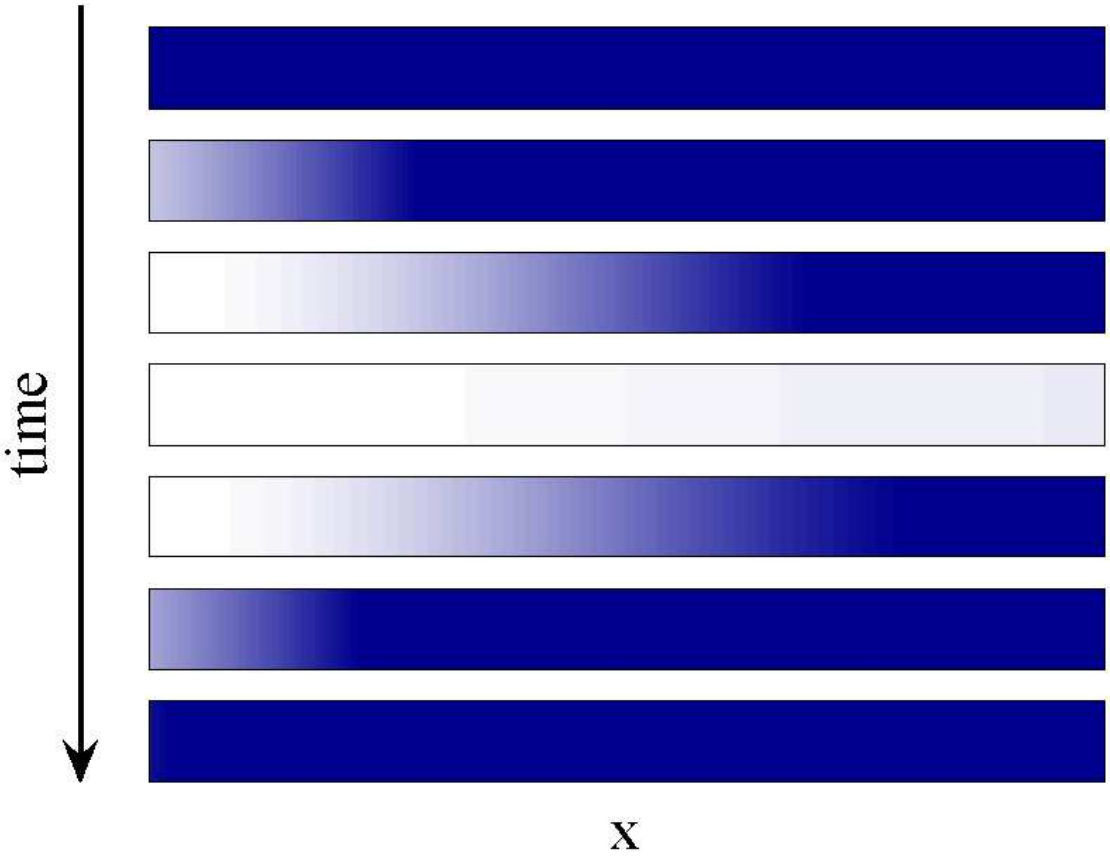

Figure 3.2. Time evolution of Bennett clocking distributed along the QCA array.

information and propagate it to the right (L2). The shift register simply moves the information from left to right. In the example shown a "1" bit, represented by a group of polarized cells (red="1"), is transported. The bit moves as cells are activated and copy the bit on the leading edge of the bit packet; cells on the trailing edge are erased to null. Because this trailing-edge cell erasure is done in the presence of a copy of the information (i.e. no information is being lost), it can be accomplished without dissipating $k_B T ln(2)$. More precisely, there is no fundamental lower limit to the energy that must be dissipated. In the Landauer-clocked majority gate, shown on the lower part of each snapshot, three bits of data (here a "0", "1",

and "1") "collide" to compute the majority function. The computation happens as the leading edge of the bit packets converge at the central device cell (L2→L3). Erasure of cells on the trailing edge is comparable to the case of the shift register except for the "loser" in the majority vote. In that case, because the output cells are in the majority state, an input line must be erased to null without a copy being present. In Figure 3.3, the "0" input to the majority gate loses the vote and the information moving forward to the right (L4 and subsequent) contains no record that the "0" was ever present. In this case information is really lost to the whole system and an energy of least $k_B T ln(2)$ must be dissipated as heat (as we will see in the next section).

The speed at which the computation occurs can influence the total power dissipated in a way unrelated to the issue of information loss. In the Landauer-clocked circuit (Figure 3.3 L1-L5) we see a wave of computational activity sweep across the circuit. The leading edge of the wave is where computation actually occurs; the trailing edge is where erasure occurs. The speed of the wave is determined by the clocking frequency and the pitch of the clocking wires. The practical upper limit of clock frequency is determined by one of two requirements: adiabatic operation or power dissipation. If the clock frequency is too fast, cells on the leading edge do not have enough time to switch smoothly to their new state and either oscillate or become stuck in metastable states. "Too fast" is relative to the tunneling time for an electron to move from one side of the molecule to the other. This can be very fast indeed; sub-picosecond times have been reported even for large molecules [72]. The gradual adiabatic nature of the switching is also a function of the width of the bit packet set by the clocking wire pitch. A broad gentle edge improves adiabaticity, at the cost of total information density in the pipeline. As the frequency approaches adiabatic breakdown, even for reversible computation like the shift register, cells on

the leading edge begin to be excited above their instantaneous ground state. This excess energy in the cell is dissipated as heat as the cells de-excite through inelastic processes (e.g. molecular vibrational states). For a large array of cells at molecular densities, this power dissipation can become the practical limitation, though THz operation of densities as high as 10^{12}devices/cm^2 may still be a possibility [13]. This heat dissipation due to operating at speeds near adiabatic breakdown is a separate issue from the heat dissipation due to information erasure—the requirement of dissipating at least $k_BTln(2)$ per erased bit holds no matter how slow the clock speed.

Bennett-clocked operation is shown in Fig. 3.3 (B1-B7) which again represents snapshots in time as the array is clocked. The computational leading edge of the clocking wave moves from left to right in B2-B4. The difference in the Bennett-clocked circuit is that there is no trailing-edge cells remain held in the active state as the computational edge moves forward. The loser in the majority gate (the green="0" input) is held in place and not erased until the results of the computation are present at the (here right-most) output edge. At that time, the output states can be copied to the next stage of computation and the clock begins to lower cells back to the null state from right to left (B4-B7). In this part of the cycle, erasure of intermediate results does occur but always in the presence of a copy. Thus no minimum amount of energy ($k_BTln(2)$) need be dissipated. At the end of the back-cycle the inputs to the computation must either be erased or copied. If they are erased, then an energy of at least $k_BTln(2)$ must be dissipated as heat for each input bit. This is unavoidable. What has been avoided is the energetic cost of erasing each of the intermediate results. The example shown in the figure is only one shift register and one majority gate—in practical cases it would be a large subsection of the calculation. In that case there are many more intermediate results than input

bits so the savings in energy dissipation by Bennett clocking could be large.

The Bennett-clocking scheme has benefits and costs which are part of the design space for the circuit. The principal benefit is lower power dissipation, which as we have seen may make the difference between molecular-scale electronics working or vaporizing. The costs include at least doubling the effective clock period to allow the forward and reverse cycles (B1-B4 and B4-B7). In addition, the amount of pipelining is reduced because for a given block of computation only one computational edge at a time can be moving across the circuit in the Bennett-clocked scheme. In Landauer clocking by contrast, several computational waves can be traversing the same block at the same time. Finally, the circuitry that provides the clocking signal has to be somewhat more complex to handle the block-by-block forward-then-backward clocking of the Bennett approach. In many circumstances, the speed and simplicity of Landauer clocking will outweigh the power dissipation benefits of Bennett clocking. It is notable that the QCA layout itself does not have to be changed to go from one to another-only the timing of the clocking needs to be altered. One could imagine switching from one mode to the other as needed.

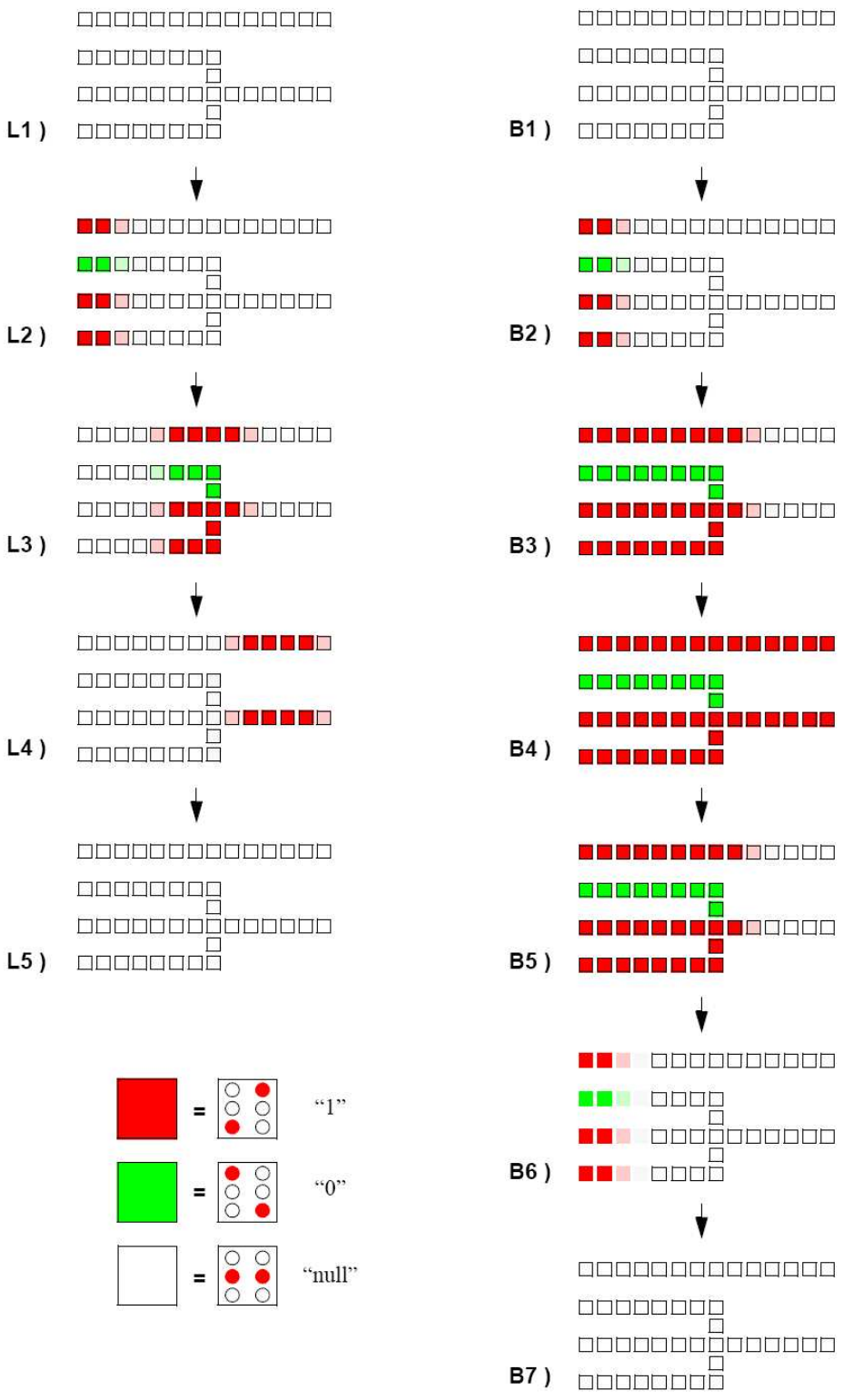

Figure 3.3. Landauer and Bennett clocking of QCA circuits.

3.4 Direct comparison of Landauer and Bennett clocking

We employ the formalism described in Section 3.2 to example circuits clocked by both Landauer and Bennett approaches to directly compare power dissipation in the two approaches. Figure 3.4 shows four QCA circuits. The first, shown in Figure 3.4 (a), is simply a QCA shift register, which can be Landauer-clocked or Bennett-clocked. A two input OR gate is formed from a three-input majority gate by fixing one input to a binary "1". Figure 3.4 (b) and (d) represent OR gates with Landauer and Bennett clocking respectively (the actual layout is identical). Fig. 3.4 (c) shows an OR gate with the addition of lines echoing the input to the output. This is the usual method of achieving Bennett-style reversible circuitry. It has the draw-back that the circuitry is more complex and intermediate results accumulate as the computation proceeds. The QCA circuit represented in Fig. 3.4 (c) is Landauer-clocked.

Figure 3.5 shows the energy dissipated per clock cycle for each of the four circuits shown in Figure 3.4, calculated using the formalism of Section 3.2. All energies are shown as a ratio to the kink energy E_k which characterizes the cell-to-cell interaction energy. The parameters were chosen to push the adiabatic limit so that dissipation amounts would be visible on the graph ($E_k = 0.19eV$, $\gamma = 0.05eV$, $f = 100GHz$, $\tau = 0.35fs$). The first pair of bars shows the very low dissipation of the shift register, whether it is Landauer-clocked or Bennett-clocked. The second pair of bars shows the dissipation of the Landauer-clocked OR gate (Figure 3.4 (b)). When the inputs are "1" and "1" (or "0" and "0") there is no erasure and the energy dissipated is less than $k_BTln(2)$. When the inputs differ information is lost and an energy of at least $k_BTln(2)$ must be dissipated. In fact the energy dissipated is about E_k, which needs to be significantly larger than $k_BTln(2)$ for the circuits to work reliably in a thermal environment. The third set of bars shows the energy

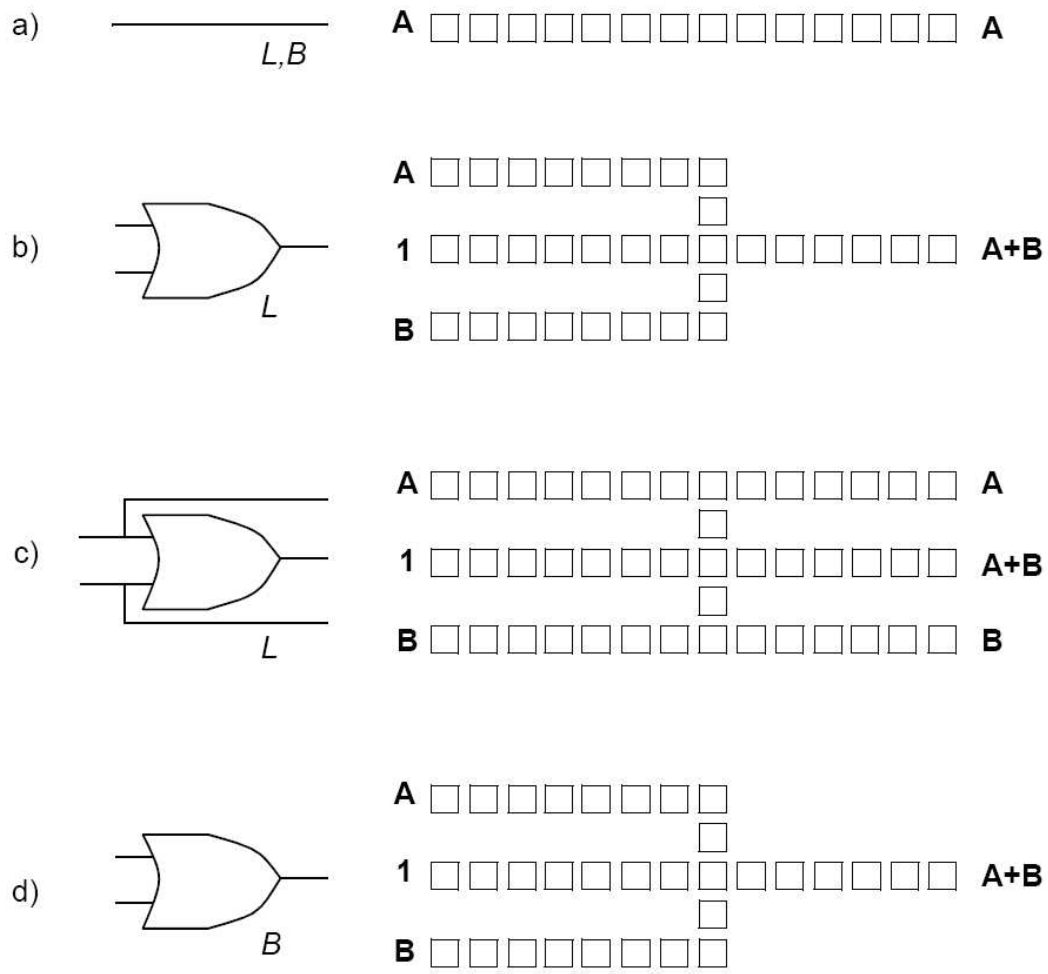

Figure 3.4. Four test QCA circuits. (a) A shift register, which can be Landauer-clocked or Bennett-clocked. (b) A Landauer-clocked OR gate. (c) A Landauer-clocked OR gate for which inputs are also echoed to the output, embedding a logically irreversible operation in a logically reversible operation. (d) A Bennett-clocked OR gate.

dissipated for the logically reversible circuit formed by combining the OR gate with echoes of the input to the output (Figure 3.4 (c)). We see that energy dissipation can indeed be lowered below $k_B T ln(2)$ by this technique even when, as here, the circuit is Landauer-clocked. As long as we keep all the intermediate results, energy

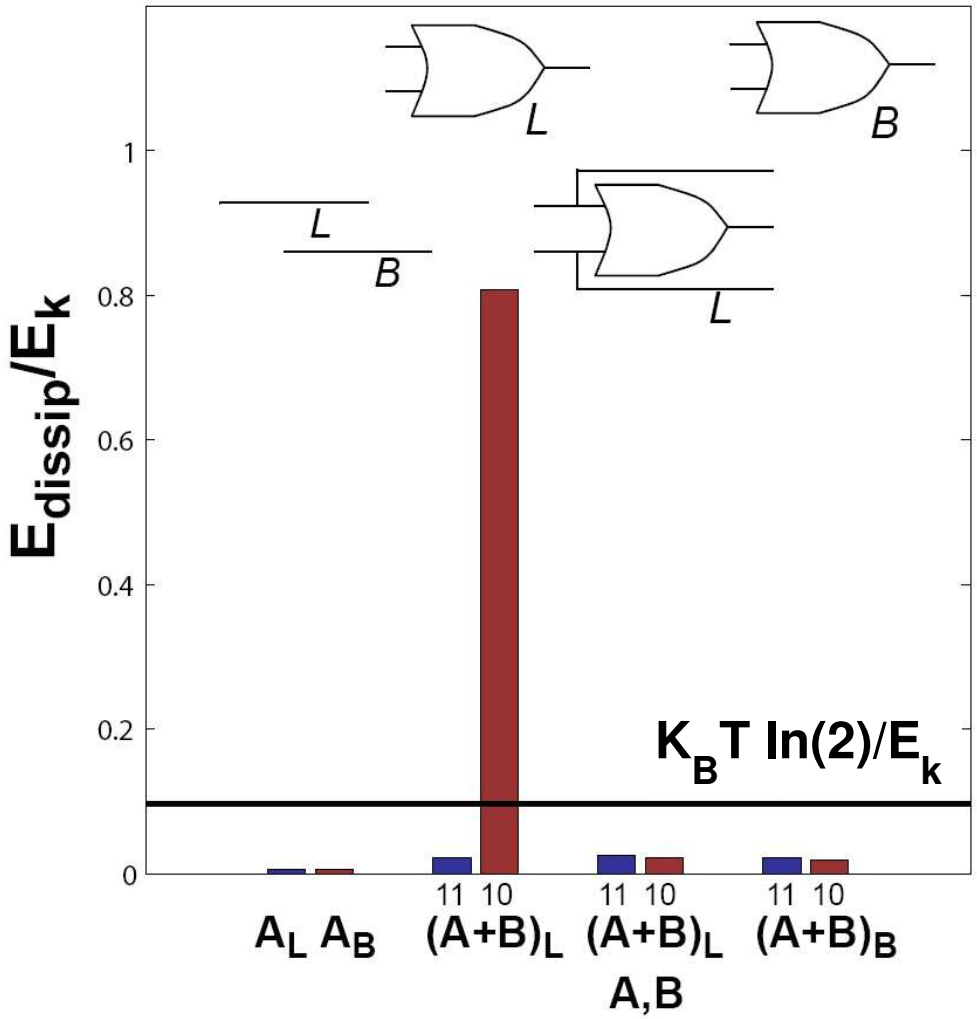

Figure 3.5. Calculated energy dissipation for the four test QCA circuits in Figure 8. The shift registers involve no information loss so dissipate less than $k_BTln(2)$. The Landauer clocked OR gate dissipates much more than $k_BTln(2)$ when the input bits differ. Echoing inputs to the output succeeds at reducing energy dissipation, but at the cost of circuit complexity. Bennett-clocking yields very low energy dissipation with no additional circuit complexity.

dissipation to the environment can be reduced to much less then $k_BTln(2)$. The fourth set of data shows the energy dissipated when the OR gate (without echoes)

is simply Bennett clocked. This is remarkable because the circuit is physically identical to the Landauer clocked OR gate, but yields vastly less energy dissipation. If the clock speed were substantially slower, the small bars in Figure 3.5 would not be visible at this scale, but the dissipation for the Landauer-clocked OR gate would remain many times larger than $k_B T ln(2)$. Figure 3.5 shows the central results of this work from which several important conclusions can be drawn.

(1). Embedding an irreversible calculation in a reversible circuit by echoing inputs to outputs does indeed result in huge reduction of the power dissipated.

(2). Bennett-clocked QCA circuits can reduce the power dissipated to much less than $k_B T ln(2)$ without changing circuit complexity. This suggests that QCA may at last provide a practical means of implementing reversible computing.

(3). We verify Landauer's principle by direct time-dependent solutions of the equations of motion for an actual circuit in thermal contact with the environment. The formalism includes the effect of thermal fluctuations from system to environment and from environment to system.

(4). The fact that the shift register dissipates much less than $k_B T ln(2)$, confirms Landauer's assertion that there is no fundamental lower limit to the energy dissipation cost of transporting information [73].

There is some confusion about the energy needed to distinguish a "1" to "0" in a thermal environment and the energy dissipated to the environment [59]. There is no doubt that the barrier to switching when an element is just holding a bit

must be larger than $k_B T ln(2)$. But there is no reason to equate barrier height with energy dissipated as heat. The key idea of Landauer's adiabatic switching is that the barrier can be lowered, the system switched, and then the barrier raised again. For a QCA shift register, the energy moving from cell to cell as a bit is shifted down the line must indeed be greater than $k_B T ln(2)$ (in the next chapter, the energy moving down the line will be discussed). But this amount of energy need not be dissipated at each step. Indeed in the Bennett approach it need not be dissipated at all. The signal energy, but not the dissipated energy, must be larger than $k_B T ln(2)$ for the signal to be robust [13, 14]. Furthermore the signal energy must be augmented from stage to stage so that the signal does not decay. The power gain is provided by the clock. As [70] points out, there is some heat dissipation in the clocking wire circuit, due to the small resistance of the wires themselves. But it can be minimized and is not a fundamental limitation.

3.5 Conclusion

Power dissipation is a crucial consideration for the future of practical computing at molecular length scale. To be successful, any technology at the molecular scale must operate near the fundamental limits of power dissipation per bit computed as a result of high densities. We describe a combination of Landauer-clocked and Bennett-clocked molecular QCA circuits here. Our direct calculation of the equations of motion coupled to the thermal bath shows that low power operation in molecular QCA is possible.

CHAPTER 4

POWER FLOW IN CLOCKED MOLECULAR QCA CIRCUITS

4.1 Introduction

In this chapter, we explore the dynamics of power flow in clocked molecular QCA circuits, particularly in fan-out, fan-in and in majority gates. Once again we solve the non-equilibrium equation of motion for clocked QCA circuits.

4.2 The theory of energy flow in a three-state QCA system

A QCA cell exchanges energy with its neighboring cells, the clock, and the thermal bath. The equations for energy flow in QCA system are derived from the instantaneous expectation value of the three-state Hamiltonian in Equation (3.1)

$$E = \langle \hat{H} \rangle = \frac{1}{3} Tr\{\hat{H}\} + \frac{\hbar}{2} \vec{\Gamma} \bullet \vec{\lambda} \tag{4.1}$$

where $\vec{\lambda}$ and $\vec{\Gamma}$ are defined in Equation (3.6) and Equation (3.3).

The instantaneous power flow in the cell is the derivative of Equation (4.1),

$$P(t) = \frac{dE}{dt} = \frac{1}{3}\frac{d}{dt}E_c(t) + \frac{\hbar}{2}\left(\frac{d}{dt}\vec{\Gamma}(t) \bullet \vec{\lambda}(t) + \vec{\Gamma}(t) \bullet \frac{d}{dt}\vec{\lambda}(t)\right) \tag{4.2}$$

Substituting Equation (3.7) into (4.2), the above equation becomes

$$P(t) = \frac{1}{3}\frac{d}{dt}E_c(t) + \frac{\hbar}{2}\left(\frac{d}{dt}\vec{\Gamma}(t) \bullet \vec{\lambda}(t) + \vec{\Gamma}(t) \bullet \left(\Omega(t) \cdot \vec{\lambda}(t) + \frac{1}{\tau} \cdot \left(\vec{\lambda}_{ss}(t) - \vec{\lambda}(t)\right)\right)\right)$$

This expression can be simplified by the fact that

$$\vec{\Gamma}(t) \bullet (\Omega(t) \cdot \vec{\lambda}(t)) = 0$$

The instantaneous power flow is therefore

$$P(t) = \frac{1}{3}\frac{d}{dt}E_c(t) + \frac{\hbar}{2}\left(\frac{d}{dt}\vec{\Gamma}(t) \bullet \vec{\lambda}(t) + \frac{1}{\tau}\vec{\Gamma}(t) \bullet \left[\vec{\lambda}_{ss}(t) - \vec{\lambda}(t)\right]\right) \quad (4.3)$$

So the total energy flow through a cell averaged over a time interval (one clock period is used so that the cell goes back to its initial state) is given by

$$E_{net} = \int_t^{t+Ts} \frac{1}{3}\frac{d}{dt'}E_c(t') + \frac{\hbar}{2}\left(\frac{d}{dt'}\vec{\Gamma}(t') \bullet \vec{\lambda}(t') + \frac{1}{\tau}\vec{\Gamma}(t') \bullet \left[\vec{\lambda}_{ss}(t') - \vec{\lambda}(t')\right]\right) dt' \quad (4.4)$$

where E_c is the clock energy, τ is the energy relaxation time constant which represents the strength of the coupling between the system and the thermal environment. $\vec{\lambda}_{ss}$ is the steady state coherence vector defined in Equation (3.6).

The above equation can be divided into four parts: (a) energy dissipated to the bath, (b) energy provided by the clock, (c) energy provided by the input and, (d) energy delivered to the output.

The energy dissipated to the bath over one clock period T_s is given by

$$E_{diss} = \frac{\hbar}{2\tau}\int_t^{t+Ts} \vec{\Gamma}(t')\left[\vec{\lambda}_{ss}(t') - \vec{\lambda}(t')\right] dt' \quad (4.5)$$

The energy provided by the clock in one clock period is

$$E_{clock} = \int_t^{t+Ts} \frac{1}{3}\frac{d}{dt'}E_c(t') + \frac{\hbar}{2}\frac{d\Gamma_8(t')}{dt'}\lambda_8(t')dt' \quad (4.6)$$

where Γ_8 and λ_8 denotes the eighth element of the vectors $\vec{\Gamma}$ and $\vec{\lambda}$.

Notice that the energy flows into the cell from the clock when the energy barriers are raised. That amount of energy will be returned to the clock when the barriers are lowered. The energy dissipated in the clocking wire circuit is not considered here.

Denote P_L as the polarization of the input (or left neighboring cells) and P_R as the polarization of the output (or right neighboring cells). The energy provided by the input (or left neighboring cells) over one clock period is

$$E_{in} = \frac{\hbar E_k}{2}\int_t^{t+Ts} \frac{dP_L(t')}{dt'}\lambda_7(t')dt' \quad (4.7)$$

The energy delivered to the output (or right neighboring cells) over one clock period is

$$E_{out} = -\frac{\hbar E_k}{2}\int_t^{t+Ts}\frac{dP_R(t')}{dt'}\lambda_7(t')dt' \tag{4.8}$$

The net change of the energy in the QCA cell system over one clock period can be expressed as

$$E_{net} = E_{in} + E_{clock} + E_{out} + E_{diss} \tag{4.9}$$

In steady state, E_{net} must be zero. Usually, the sign of the input energy is positive and the signs of the output energy and the energy dissipated to bath are negative.

4.3 Information flow in clocked QCA circuits

Information is transported from cell to cell directed by clock signals. With appropriate layout, QCA information can be duplicated and fan-outs and fan-ins can be realized. Figure 4.1 shows the layouts of three QCA circuits: one-to-two fan-out and two-to-one fan-in, one-to-three fan-out and three-to-one fan-in, and one-to-four fan-out and four-to-one fan-in. In Column 3, one input signal line propagates into two, three and four signal lines correspond to Figure 4.1(a), (b) and (c) respectively. In Column 7, those signal lines merge into one signal line. Landauer clocking is employed in the QCA circuits to achieve adiabatic switching.

Figure 4.2 illustrates the information flow in a circuit constructed with one-to-two fan-out and two-to-one fan-in at different stages of time. The fully polarized "1" cell is colored in red. The white cell is in a null state, holding no information. The pink cell represents not fully polarized cell, where a transition between "1" and null is made. In the initial state, all clocks are low (inactive) and all cells are in the null state. As clocks are activated from left to right, the signal propagates from left to right. When the signal moves to the cell in the third column, it splits into

two signal lines because of interaction with its neighboring upper cell and lower cell. Those two signal lines propagate independently to their right cells till they merge into one signal line in the seventh column. The merged signal is then moved along the line towards right. Finally, all clocks are deactivated and all cells go back to null state.

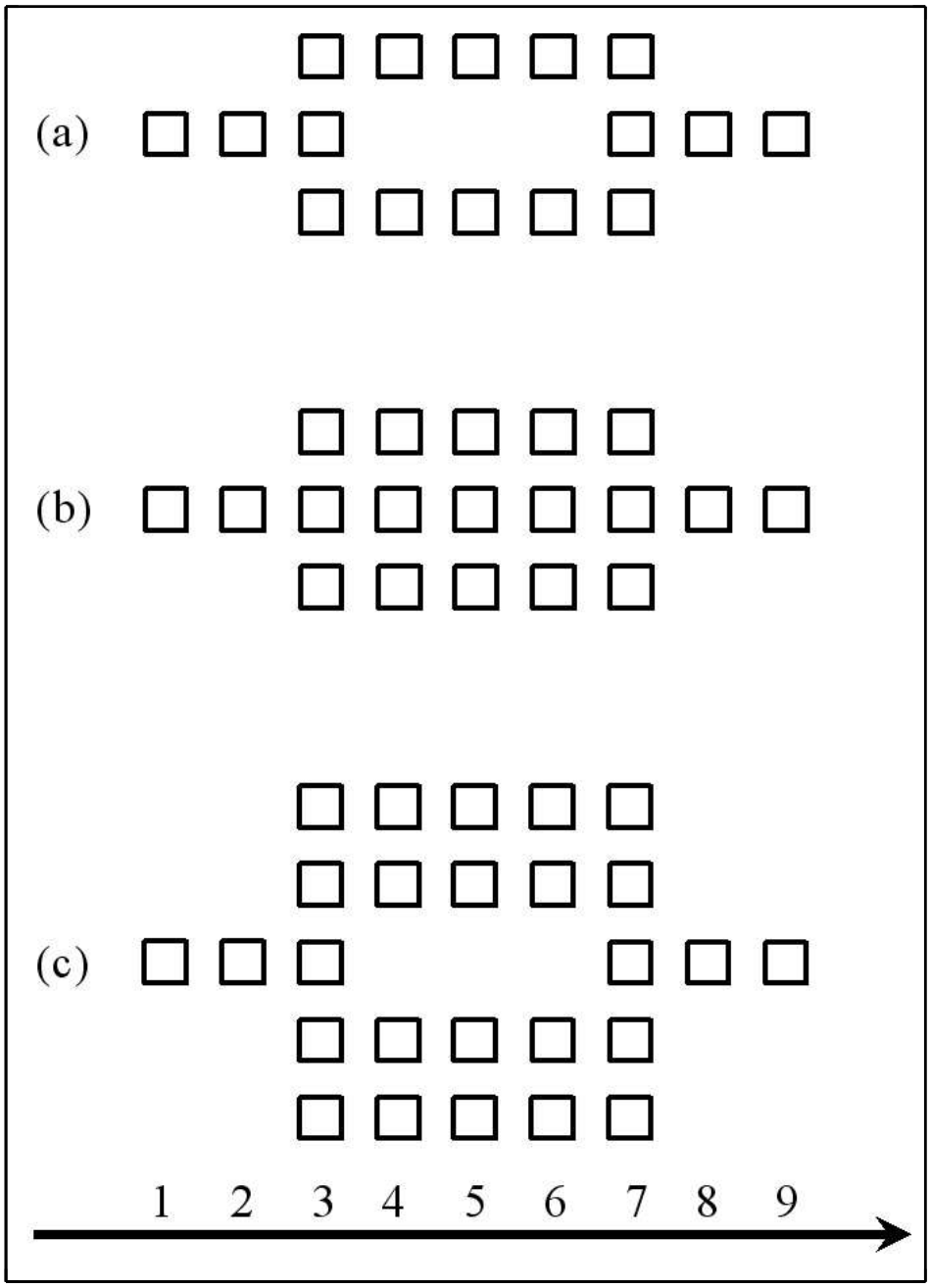

Figure 4.1. The layout of fan-outs and fan-ins for (a) one-to-two fan-out and two -to-one fan-in. (b) one-to-three fan-out and three-to-one fan-in. (c) one-to-four fan-out and four-to-one fan-in. In Column 3, one input signal line propagates into two (or three, four) signal lines. In Column 7, two (or three, four) signal lines merge into one signal line.

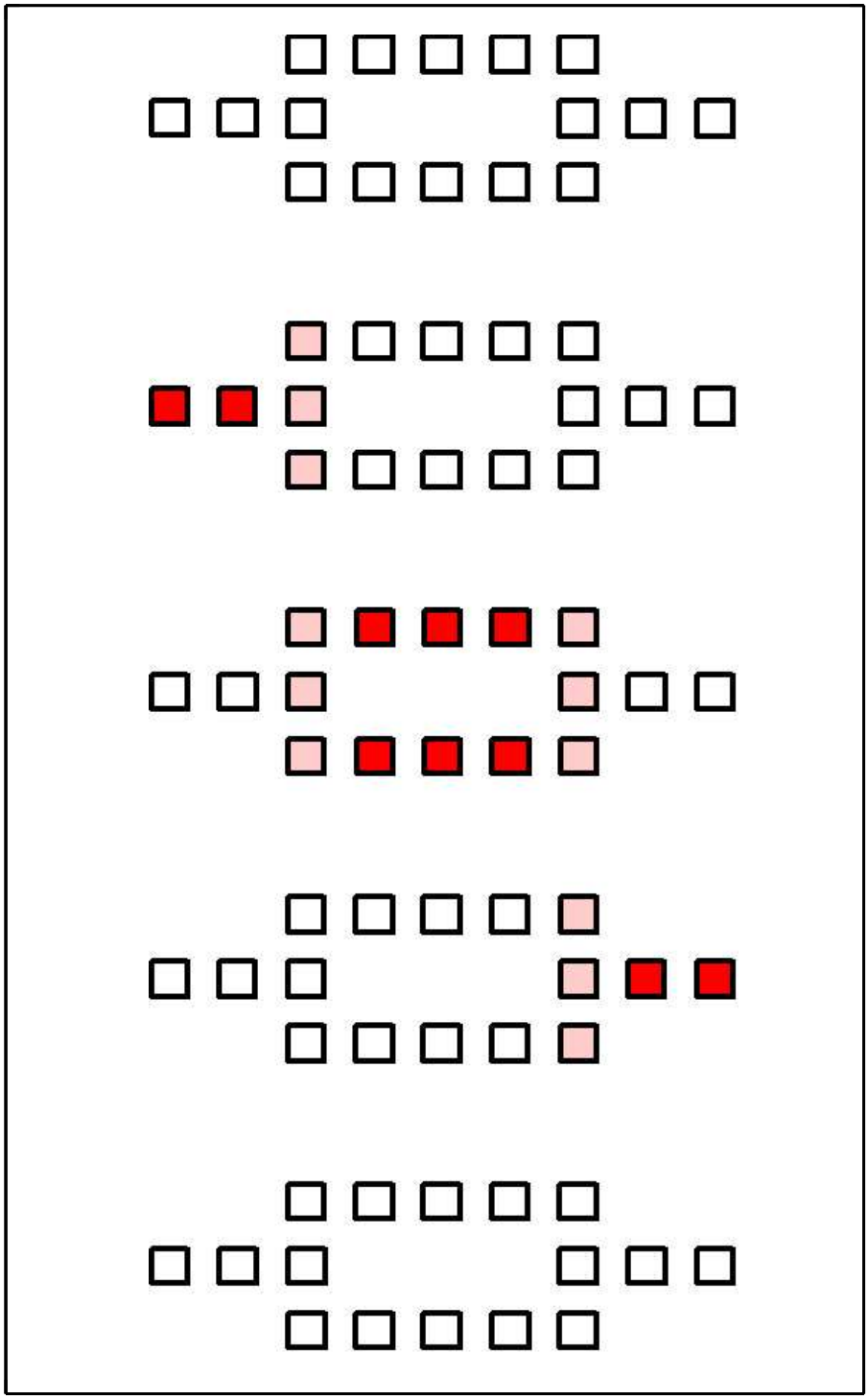

Figure 4.2. Information flow in a circuit constructed with one-to-two fan-out and two-to-one fan-in at different stages of time. The red cell represents a "1" stored in the cell.

4.4 Power flow in clocked QCA circuits

The coherence vector formalism with dissipation incorporated is employed to examine the energy flow in QCA circuits. The parameters are chosen to minimize the energy dissipation so that there is no dissipation due to the operating speed ($E_k = 0.2ev$, $\gamma = 0.04ev$, $f = 100\text{GHz}$, $\tau = 3.3 \times 10^{-16}$ s).

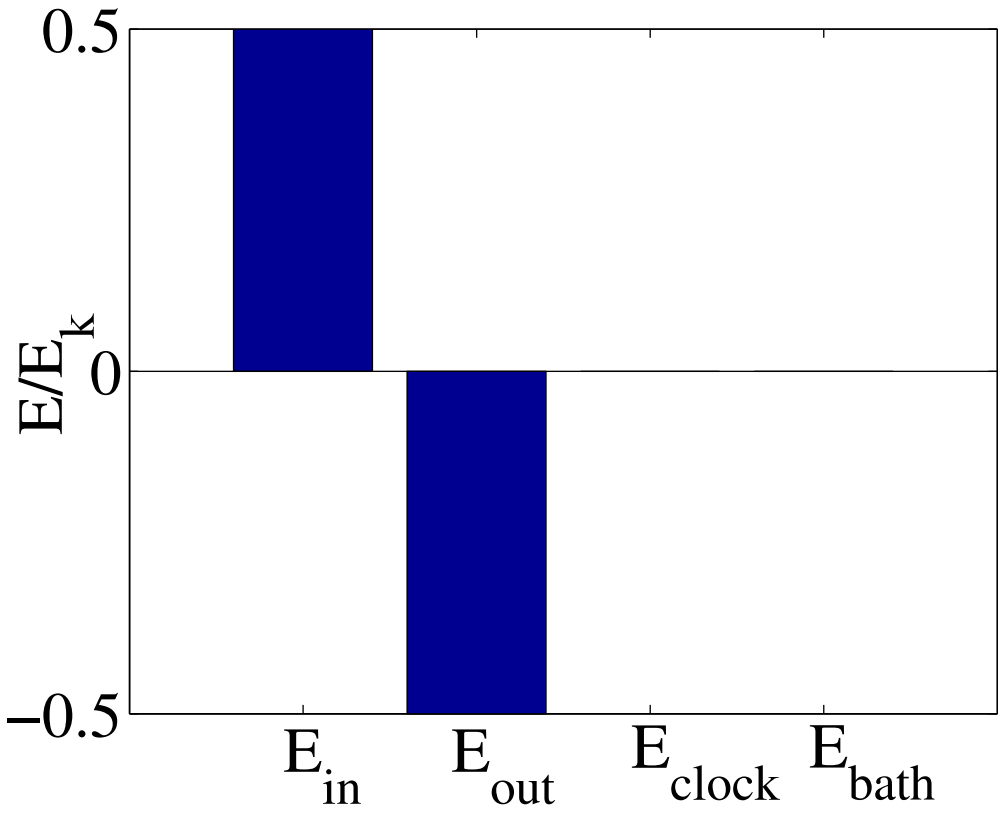

Figure 4.3. Steady state energy flow in a QCA shift register cell in one clock cycle.

Let's first take a look at the simplest circuit: the QCA shift register. Figure 4.3 shows the steady-state energy flow averaged over one clock cycle in a shift register cell. All energies are shown as a ratio to the kink energy E_k which characterizes the cell-to-cell interaction. Energy flow from the input (left neighboring cell) equals to the energy flow to the output (right neighboring cell), which indicates that the net

power gain is unity. The energy provided by the clock equals the energy dissipated to the thermal bath, which are both very small and not visible in the graph. The signal energy should be and is much greater than $k_B T ln(2)$ to be distinguishable in the thermal environment. Note that this amount of energy is transported from cell to cell rather than dissipated to the thermal bath.

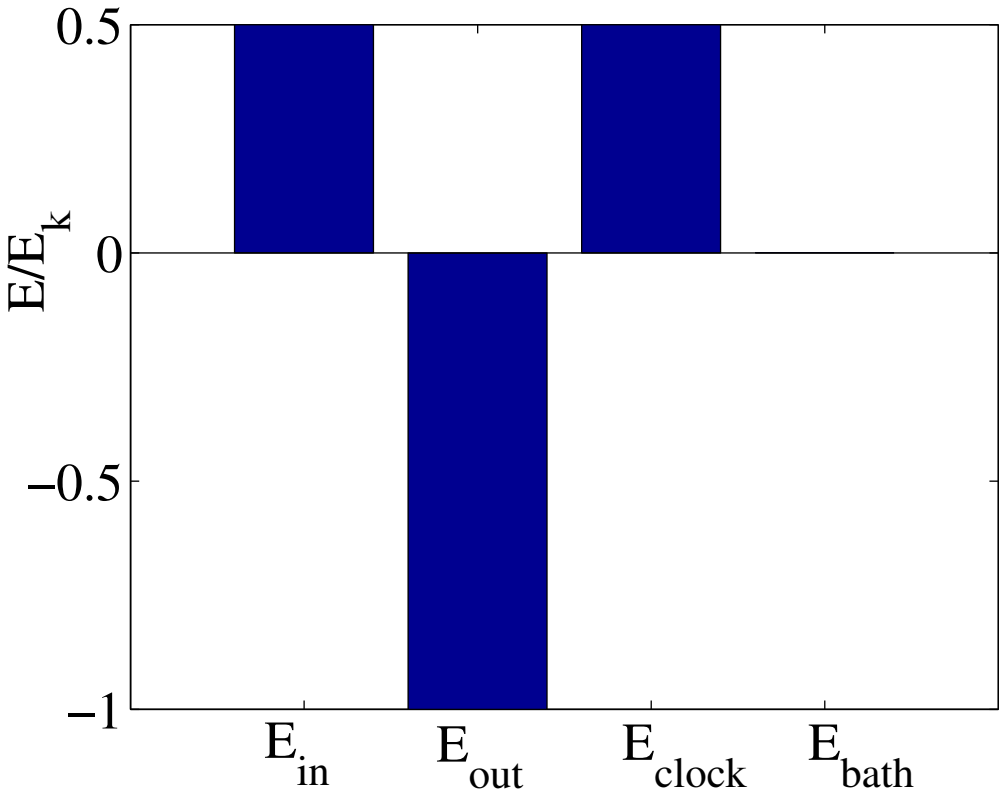

Figure 4.4. The steady state energy flow over one clock period in the third column of a one-to-two fan-out and two-to-one fan-in described in Figure 4.2.

Since the one-to-many fan-outs and many-to-one fan ins act as regular shift registers except for the third column and seventh column, we are particularly interested in the steady state energy flow in the third column. Figure 4.4 illustrates the total energy flow over one clock period in the third column of a one-to-two fan-out and two-to-one fan-in described in Figure 4.2. The output energy is twice the input en-

ergy because there are two lines of information propagated to the right and only one line of information from the left. The work done by the clock in the third column thus provides the necessary energy ($0.5E_k$) for power gain. The energy dissipated to the thermal bath is still small because no bit erasure occurs.

The energy flow in the clock in each column of the layout in Figure 4.1 is plotted in Figure 4.5 to examine the role of clocking in fan-outs and fan-ins. In Column 3 where fan-outs occur, the clock provides the necessary energy for power gain. For fan-out of 2 (or 3 and 4) lines, energy provided by the clock is $E_k/2$ (or E_k and $3E_k/2$). In Column 7 where fan-ins happen, the amount of the energy that the clock provides for fan-outs is returned back to the clock. And that amount of energy is again not dissipated to the environment. Hence the clock provides energy needed for power gain while that amount of energy stored in the system is returned back to the clock in fan-ins. It's notable that for each fan-out (fan-in), the energy provided by the clock is about one half E_k, which indicates that there is $E_k/2$ amount of energy transported in one single cell wire. A simple analysis from the Hamiltonian matrix tells us why it is $E_k/2$. The Columbic interaction between two cells is E_k. Therefore the energy stored in one cell is just half of that E_k, and this amount of energy is moved along the QCA line.

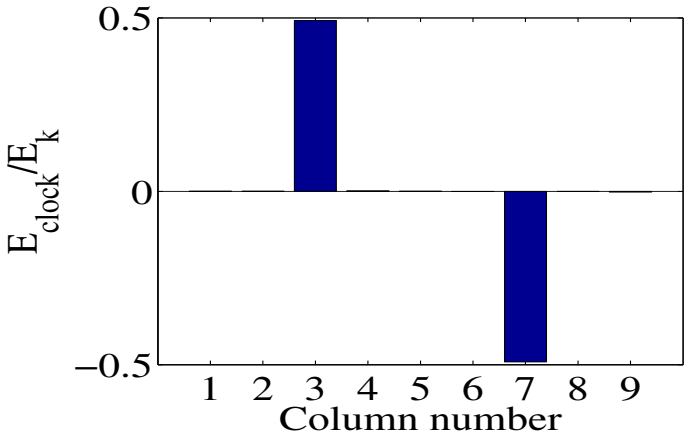

(a)

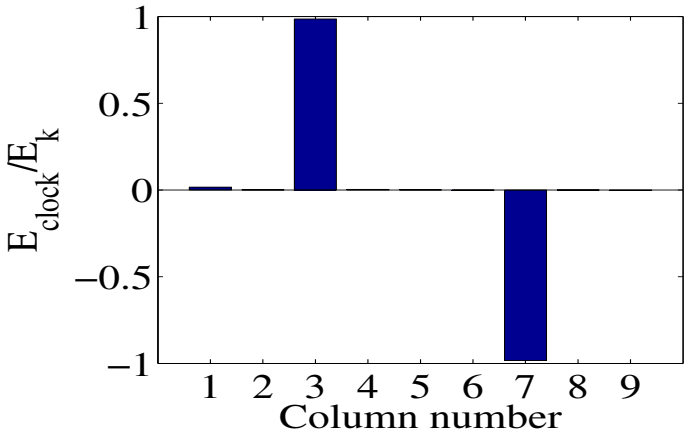

(b)

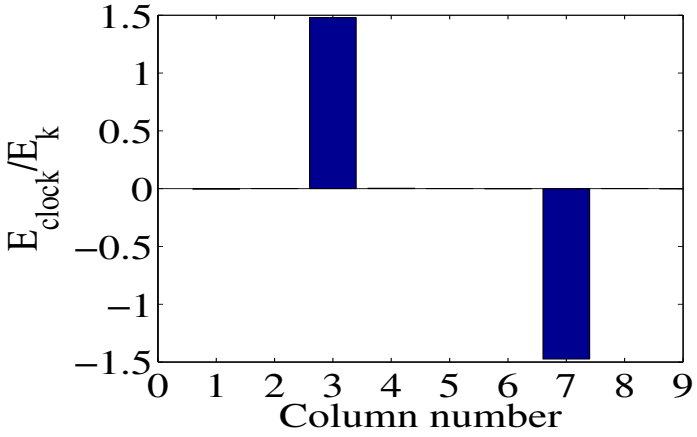

(c)

Figure 4.5. The energy flow in the clock in each column of layout in the circuit (a) one-to-two fan-out, two-to-one fan-in (b) one-to-three fan-out, three-to-one fan-in (c) one-to-four fan-out, four-to-one fan-in.

More complex QCA fan-out circuit can be constructed hierarchically with appropriate layout. Figure 4.6 shows the layout of a one-to-eight fan-out constructed with three stages of one-to-two fan-out.

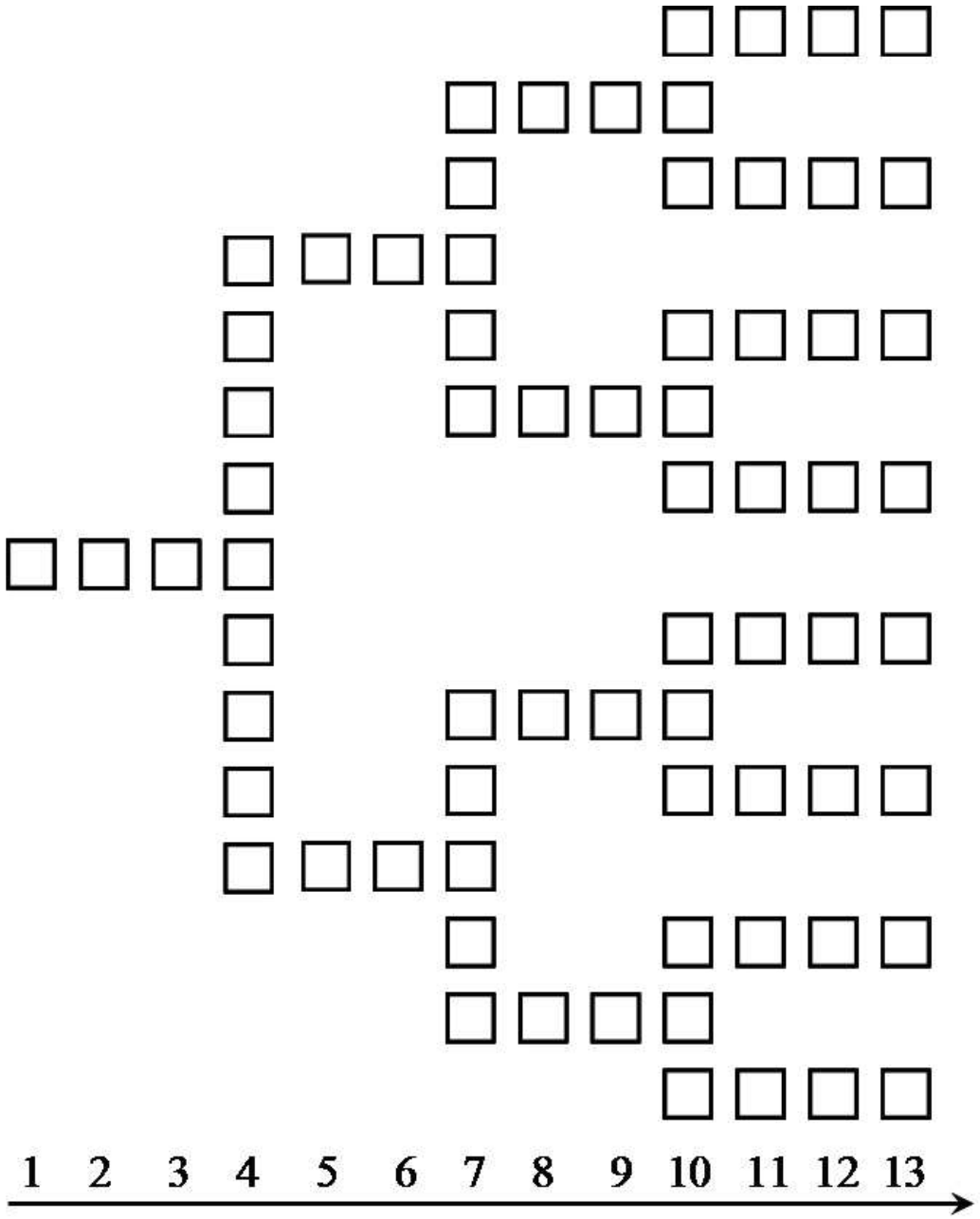

Figure 4.6. The layout of a one-to-eight fan-out constructed with three stages of one-to-two fan-out.

The energy provided by the clock in each column of the layout per clock cycle is illustrated in Figure 4.7. In Column 4, one line of information splits into two lines of information, where the clock provides $E_k/2$ amount of energy. The clock provides E_k amount of energy in Column 7 where two lines of information copies into four lines of information. In Column 10, $2E_k$ amount of energy is provided by the clock for another power gain of two. Therefore, for a one-to-eight fan-out, a total energy of $3.5E_k$ is supplied by the clock. The clock is therefore essential in the QCA circuit, as it not only enables data pipelining for the circuitry but also supplies power gain and amplifies weakened signals. The results of the one-to-eight fan-out QCA circuitry can be fed to conventional CMOS circuits.

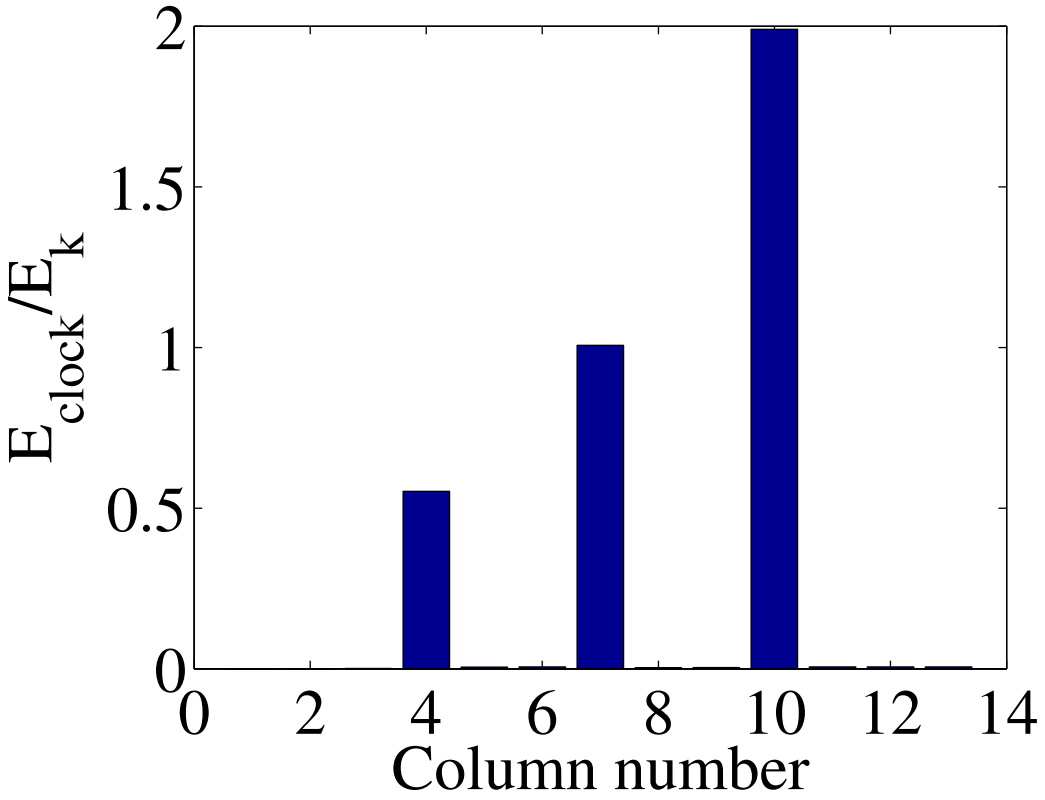

Figure 4.7. The energy provided by the clock per clock cycle in each column of the layout in Figure 4.6.

Figure 4.8 shows the schematic and the power flow stream of the interconnection of the QCA circuitry to conventional CMOS circuits. The clock circuitry augments the signal from the QCA circuitry and the amplified signal is then connected to the conventional CMOS circuit so that it can be more reliably measured at the output.

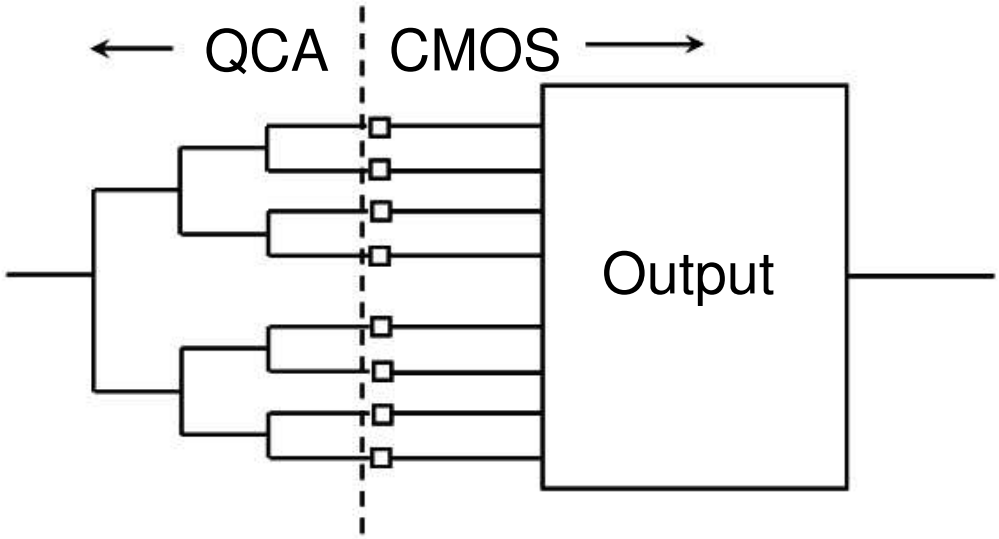

(a)

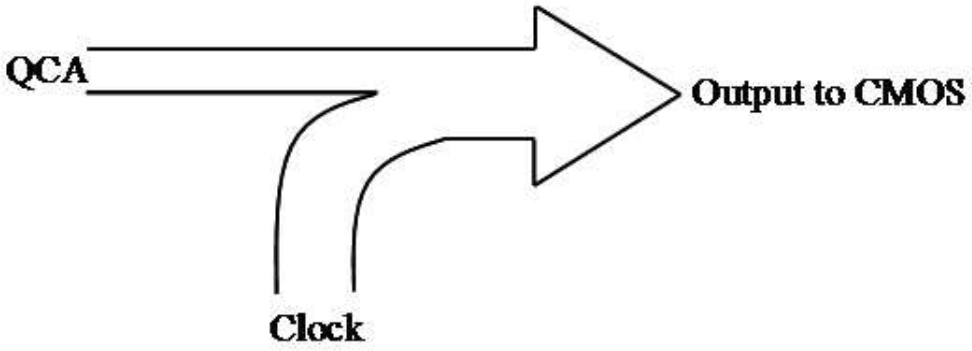

(b)

Figure 4.8. The schematic and the power flow stream of the interconnection of the QCA circuitry to conventional CMOS circuits.

All the circuits we studied for power flow so far are logically reversible circuits, with no bit erasure involved. Any logic gate that has more inputs than outputs is

a logically irreversible circuit since the inputs can not be deduced from the output. It will inevitably dissipate at least a $k_BTln(2)$ to the environment. It's instructive to study the power flow in a majority gate as bit erasure can be explicitly observed. The layout of a majority gate has been shown in Figure 3.3. A majority gate with three same inputs can be seen as a three-to-one fan-in. The power flow over one clock cycle in the majority gate with same inputs is demonstrated in Figure 4.9(a). Since there is no information lost, the energy dissipated is arbitrarily small. The clock provides the energy difference between the input power and output power. The work done by the clock is negative as the energy stored in the system (which is E_k) goes back to the clock. When input bits differ, shown in Figure 3.3 (a) L3 stage, the minority of the input bits ("0" in the top line) is erased. This results in an amount of energy much greater than $k_BTln(2)$ dissipated to the thermal bath while the energy provided by the input and delivered to the output remains the same, as is indicated in Figure 4.9 (b). In this case, only part of the stored energy goes to the clock, the rest of the energy is dissipated to the thermal bath because of information destruction.

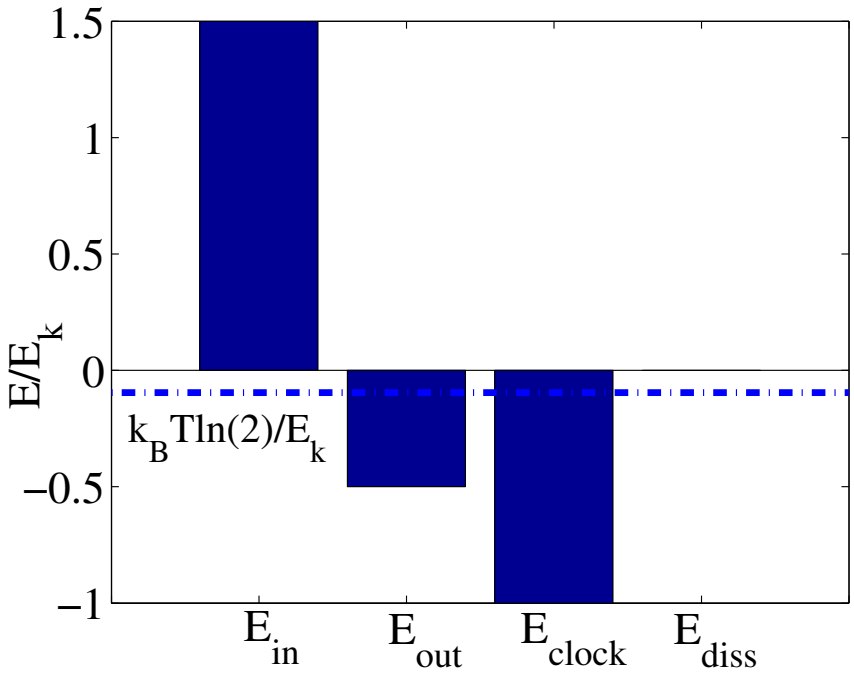

(a)

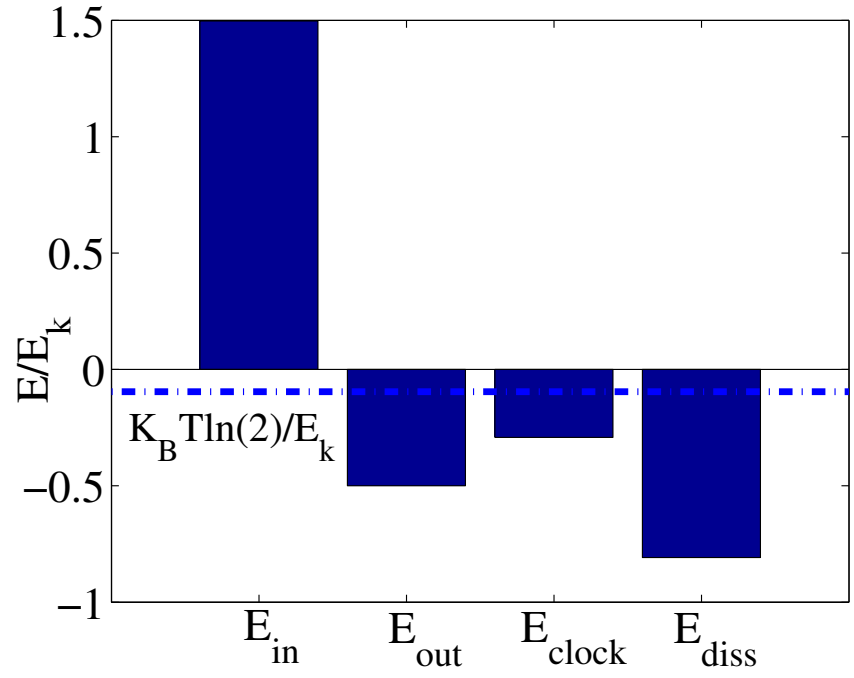

(b)

Figure 4.9. Steady state energy flow in a three input majority gate when (a) All inputs are the same (b) One of the inputs differ.

4.5 Conclusion

The energy flow in clocked QCA circuits explains how a QCA cell is interacting with its surroundings and how energy is exchanged between them. We studied the energy flow in clocked QCA circuits, especially in fan-outs, fan-ins and majority gates. Our calculation of equation of motion shows that clocking plays an important role in QCA circuits, as it provides power gain and make up for the energy lost due to the speed of computation.

CHAPTER 5

ROBUSTNESS IN CLOCKED MOLECULAR QCA

5.1 Introduction

Chapter 2 examined robustness in a semi-infinite metal-dot QCA shift register considering both thermal and speed effects and manufacturing variations. In molecular QCA systems, the kink energy is much larger; allowing room temperature operation. Though thermal fluctuations are therefore small, the exact control of the size, position and orientation of each cell in molecular QCA circuit is challenging. A defect-tolerant architecture is necessary for obtaining reliable signals with imperfect devices.

QCA approach is inherently robust against disorder and can be made even more so by simply using wider wires to build in redundancy at every stage. Other defect tolerant strategies in QCA have been described in [42, 43, 44]. Analysis of missing cell defects in QCA wires [80] and defects due to displacement disorders and temperature effect have been studied in [81]. Defects due to cell rotation have not been examined. In this chapter, we study robustness in a molecular semi-infinite shift register, with single cell and three-cell widths, in terms of displacement and rotational disorders. The key results are phase plots of working parameter space with both displacement and rotational disorders. Our study shows that the QCA architecture exhibits a high degree of robustness.

5.2 Coulombic interaction between two arbitrary positioned cells in a three-state system

When QCA cells are not uniformly spaced and have different orientations, the geometric factor $f_{j,m}$ in Hamiltonian (Equation (3.1) in Chapter 3) is no longer unity. The geometric factor can be calculated from a nine-state Hamiltonian basis which still explicitly accounts for spatial relationship of cells. The reduction of Hamiltonian from full basis to nine-state basis and then to the three-state approximation has been detailed in [79]. In the nine-state basis, each electron is confined to a single side of the cell, where the tunneling between the sites in two sides of the cell is suppressed. The nine-state basis vectors with the corresponding charge configuration at six sites within a cell is listed in Figure 5.1.

The nine-state Hamiltonian is therefore

$$H^{(9)} = \sum_i (E_i + V_i)\hat{n}_j + \sum_{i>j} t_{i,j}(\hat{a}_i^\dagger \hat{a}_j + \hat{a}_j^\dagger \hat{a}_i) + \sum_{i>j} V_Q \frac{\hat{n}_i \hat{n}_j}{|R_i - R_j|} \qquad (5.1)$$

The first term of Equation 5.1 represents the on site energy of each dot. E_i is the occupancy energy of site i, including the positive neutralizing background charge and the effects of the clock. V_i is the potential energy of a site i due to charges in neighboring cells. The second terms accounts for the tunneling energy between sites. $t_{i,j}$ is the tunneling energy between site i and site j. $\hat{a}_i(\hat{a}_i^\dagger)$ annihilates (creates) an electron on site i. The number operator for electrons on site i is

$$\hat{n}_i = \hat{a}_i^\dagger \hat{a}_i.$$

The last term corresponds to the Coulombic interaction between the electrons on different sites within a cell, where

$$V_Q = \frac{1}{4\pi\epsilon},$$

ϵ is the permittivity in free space and $|R_i - R_j|$ is the distance between site i and site j.

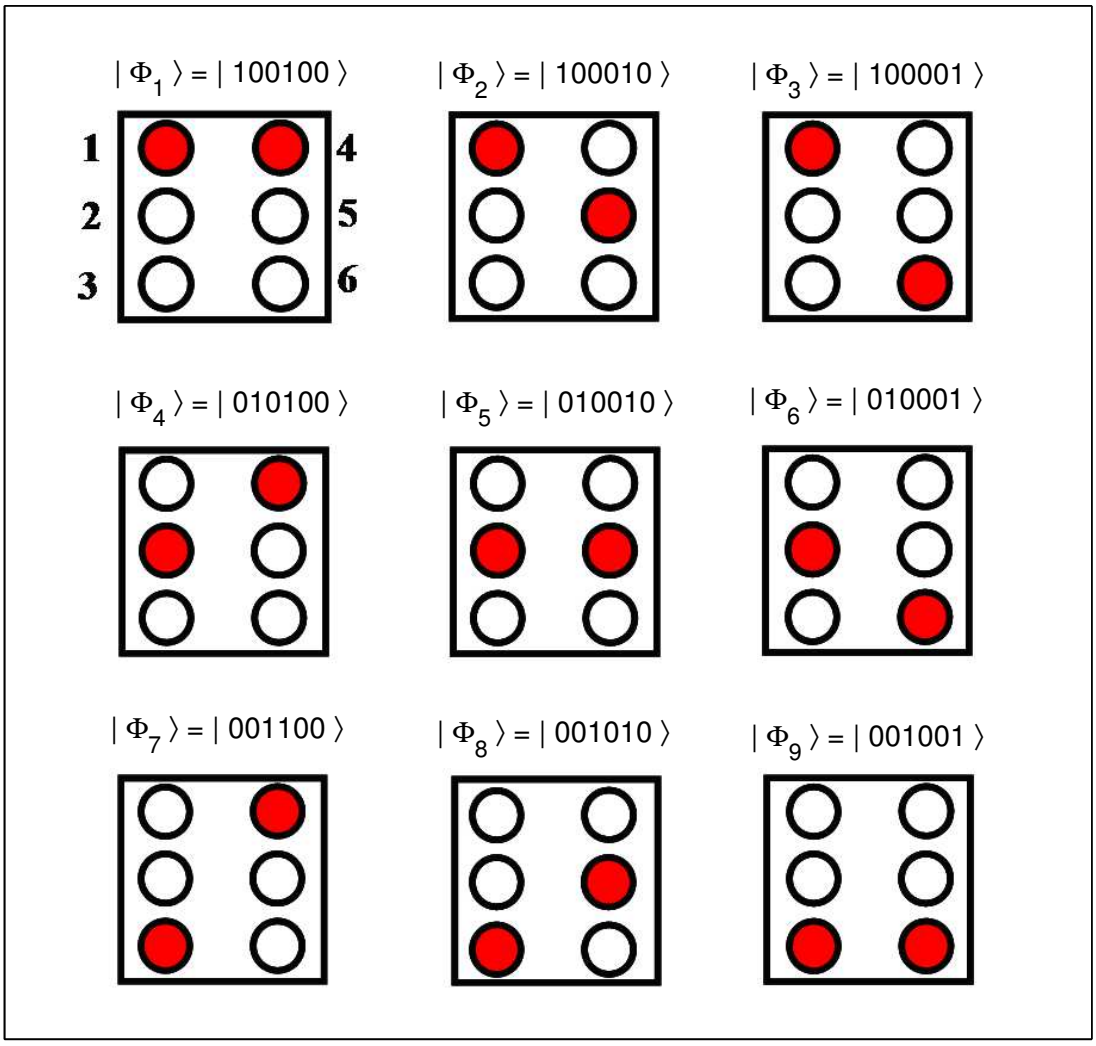

Figure 5.1. Nine-state basis vectors with the corresponding charge configuration at six sites within a cell.

The Coulombic interaction between two cells is the energy difference between two fully polarized cells with the same polarization and opposite polarization.

$$E = \langle\Phi_7|\sum_i (E_i + V_i)\hat{n}_i|\Phi_7\rangle - \langle\Phi_3|\sum_i (E_i + V_i)\hat{n}_i|\Phi_3\rangle$$

where $\sum_i (E_i + V_i)\hat{n}_i$ is the term in a nine-state Hamiltonian and Φ_i is the nine state basic vector listed in Figure 5.1. The geometric factor is then the ratio of Coulombic interaction between two arbitrary positioned neighboring cells with arbitrary orien-

tation and Coulombic interaction between two horizontally (or vertically) aligned standard cells.

5.3 Disorder in QCA architecture

Thermal effects and manufacturing defects are most common disorders in QCA architecture. Thermal fluctuation can excite QCA cell array above its ground state and switch some of the cells into wrong states. The maximum operating temperature is limited by the size of the QCA cells. The Columbic interaction energy between two cells is inversely proportional to the cell size, which can be obtained from electrostatic calculation. The distance between two corner dots in a QCA cell is $a = 1nm$ and the distance between two horizontally aligned cells (from center of one cell to the center of another cell) is $2a$. The kink energy is large enough (about $0.2ev$) that the molecular systems can be considered at zero temperature.

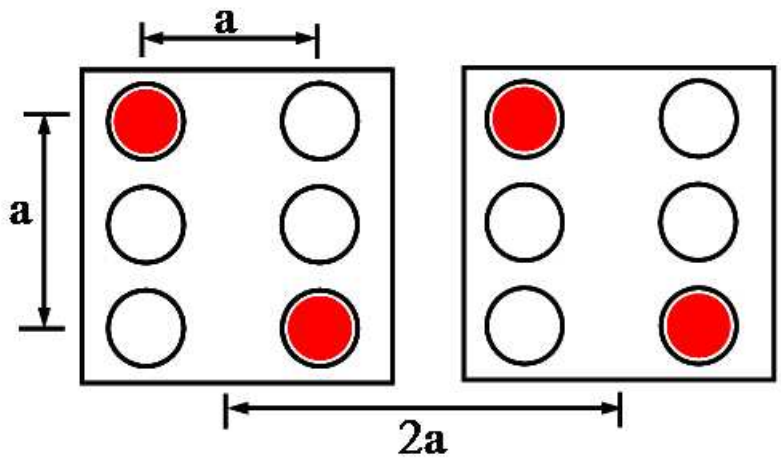

Figure 5.2. The geometry of two neighboring QCA cells.

Because of the substrate interactions and inter-molecular interactions, molecular arrays are highly ordered. But defects due to rotated cells and cells displaced from

ideal places still exist, because deviation from ideal cell positions and rotation of molecules are inevitable.

The displacement disorder happens when the cell is displaced from its original place. Neighboring cells with shorter distance have stronger Coulombic interaction than the ones with longer distance. The Coulombic interaction between cells decays as the inverse fifth power of the distance between them [79]. Therefore it is sufficient to consider the interaction between each cell and its eight surrounding neighbors. When the displaced cell is about 45 degree to its neighboring cell, they will induce opposite polarizations. The closer they are the stronger inversion they have. Figure 5.3 shows the interaction with two cells diagonally aligned. The diagonal interaction of the neighboring cells is implemented to realize inverters in QCA architecture.

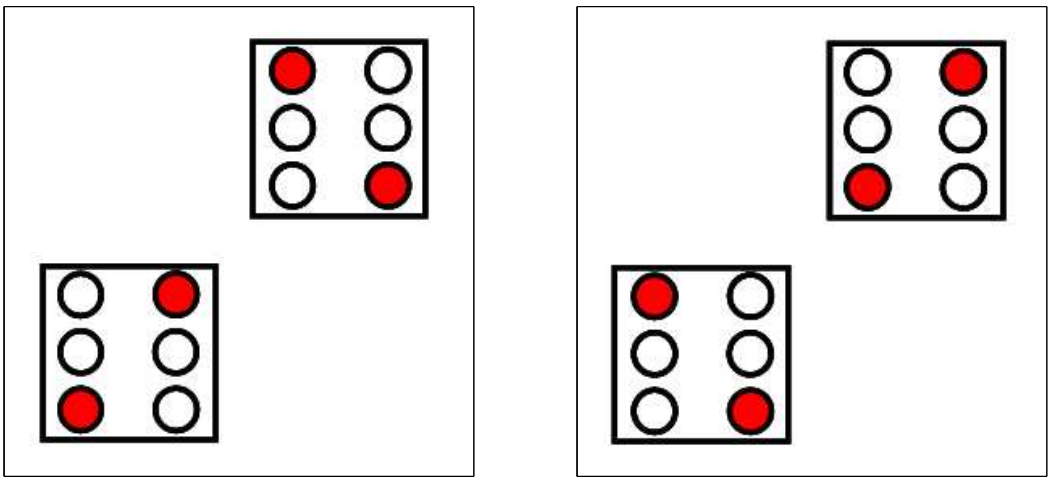

Figure 5.3. The interaction of two diagonally aligned cells.

The Coulombic interaction between a normal cell and a rotated cell is weaker than the interaction between two unrotated cells. A rotated cell is one that has been rotated around its center. Figure 5.4 shows the interaction energy between one normal cell and one cell rotated from 0° to 45° (because of symmetric geometry,

we only need to consider rotation angle from 0° to 45°) as a ratio to the interaction energy between two neighboring normal cells. The distance between two cells is fixed to 2a. With the increase of a cell's rotational angle, the interaction between the two cells becomes weaker. When the cell is rotated 45°, it will have no interaction on its neighboring normal cell. This feature can be exploited in coplanar non-interfering wire crossing, with one line of normal cells and one line of 45° rotated cells crossing each other without interference of signals [5]. When the cell is rotated 90°, the two neighboring cells will have the same polarization again. If both cells are rotated 45 degree, they will have the opposite polarization. A line of 45 degree rotated cells functions as an inverter chain, shown in Figure 5.5. The polarization alternates

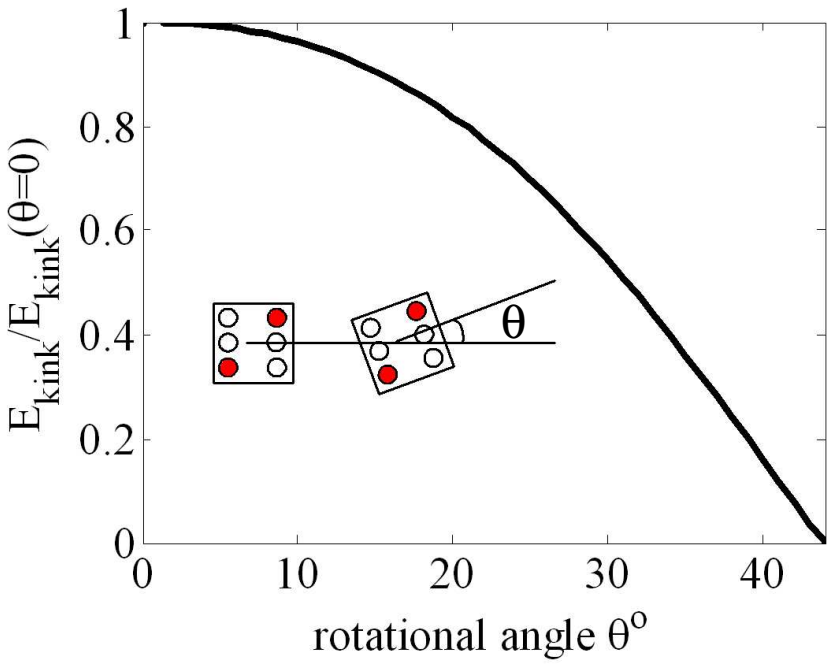

Figure 5.4. Coulomb interaction between one normal cell and one cell rotated from 0° to 45° as a ratio to the interaction between two neighboring normal cells. The distance between two cells is fixed at 2a.

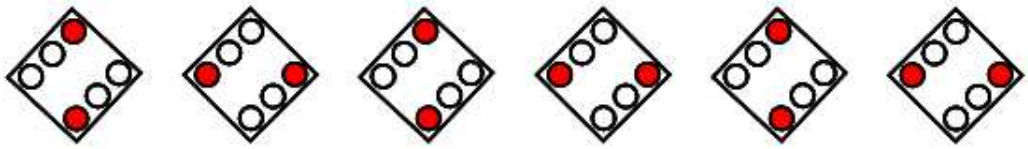

Figure 5.5. An inverter chain composed of a line of 45 degree rotated cells.

5.4 Robustness in molecular QCA shift registers

We examine robustness in a semi-infinite clocked molecular QCA shift register with respect to both displacement and rotational disorder. A semi-infinite shift register can be simulated with a finite number of cells. It is constructed with four cells in a line with the last cell connected to the first cell so that the information moves along the shift register chain infinitely. A four-phase clocking scheme is employed to realize adiabatic switching so that there are always two copies of bits moving along the chain. We solve the time dependent, non-equilibrium equation of motion at room temperature described in Equation (3.7). The three-state Hamiltonian includes the geometry factor that accounts for the orientation and positioning of the neighboring cells. In the simulation, we examined an array of 500 cells. Each cell is displaced randomly in the x direction by Δx and in the y direction by Δy. Δx and Δy are chosen randomly in the interval $[-\delta, +\delta] \times a$. $\Delta\theta$ is chosen randomly in the interval $[-\theta, +\theta]$.

Figure 5.6 shows the phase plot of the working space as a function of both δ and θ. Points with circle and cross represent working and failing circuit respectively. The shaded area is where the circuit works and the white area is where the circuit fails. A working circuit means that the output of the shift register chain has the

same polarization as the input. In a successful single cell wide shift register chain, all the cells are switched to the same polarization as the input (not necessarily fully polarized). If the output of the shift register chain has the opposite polarization as the input, it is considered as a failing circuit. In a single wire shift register, if one cell is switched to the wrong state, the rest of the cells to its right will be copying that wrong information along the array. When there is only rotational disorder ($\delta = 0$), the shift register succeeds when $\theta \leq 21°$. With the increase of the displacement disorder, the tolerance to rotational disorder decreases. When there is only displacement disorder ($\theta = 0$), the shift register works when $\delta \leq 0.35$.

Figure 5.7 demonstrates the geometry of the shift register with displacement and rotational disorders in the cases where the circuit works and fails. The single wire QCA shift register displays a high order of robustness in presence of manufacturing defects.

Adding redundancy can improve the defect tolerance in the QCA system. Figure 5.8 illustrates the phase plot of the working space as a function of both δ and θ in a three-cell wide shift register. As is shown from the figure, the tolerance to the rotational disorder has improved by $\pm 5°$ when displacement factor $\delta < 0.3$. Even when one or several of the cells in the QCA array flip to the wrong state, the rest of the cells copy the right information to the output.

Figure 5.9 demonstrates the geometry of the three-cell wide shift register with displacement and rotational disorders in cases when the circuit succeeds and fails. This figure indicates that the robustness in QCA can be improved by using wider wires to build redundancy in every stage of the circuit. The highly disordered geometry of a functioning QCA array exhibits a high order of the robustness in molecular QCA system due to the strong coupling between the molecular QCA cells.

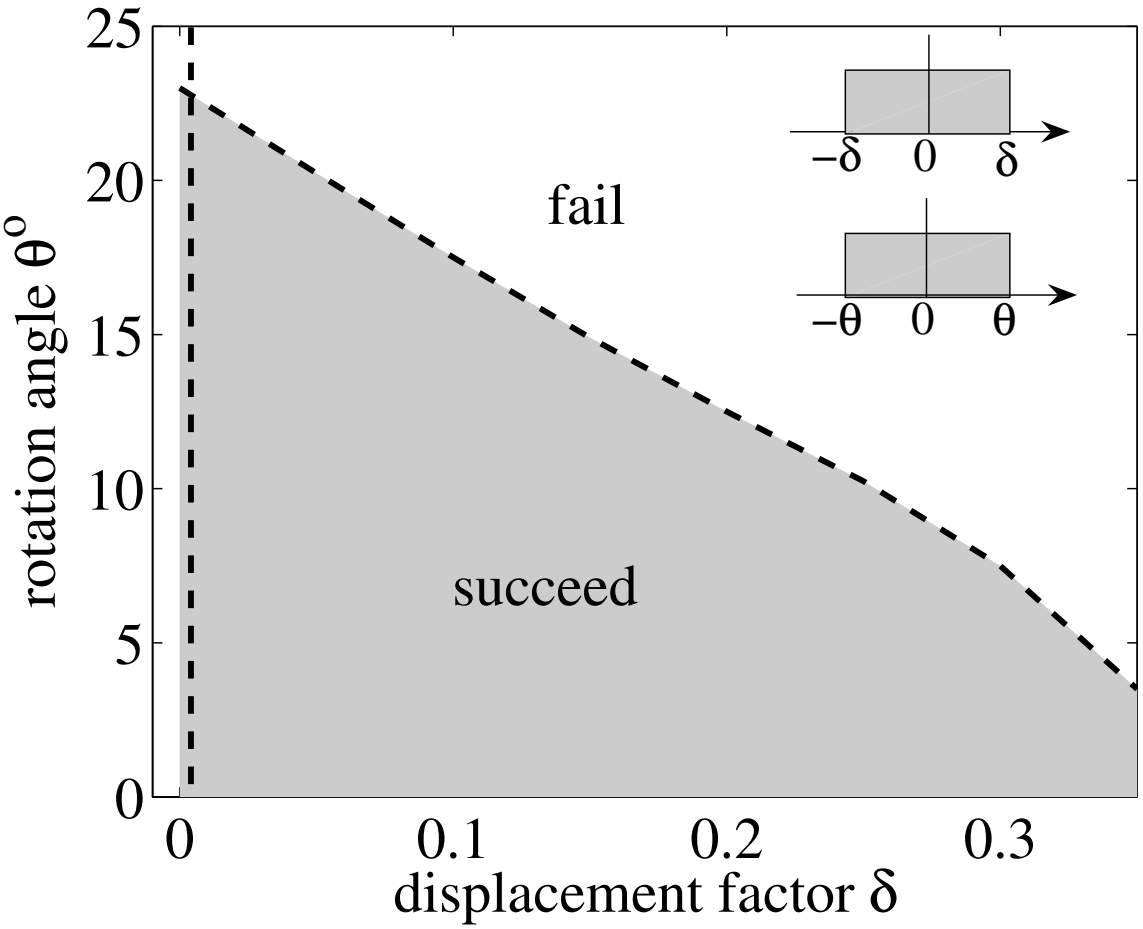

Figure 5.6. The phase plot of the working space as a function of both displacement factor δ and rotational angle θ in a single cell wide shift register.

5.5 Conclusion

Defect tolerance is critical for molecular QCA circuits because of the inevitable defects in molecular QCA fabrication. In this chapter, we examine the robustness of the single cell wide and three-cell wide molecular QCA shift registers in terms of displacement and rotational disorders. We obtain phase plots of working space as a function of both displacement and rotational disorder. Our results show that QCA approach is robust and defect tolerance can be simply improved with wider wires.

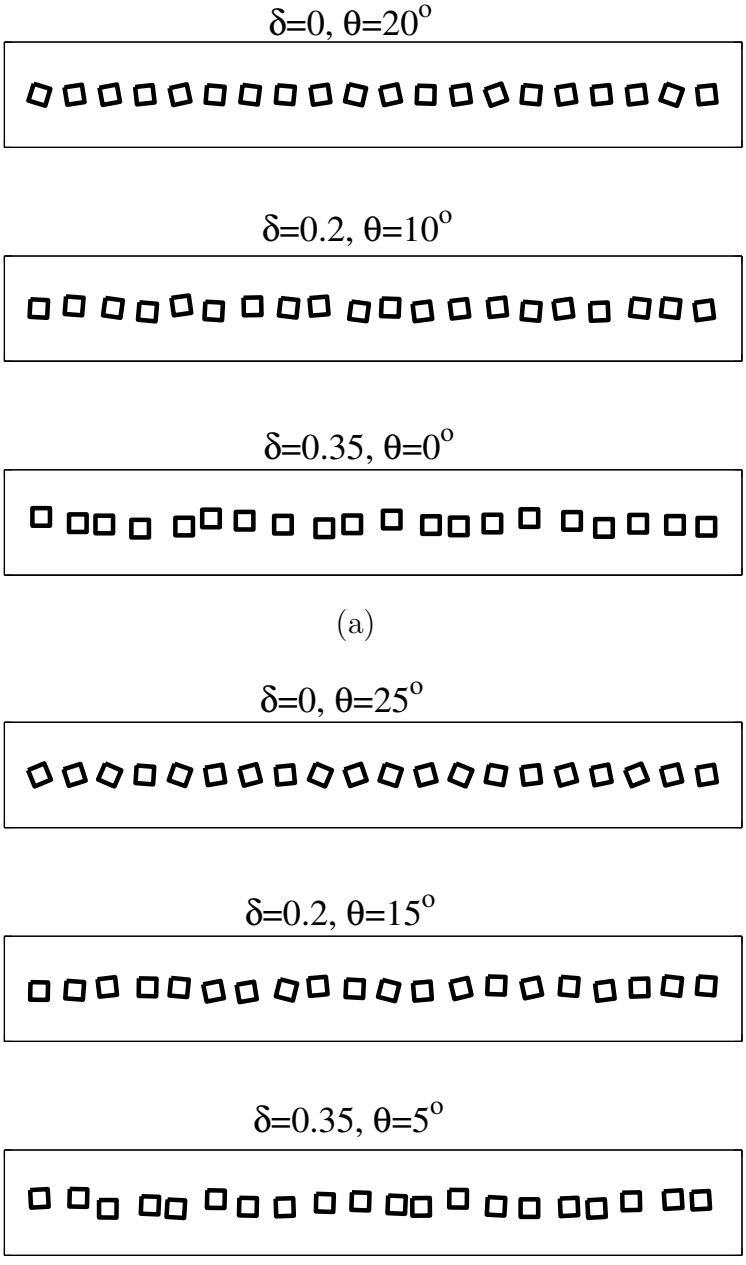

Figure 5.7. The geometry of the single cell wide shift register; (a) three cases when the circuit works (b) three cases when the circuit fails.

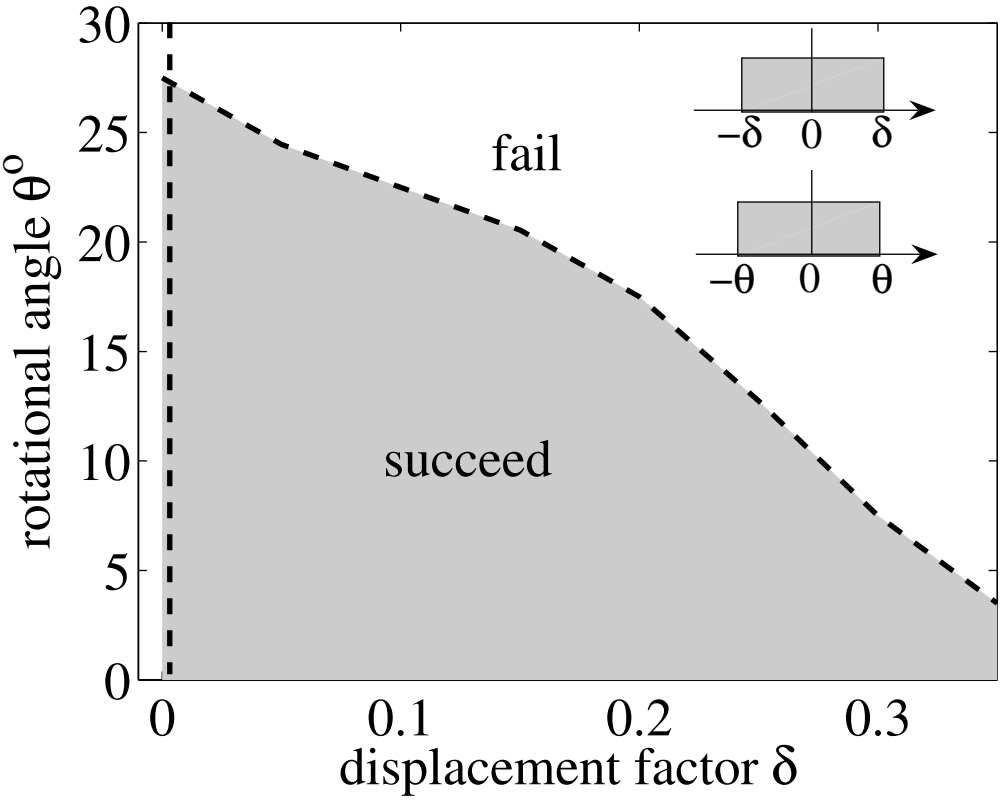

Figure 5.8. the phase plot of the working space as a function of both δ and θ in a three-cell wide shift register.

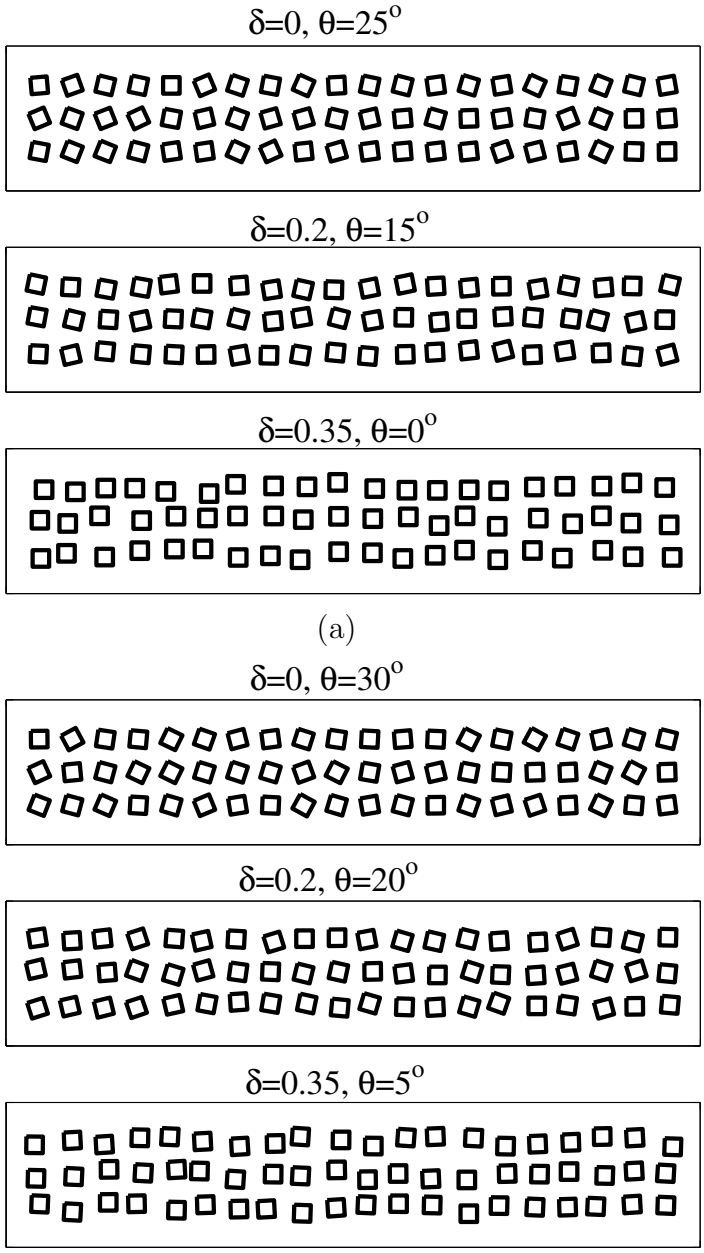

Figure 5.9. The geometry of the three-cell wide shift register; (a) three cases when the circuit works (b) three cases when the circuit fails.

CHAPTER 6

CONCLUSION

The QCA paradigm encodes bit information by charge configuration within a cell instead of current switches of transistors in conventional CMOS circuits. This revolutionary approach provides an alternate way for transistor-less computation at the nanoscale.

QCA logic devices such as binary wires, majority gates, shift registers and fan outs built with metallic tunnel junctions and very small capacitors have been successfully fabricated [25, 26, 27, 28]. Power gain in metal-dot QCA system has been measured experimentally [29]. Although limited by the fabrication method to very low operation temperature, the functioning metal-dot QCA devices provide valuable demonstrations of QCA circuits and strong evidence of the applicability of QCA system. They serve as prototypes for ultimate small molecular QCA system that can function at room temperature.

Significant research has been conducted both theoretically and experimentally on the implementation of molecular QCA cells which are constructed using mixed valence compounds [27-34]. Two-dot half cells and four-dot cells have been synthesized and direct measurements of bistable switching required for QCA operation have been reported [38, 39, 40, 41]. The fabrication of molecular QCA devices are still under way.

QCA clocking schemes have been developed to adiabatically switch the QCA cells

between active state and null state, reducing the power dissipated to the thermal environment to a minimum.

This thesis provides a theoretical study on the performance in both clocked metallic and molecular QCA circuits. The robustness with regard to thermal fluctuation, switching speed and capacitance variation due to manufacturing imperfections in a semi-infinite metal-dot QCA shift register is studied in Chapter 2. A phase plot of the working space with respect to effect of temperature and speed is obtained by directly solving a time dependant master equation. Our simulation shows that the metal-dot QCA shift register can function without an error with a random capacitance deviation of $\pm 10\%$ from the standard capacitance parameters. The performance of the metal-dot QCA shift register can be greatly improved with scaling down the capacitances. Energy dissipation and energy flow in clocked molecular QCA circuits are studied in Chapter 3 and Chapter 4. The ideas of Bennett are applied in Chapter 3 to switch QCA cells in the most power efficient manner, reducing the power dissipation to a minimum. A coherence vector formalism with dissipation incorporated through a time relaxation approximation in an open system coupling to the thermal bath is developed to study the thermodynamics in the QCA system. The comparison of the energy dissipated to the thermal environment in the Landauer clocked and Bennett clocked QCA circuits suggest that QCA may provide a practical means of implementing reversible computing and illustrates the principle that there is no fundamental lower limit to the energy dissipation cost of transporting information. Our results are not a proof of the correctness of the Landauer-Bennett analysis, but they certainly demonstrate its correctness in this concrete system. QCA cells exchange energy with its neighboring cells, the clock and the thermal bath. The energy flow in presence of information flow in clocked molecular QCA circuits especially in fan-outs, fan-ins and majority gates is stud-

ied in Chapter 4. Our calculations show the key role that clocking plays in QCA circuits, as it not only enables data pipelining but also provides power gain and augments weakened signal at every stage. Our results show that $E_k/2$ amount of energy is transported along the QCA array and that amount of energy need not be dissipated as long as there is no bit erasure involved. The robustness in clocked molecular QCA circuits is examined in Chapter 5. The robustness in a single cell wide and three-cell wide molecular QCA shift register in terms of manufacturing imperfections, displacement disorder and rotational disorder, is studied. Our results show that QCA approach is inherently robust and defect tolerance can be simply improved using wider wires to build redundancy at every stage.

This thesis focuses on the robustness in metallic and molecular QCA shift register, other QCA circuits have not been examined. Future work can be extended to the robustness in more complex circuits like majority gates or full adders. More explicit parameter variations in defects during the fabrication process can be added to test the robustness in molecular QCA system, for example, cells with non-uniform sizes, distorted shape of cells, and missing cells etc.

REFERENCES

[1] Lent, C. S.; Tougaw, P. D.; Porod, W. and Bernstein, G. H., *Nanotechnology,* 4, 49, 1993.

[2] Lent C. S. and Tougaw P. D., "Lines of interacting quantum-dot cells: a binary wire," *J. Appl. Phys.,* vol. 74, pp. 6227-33, Nov. 1993.

[3] Lent C. S., Tougaw P. D. and Porod W., "Bistable saturation in coupled quantum dots for quantum cellular automata," *Appl. Phys. Lett.,* vol. 62, pp. 714-716, Feb. 1993.

[4] Lent C. S. and Tougaw P. D., "Bistable saturation due to single electron charging in rings of tunnel junctions," *J. Appl. Phys.,* vol. 75, pp. 4077-80, Apr. 1994.

[5] Tougaw P. D. and Lent C. S., "Logical devices implemented using quantum cellular automata," *J. Appl. Phys.,* vol. 75, pp. 1818-25, Feb. 1994.

[6] Lent C. S., Tougaw P. D. and Porod W., "Quantum cellular automata: the physics of computing with arrays of quantum dot molecules," *Proceedings of the Workshop on Physics and Computation - PhysComp '94,* pp. 5-13, 1994.

[7] Tougaw P. D. and Lent C. S., "Effect of stray charge on quantum cellular automata," *Jpn. J. Appl. Phys.,* vol. 34, pp. 4373-4375, Part 1, No. 8B, Aug. 1995.

[8] Tougaw P. D. and Lent C. S., "Dynamic behavior of quantum cellular automata," *J. Appl. Phys.,* vol. 80, pp. 4722-4736, Oct. 1996.

[9] Lent C. S. and Tougaw P. D., "A device architecture for computing with quantum dots," *Proc. IEEE,* 85, pp. 541-557, Apr. 1997.

[10] Toth G. and Lent C. S., "Quasiadiabatic switching for metal-island quantum-dot cellular automata," *J. Appl. Phys.,* vol. 85, pp. 2977-2984, Mar. 1999.

[11] Toth G. and Lent C. S., "Role of correlation in the operation of quantum-dot cellular automata," *J. Appl. Phys.,* vol. 89, pp. 7943-7953, Jun. 2001.

[12] Toth G. and Lent C. S., "Quantum computing with quantum-dot cellular automata," *Phys. Rev. A,* vol. 63, 052315, pp. 1-9, 2001.

[13] Timler J. and Lent C. S., "Power gain and dissipation in quantum-dot cellular automata," *J. Appl. Phys.,* vol. 91, pp. 823-831, Jan. 2002.

[14] Timler J. and Lent C. S., "Maxwell's demon and quantum-dot cellular automata," *J. Appl. Phys.,* vol. 94, pp. 1050-1060, 2003.

[15] Bazan G., Orlov A. O., Snider G. L., Bernstein G. H., "Charge detector realization for AlGaAs/GaAs quantum-dot cellular automata," *J. Vac. Sci. Tech.* B vol 14, pp. 4046-4050, 1996.

[16] Single C., Augke R., Prins E. E., Wharam D. A. and Kern D. P., "Towards quantum cellular automata operation in silicon: transport properties of silicon multiple dot structures," *Superlatt. and Microstr.,* vol. 28, pp. 429-434, Nov. 2000.

[17] Single C., Rugke A. and Prins E. E., "Simultaneous operation of two adjacent double dots in silicon," *Appl. Phys. Lett.,* vol. 78, pp. 1421-1423 Mar. 2001.

[18] Cowburn R. P. and Welland M. E., "Room temperature magnetic quantum cellular automata," *Science,* Vol. 287, pp. 1466-1468, Feb. 2000.

[19] Csaba G. and Porod W., "Simulation of Field Coupled Computing Architectures Based on Magnetic Dot Arrays," *J. Comp. Elect.,* vol. 1, pp. 87-91, 2002.

[20] Imre A., Zhou L., Orlov A. O., Csaba G., Bernstein G. H., Porod W. and Metlushko V., "Application of mesoscopic magneti rings for logic devices," *4th IEEE Conference on Nanotechnology,* pp. 137-139, 2004.

[21] Imre A., Csaba G., Ji L., Orlov A. O., Bernstein G. H., Porod W., "Majority Logic Gate for Magnetic Quantum-Dot Cellular Automata," *Science,* vol. 311 pp. 205-208, 2006.

[22] Orlov A. O., Amlani I., Bernstein G. H., Lent C. S. and Snider G. L., "Realization of a functional cell for quantum-dot cellular automata," *Science* 277, pp. 928-930, Aug. 1997.

[23] Amlani I., Orlov A. O., Snider G. L., Lent C. S. and Bernstein G. H., "External charge state detection of a double-dot system," *Appl. Phys. Lett.,* vol. 71, pp. 1730-1732, Sep. 1997.

[24] Amlani I., Orlov A. O., Snider G. L., Lent C. S. and Bernstein G. H., "Demonstration of a six-dot quantum cellular automata system," *Appl. Phys. Lett.,* vol. 72, pp. 2179-2181, Apr. 1998.

[25] Amlani I., Orlov A. O., Toth G., Lent C. S., Bernstein G. H. and Snider G. L., "Digital logic gate using quantum-dot cellular automata," *Science,* vol. 284, pp. 289-291, Apr. 1999.

[26] Orlov A. O., Amlani I., Toth G., Lent C. S., Bernstein G. H. and Snider G. L., "Experimental demonstration of a binary wire for quantum-dot cellular automata," *Appl. Phys. Lett.,* vol. 74, pp. 2875-2877, May 1999.

[27] Amlani I., Orlov A. O., Kummamuru R. K., Bernstein G. H., Lent C. S. and Snider G. L., "Experimental demonstration of a leadless quantum-dot cellular automata cell," *Appl. Phys. Lett.,* vol. 77, pp. 738-740, Jul. 2000.

[28] Orlov A. O., Amlani I., Kummamuru R. K., Ramasubramaniam R., Toth G., Lent C. S., Bernstein G. H. and Snider G. L., "Experimental demonstration of clocked single-electron switching in quantum-dot cellular automata," *Appl. Phys. Lett.,* vol. 77, pp. 295-297, Jul. 2000.

[29] Kummamuru R. K., Timler J., Toth G., Lent C. S., Ramasubramaniam R., Orlov A. O., Bernstein G. H. and Snider G. L., "Power gain in a quantum-dot cellular automata latch," *Appl. Phys. Lett.,* vol. 81, pp. 1332-1334, Aug. 2002.

[30] Kummamuru R. K., Orlov A. O., Lent C. S., Bernstein G. H. and Snider G. L., "Operation of a quantum-dot cellular (QCA) shift register and analysis of errors," *IEEE Trans. Elect.* Dev., vol 50, pp. 1906-1913, 2003.

[31] Lent C. S., "Bypassing the Transistor Paradigm," *Science,* vol. 228, pp. 1597-1598, 2000.

[32] Hennessy K. and Lent C. S., "Clocking of molecular quantum-dot cellular automata," *J. Vac. Sci. Tech. B,* vol. 19, pp. 1752-1755, Sep. 2001.

[33] Blair E. and Lent C. S., "An architecture for molecular computing using quantum-dot cellular automata," *IEEE-NANO Third IEEE Conference on Nanotechnology,* Volume 1, 2003, pp. 402 -405.

[34] Lieberman M., Chellamma S., Varughese B., Wang Y. L., Lent C. S., Bernstein G. H., Snider G. and Peiris F. C., "Quantum-dot cellular automata at a molecular scale," *Ann. N.Y. Acad. Sci.,* vol. 960, 2002.

[35] Lent C. S., Isaksen B. and Lieberman M., "Molecular quantum-dot cellular automata," *J. Am. Chem. Soc.,* vol. 125, pp. 1056-1063, 2003.

[36] Lent C. S. and Isaksen B., "Clocked molecular quantum-dot cellular automata", *IEEE Trans. on Electron Devices,* 50, 1890-1896 2003.

[37] Manimarian M., Snider G. L., Lent C. S., Sarveswaran V., Lieberman M., Li Z. and Fehlner T. P., "Scanning tunneling microscopy and spectroscopy investigations of QCA molecules," *Ultramicroscopy,* vol. 97, pp. 55-63 2003.

[38] Li Z., Beatty A. M. and Fehlner T. P., "Molecular QCA Cells. 1. "Structure and functionalization of an unsymmetrical dinuclear mixed-valence complex for surface binding." *Inorg. Chem.,* vol. 42, pp. 5707-5714 2003.

[39] Li Z. and Fehlner T. P., "Molecular QCA Cells. 2. "Electrochemical characterization of an unsymmetrical dinuclear mixed-valence complex bound to a au surface by an organic linker," *Inorg. Chem.,* vol. 42, pp. 5715-5721, 2003.

[40] Qi H., Sharma S., Li Z., Snider G. L., Orlov A. O., Lent C. S. and Fehlner T. P., "Molecular qca cells. electric field driven switching of a silicon surface bound array of vertically oriented two-dot molecular quantum cellular automata," *J. Am. Chem. Soc.,* vol 125, pp. 15250-15259, Dec. 2003.

[41] Jiao J., Long G. J., Grandjean F., Beatty A. M. and Fehlner T. P., "Building blocks for the molecular expression of quantum cellular automata. isolation and characterization of a covalently bonded square array of two ferrocenium and two ferrocene complexes," *J. Am. Chem. Soc.,* vol. 125, pp. 7522, 2003.

[42] Huang J., Tahoori M. B. and Lombardi F., "Defect characterization for scaling of QCA devices", *IEEE Symposium on Defect and Fault Tolerant (DFT),* 2004.

[43] Fijany A. and Toomarian B. N., "New design for quantum dots cellular automata to obtain fault tolerant logic gates," *J. of Nanoparticle Res.,* vol. 3, pp.27-37, Feb. 2001.

[44] Walus K., Budiman R. A. and Jullien G. A., "Effects of morphological variations of self-assembled nanostructures on quantum-dot cellular automata (QCA) circuits", *Frontiers of Integration, An International Workshop on Integrating Nanotechnologies,* 2002.

[45] Lent C. S., Tougaw P. D., Brazhnik Y., Weng W., Porod W., Liu R. W. and Huang Y. F., "Quantum cellular neural networks," *Superlatt. and Microstr.,* vol. 20, pp. 473-478, 1996.

[46] Gin A., Williams S., Meng H. Y. and Tougaw P. D., "Hierarchical design of quantum-dot cellular automata devices," *J. Appl. Phys.,* vol. 85, pp. 3713-3720, 1999.

[47] Niemier M. T. and Kogge P. M., "Logic-in-wire: Using quantum dots to implement a microprocessor", *International Conference on Electronics, Circuits, and Systems (ICECS '99),* 1999.

[48] Pasky J. R., Henry L. and Tougaw P. D., "Regular arrays of quantum-dot cellular automata macrocells," *J. Appl. Phys.,* vol. 87, pp. 8604-8609, June 2000.

[49] Csurgay A. I., Porod W. and Lent C. S., "Signal processing with near-neighbor-coupled time-varying quantum-dot arrays," *IEEE Trans. Circuits Sys. I-Fund. Theor. Appl.,* vol. 47, pp. 1212-1223, Aug. 2000.

[50] Niemier M. T. and Kogge P. M., "Problems in designing with QCAs: layout=timing," *Int. J. of Circuit Theor. and Appl.,* vol. 29, pp. 49-62, 2001.

[51] Cardenas-Barrera J. L., Platoniotis K. N. and Venetsanopoulos A. N., "QCA implementation of a multichannel filter for image processing," *Math. Prob. in Eng.,* vol. 8, pp. 87-99, 2002.

[52] Frost S. E., Rodrigues A. F., Janiszewski A. W., Rausch R. T. and Kogge P. M., "Memory in motion: A study of storage structures in QCA", *1st Workshop on Non-Silicon Computation,* 2002.

[53] Niemier M. T., Rodrigues A. F. and Kogge P. M., "A potentially implementable FPGA for quantum dot cellular automata", *1st Workshop on Non-Silicon Computation,* 2002.

[54] Armstrong C. D. and Humphreys W. M., "The development of design tools for fault tolerant quantum dot cellular automata based logic", *2nd International Workshop on Quantum Dots for Quantum Computing and Classical Size Effect Circuits,* 2003.

[55] Tahoori M. B., Huang J., Momenzadeh M. and Lombardi F., "Testing quantum cellular automata", *IEEE Transaction on Nanotechnology (TNANO),* December 2004.

[56] Dimitrov V. S., Jullien G. A. and Walus K., "Quantum-dot cellular automata carry-lookahead adder and barrel shifter", *presented at IEEE Emerging Telecommunications Technologies Conference,* 2002.

[57] Walus K., Vetteth A., Jullien G. A. and Dimitrov V. S., "RAM design using quantum-dot cellular automata", *NanoTechnology Conference,* vol 2, pp. 160-163, 2003.

[58] Walus K., QCADesigner Home Page, http://www.atips.ca/projects/qcadesigner/.

[59] Zhirnov V. V., Cavin R. K., Hutchby J. A. and Bourianoff G. I., "Limits to binary logic switch scaling-A gedanken model," *Proc. IEEE,* vol. 91, pp. 1934, 2003.

[60] Leff, H. and Rex, A., "Maxwell's Demon 2", *IOP, Bristol,* 2003.

[61] Bennett, C. H., "Notes on Landauer's principle, reversible computation, and maxwell's demon," *Studies in History and Philosophy of Modern Phys.,* vol. 34, pp. 501, 2003.

[62] Bennett, C. H., "Notes on the history of reversible computation," *IBM J. Res. Dev.,* vol 32, pp. 16-23, 1988.

[63] Szilard L., "On the decrease of entropy in a thermodynamic system by the intervention of intelligent beings," *Z. Physik,* vol. 53, pp. 840-856, 1929; translation by A. Rapoport and M. Knoller, reprinted in [1] pp. 110-119 (2nd edition).

[64] Brillouin, L., "Maxwell's Demon Cannot Operate: Information and Entropy. I," *J. Appl. Phys.,* vol. 22, pp. 334-337, 1951.

[65] Landauer, R., "Irreversiblility and heat generation in the computing process," *IBM J. Res. Dev.,* vol 5, pp. 183-191, 1988.

[66] Keyes R. W. and Landauer R., "Minimal energy dissipation in logic," *IBM J. Res. Dev.,* vol 14, pp. 152-157, 1970.

[67] Meindl J., Chen Q. and Davis J., "Limits on silicon nanoelectronics for terascale integration," *Science,* vol. 293, 2044, 2001.

[68] Bennett C. H., "Logical reversibility of computation," *IBM J. of Res. Dev.,* vol. 17, pp. 525-532, Nov. 1973.

[69] Keyes R. W., "Fundamental limits of silicon technology," *Proc. IEEE,* vol. 89, pp. 227, 2001.

[70] Cavin R. K., Zhirnov V. V., Hutchby J. A. and Bourianoff G. I., "Energy barriers, demons, and minimum energy operation of electronic devices," *Noise in Devices and Circuits III,* edited by Balandin A., Danneville F., Deen M. J., Fleetwood D. M., *Proc. of SPIE,* vol. 5844, SPIE, Bellingham, WA, pp. 1-9, 2005

[71] Mahler G. and Weberrub V. A., *Quantum networks: Dynamics of open nanostructures,* Springer, New York, 1995.

[72] Martini I. B., Ma B., Ros T. D., Helgeson R., Wudl F. and Schwartz B. J., "Ultrafast competition between energy and charge transfer in a functionalized electron donorrfullerene derivative," *Chem. Phys. Lett.,* vol. 327, pp. 253-262, 2000.

[73] Landauer R., "Energy requirements in communication," *Appl. Phys. Lett.,* vol. 51, pp 2056-2058, 1987.

[74] Landauer R., "Uncertainty principle and minimal energy dissipation in the computer," *Intern. J. Theoretical Phys.,* vol 21, pp. 283, 1982.

[75] Wasshuber C., *Computational single-electronics,* Springer WienNewYork, 2001.

[76] SIMON homepage, http://www.lybrary.com/simon/.

[77] Kummamuru R.K., Liu M., Orlov A. O. , Lent C. S. , Bernstein G. H. and Snider G. L., "Temperature dependance of locked state in QCA latch," *Microelectronics Journal* vol.36, pp.304-307, 2005.

[78] Grabert H. and Devoret M. H., *Single Charge Tunneling, Coulomb Blockade Phenomena in Nanostructures,* Plenum Press, 1992.

[79] Timler J, "Energy dissipation and power gain in quantum-dot cellular automata," *PhD thesis*, University of Notre Dame, Dept. of Electrical Engineering, May 2003

[80] Dysart T. J., Kogge P. M. , Craig S. Lent and Liu M.," An analysis of missing cell defects in quantum-dot cellular automata,"*IEEE NANOARCH*, May, 2005

[81] Khatun M., Barclay T., Sturzu I. and Tougaw P. D., "Fault tolerance calculations for clocked quantum-dot cellular automata devices," *J. Appl. Phys.* vol 98, pp. 094904, 2005.

[82] Bernstein G. H., Bazan G., Chen M. H., Lent C. S., Merz J. L., Orlov A. O., Porod W., Snider G. L., Tougaw P. D., "Practical issues in the realization of quantum-dot cellular automata," *Superlatt. and Microstr.* vol 20, pp. 447-459, 1996.

[83] Lu Y., Lent C. S., "Model Hamiltonian of molecular quantum-dot cellular automata," *in preparation*

[84] Likharev K. K. and Korotkov A. N.,""Single-Electron Parametron": Reversible Computation in a Discrete-State System," *Science* vol 273, pp. 763-765, 1996.